ANUARUL INSTITUTULUI GEOLOGIC AL ROMÂNIEI

ISSN 1453-357X

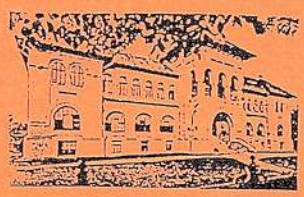

Vol. 72
Part II

Paper presented at the XVI Congress
of the Carpathian-Balkan
Geological Association
(Viena, 1998)

Institutul Geologic al României
Bucureşti – 2000

GEOLOGICAL INSTITUTE OF ROMANIA
Director General Dr. G. Udubaşa Member of the Romanian Academy

The **Geological Institute of Romania** is now publishing the following periodicals:

Romanian Journal of Mineralogy
Romanian Journal of Petrology
Romanian Journal of Mineral Deposits
Romanian Journal of Paleontology
Romanian Journal of Stratigraphy
Romanian Journal of Tectonics and Regional Geology
Romanian Journal of Geophysics
Anuarul Institutului Geologic al României
Memoriile Institutului Geologic al României

Romanian Journals supersede "Dări de Seamă ale Şedinţelor" and "Studii Tehnice şi Economice", whose apparition goes back to 1910. Besides regular volumes, each series may occasionally contain Supplements (for abstracts and excursion guides to congresses and symposia held in Romania) and Special Issues (for larger papers of special interest). "Anuarul Institutului Geologic al României" will appear in a new form, containing both the annual activity report and review papers.

Editorial Office:
Geological Institute of Romania
Str. Caransebeş Nr. 1
RO – 79678 Bucureşti – 32
Tel. (+40) 1 224 20 91, 224 15 30
Fax (+40) 1 224 04 04
e-mail UDUBASA@IGR.RO

The editor has changed the name as follows: Institutul Geologic al României (1906–1952), Comitetul Geologic (1953–1966), Comitetul de Stat al Geologiei (1967–1969), Institutul Geologic (1970–1974), Institutul de Geologie şi Geofizică (1975–1993), Institutul Geologic al României (since 1994).

ANUARUL INSTITUTULUI GEOLOGIC AL ROMÂNIEI supersedes ANUARUL INSTITUTULUI DE GEOLOGIE ŞI GEOFIZICĂ.

The manuscripts should be sent to the scientific editor and/or executive secretary. Correspondence concerning advertisments, announcements and subscriptions should be sent to the Managing Editor.

ISSN 1453–357X
Classification index for libraries 55(058)

Printed by the Geological Institute of Romania
Bucharest

CONTENTS

An. Inst. Geol. Rom., 72, part. II, p. 3-8, Bucureşti, 2000

UPPER PLIOCENE VEGETATIONAL PHASES SOUTH PERICARPATHIANS DEPRESSION, ROMANIA

Emanuel DEMETRESCU

Geological Institute of Romania, 1 Caransebeş St., RO-79678 Bucharest 32

Key words: Palynostratigraphy. Upper Pliocene. Romania.

Abstract: A detailed succession of ten palynologic assemblages consisting of pollen and spores and freshwater cysts is presented. All morphotypes have been delivered along the South peri-Carpathians area during a period of time when most of the tardy Magnoliophyta families have started their development. Based upon their distribution and paleoenvironmental significance during the Upper Pliocene, a ten-level palynostratigraphic scale of specific occurrence is proposed.

Introduction

The material has been collected from eight sections (Fig. 1), and consists of dark to light grey clays and coaly clays.

The palynologic characterization is based upon ten groups of pollen and spores delivered from land-growing taxa plus a suite of four spectra predominantly encompassing pollen of both emergent and submerged aquatic plants. All are regarded as assemblages rather than "associations" to stress upon the absence of biostratigraphic markers. This mode of viewing things has been carried by the fact that the growing of vegetation has been tributary - at least in this area - to environmental and depositional instead of biostratigraphic control. Owing to high vertical and horizontal fluctuations from one site to another as an effect of sedimentary conditions in alluvial plains, there is not a single taxon as reliable for biochronostratigraphic purpose as necessary. It goes without saying that, under the circumstances, one cannot establish a stratigraphic scale in terms of ISG recommendations but solely resume to present these groups as they succeed in the studied deposits.

The respective assemblages (aquatics included) define fourteen intervals or levels (Table 1), each having a particular reproducible degree (RD). This attribute has been assimilated after that referable to biochronological associations (Geux, 1987) yet bears no such a significance in the case here discussed. As seen in Table 1 eight spectra can be grouped to result eventually only ten characteristic assemblages or "palyno-levels" whose position is labelled base upwards. Some of these taxa have a restricted occurrence, others extend throughout the whole area and several out of those recovered from the upper interval make up assemblages that interpenetrate with one another vertically and show a discontinuous distribution laterally. Palynologic delimitation based on these levels of occurrence is illustrated in Figure 2.

Discussion

The suite of vegetational phases starts with a very diversified spectrum predominantly arboreal represented by a remarkable gymnosperm and angiosperm assemblage. It has been recovered from the lower third of the Parscovian sub-stage and represents the so-called Tertiary relics. *Cedrus, Taxus* and *Keteleeria* should be mentioned amongst Gymnospermae. Taxodiaceae have delivered *Glyptostrobus europeus* and *Cryptomeria* sp. Pollen of *Sequoia* also occurs in relative high percentage. The content of humic substances at this level documents the existence of an environment rich in humic clays for which *Sequoia* trees are supposed to have a high affinity. Other morphotypes indicative of warm climate are *Sciadopitys, Tsuga* and *Ginkgo*. Angiospermae include *Symplocos, Nyssa, Catalpa bignonioides, Liquidambar, Carya, Pterocarya, Myrica* and the liana *Parthenocissus*. Broad-leaved forms such as *Castanea* and other Fagaceae have had an important participation, *Castanea* particularly suggesting coastal low land forests. The couple

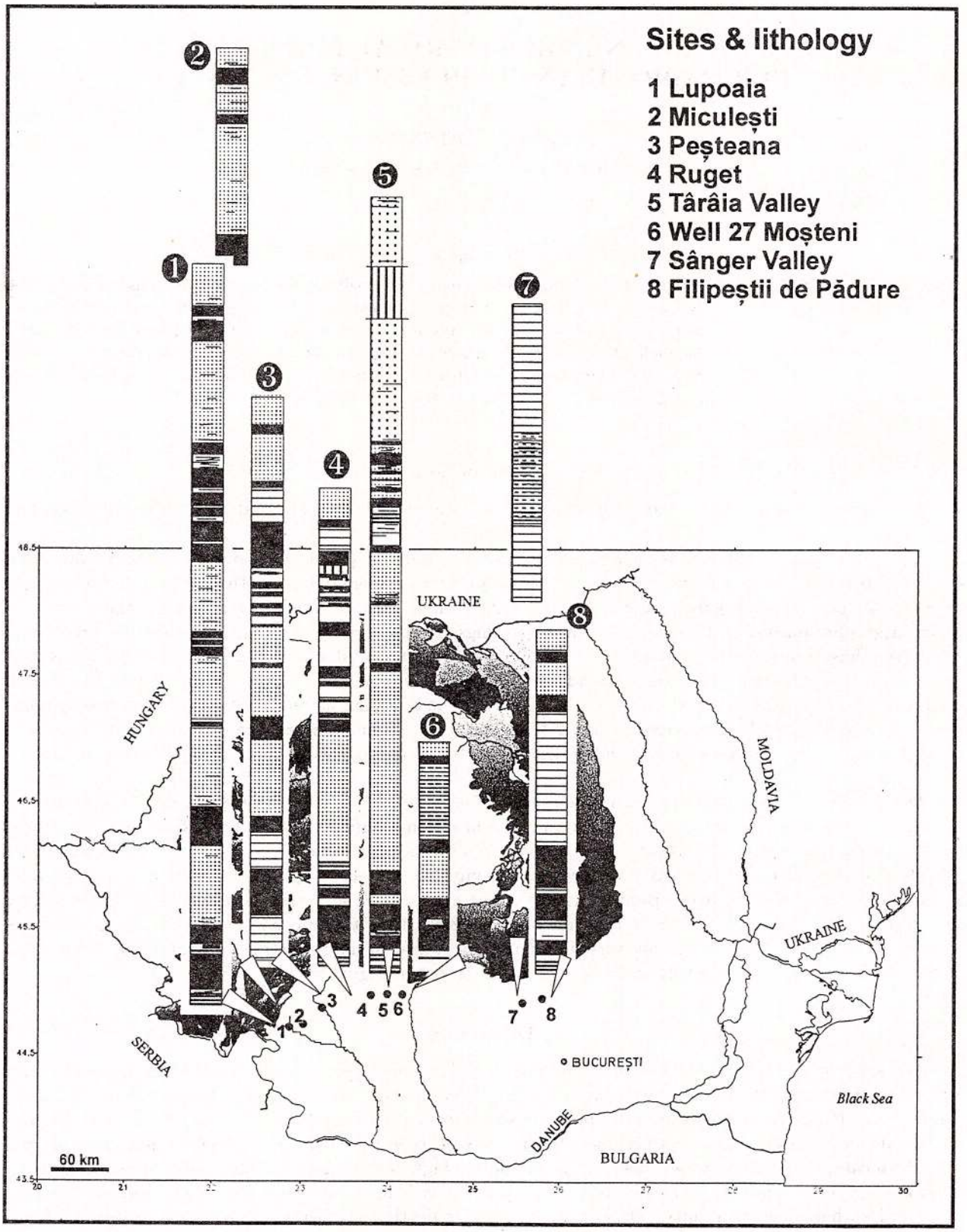

Fig. 1 – Sketch map showing the studied area sampled sections; columns are not at scale.

Table 1

Levels	Characteristic assemblages		RD	Sections
	Leading taxa and/or indicative group	Main constituents (besides leading species)		
10	*Artemisia-Selaginella*	*Polygala*, Graminae, div. mosses spores	2	2, 5
	Aquatics IV - *Pediastrum*	other Hydrodyctiaceae and Zygnemataceae		
9	*Spergularia-Gypsophila*	*Hibiscus, Buplerum, ?Filipendula, Polygala*	4	1-3, 5
8	*Acacia*-Oleaceae	*Jasminum, Syringa, Ligustrum, Olea, Fraxinus, Aesculus, Rhus*	5	1-3, 5, 7
7	Shrubs III	*Myricaria, Tamarix, Spirea, Staphylea*	1	7
6	Aquatics III - *Utricularia*	*Potamogeton, Nelumbo, Menyanthes, Sagittaria, asperula, Nymphoides, Nymphaea, Nuphar*	4	1, 4, 5, 7
	Aquatics II - *Stratiotes*	*Heleocharis, Hydrocharis, Parnassia, Epilobium, Pedicularis*	5	1, 3-5, 7
5	Shrubs II	*Lonicera, Sambucus, Viburnum, Eleagnus Crataegus, Corylus, Alnus,*	2	5, 7
4	Cupressaceae-Taxodiaceae Pinaceae	*Larix, Juniperus, Picea,* Betulaceae, *Acer*	4	1, 3, 5, 7
	Herbs & Bushes	*Dipsacus, Polygonum, Rumex, Malva, Geranium*	3	1, 3, 5
3	Aquatics I	*Lysimachia, Myriophyllum, Geranium ?palustris, Batrachium, Ceratophyllum, Azolla, Salvinia,* Zygnemataceae	3	1, 3, 5
2	*Sphagnum-Drosera*	Pteridophyta and fungi	5	1, 3, 5, 6, 8
	Shrubs I - Ericaceae	*Salix, Carex, Phragmites*	7	1-6, 8
1	Tertiary relics	*Ginkgo, Keteleeria, Cathaya, Tsuga, Taxodium, Glyptostrobus, Sciadopytis, Symplocos, Liquidambar, Carya, Pterocarya*	7	1-6, 8

Symplocos-Nyssa may indicate high groundwater table. The humid conditions are also reflected by the occurrence of *Sequoia-Taxodium-Sciadopitys* all standing for wetter and warmer climate. *Symplocos* also documents the existence of Mediterranean and paleosubtropical conditions. It could have not developed if the winter temperature would have not been well above 0^0C.

Towards the upper part of this interval a dilution in the constituency of this first assemblage has been observed. This is consistent with the trend of switching toward a shrubbery phase with Ericaceae, Salicaceae and *Myrica* that followed above and characterizes the second group of this succession. All environmental conditions have changed, the palynologic spectrum becoming more scarce. The advent of Ericaceae may stand for a reduction in nutrient supply and the existence of more drained soils. The climatic deterioration is also suggested by the presence of *Corylus* and the following *Sphagnum-Drosera* couple accompanied by Pteridophyta and fungal remains consisting of various ascospores and hypae. The most remarkable taxon out of this assemblage is *Drosera*, which indicates the development of peat-forming bogs.

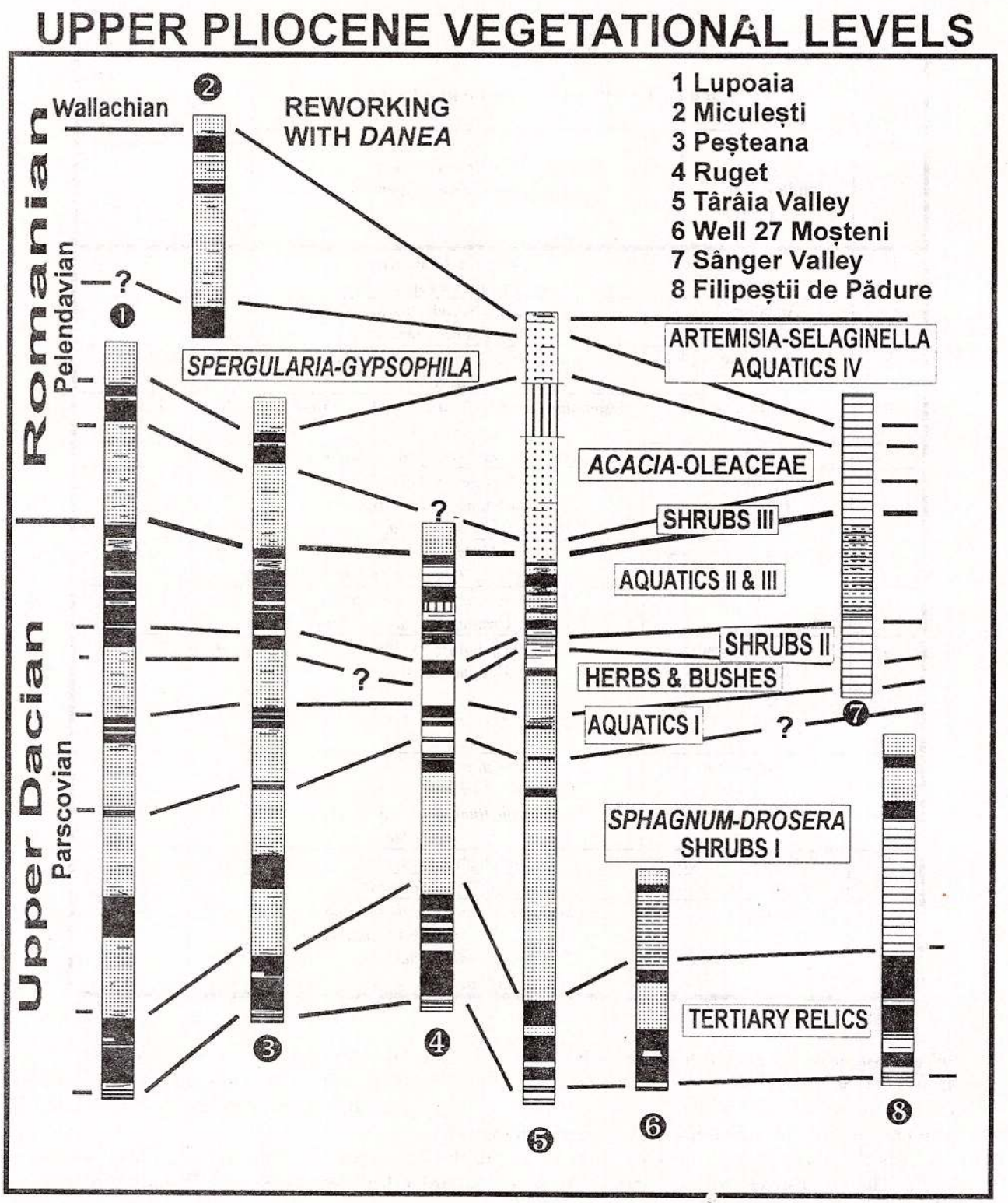

Fig. 2 – Stratigraphic delimitation based upon palynomorph distribution according to Table 1.

The third phase chiefly characterizes a more humid habitat with aquatics sensibly increasing. In addition to very well preserved massulae of Salviniaceae a suit of aquatic morphotypes of both lacustrine and riparian habitat do occur at this level. Pollen derived from other plants is not particularly significant and accumulated during a period of time when the pollen rain dropped from more distant, arboreal taxa, thus from extra-local sources (e. g., Pinaceae, Fagaceae and Juglandaceae).

The material from the immediate overlying intervals suggests a relative decline in the climatic regime, with two assemblages which mix up with one another: they are herbs and bushes and Cupressaceae-Taxodiaceae-Pinaceae group. The palynocontent is dominated by *Picea, Larix* and *Juniperus* to which add *Pinus* and *Abies*. *Juniperus* possibly had a scattered distribution. It generally grows on elevated sites and the fact that pollen of this taxon, not exceeding 9 %, does persist in this interval accounts for our supposition that cooler conditions either have existed at regional scale or have functioned as micro-climate. After all the whole assemblage seems to suggest the existence of such a climatic regime and is consistent with the presence of herbs and bushes continuing their development from the underlying interval. For all that, this community out of which the deciduous taxa are almost missing (Fagaceae 1.8 %, Juglandaceae 0.0 %, *Tilia, Celtis* and *Ulmus* between 0.7 and 1,2 %) does not indicate necessarily a deterioration of climatic conditions. Jacobson (1979), studying the paleoecology of *Pinus strobus* (White Pine) has shown that an increasing in accumulation of pine litter increases soil acidity which reduces, in turn, the bacterial decomposition and ultimately acts like a barrier stratum for other seeds which can no more reach the mineral soil and germinate. It is reasonable to assume that a similar mechanism might also had taken place in relationship with other coniferous types producing heavy litter accumulation which possible has led to such a situation in this area. In the case of this particular level the possibility of transport from outside the sector is not considered, primarily due to the coherence the respective assemblage shows. Erdtman (1969) has stated that *Picea* produces pollen grains with high settling velocity which are not dispersed far from the source.

Further on, following a short and passing shrubbery phase (Shrubs II), during which no noticeable event has been remarked, the depositional area must have suffered a strong subsidence as proved by a sudden advent of submerged lacustrine representatives of the Aquatics II and III, respectively. They characterize much deeper environments and have been accompanied by riparian hydrophylous types. It is pointed out the particular significance some species have for they release their micro-organs directly into the water. It is the case of *Stratiotes, Heleocharis* and *Hydrocharis*, all belonging to the Aquatics II assemblage. Such pollen possesses a very thin exine and their well preserved state demonstrates beyond doubt that the whole organic fraction has not been removed after settling nor has been strongly affected after settling. One can consider the respective occurrence as being highly indicative from both stratigraphical and paleoenvironmental viewpoints for it documents the existence of a unique interval of distribution plus the fact that the deeper lacustrine habitat has covered much larger sectors. With this aquatic inter-phase the sequence of Upper Dacian (Parscovian) comes to an end. What follows above beginning with Shrubs III belongs to the Romanian stage and characterizes its first sub-stage: the Pelendavian.

Most of the taxa here still have the riparian status but some have certainly inhabited the floodplain area. In terms of vegetation change this population of shrubs and sub-arboreal species characterizes an interval of transition toward more arid and warm a climate. Although the percentage value of *Tamarix* and *Myricaria* is rather low (2 % and 4 % respectively), one should not overlook that they are entomophylous species and this suggests a controlled dispersal from local sources.

Farther on the development of *Acacia* - Oleaceae merely confirms the existence of warmer climatic conditions. Desiccation has accentuated the attributes of open land environment which has favoured the continually reducing process of the depositional zone during which the organic particles have suffered a more intense degradation. Through time the aridity has increased and the main taxa likely to inhabit and compete under such conditions have mostly been herbaceous as it is documented by the occurrence of *Spergularia* - *Gypsophila* couple plus some Fabaceae and composits.

This situation went on this way until a new phase of fluvial regime has been initiated. The fluvial activity led to a slight development of frewshwater algae and especially Hydrodyctiaceae (*Pediastrum*).

The presence of micro-organs delivered from wild-growing herbaceous vegetation plus the occurrence of *Artemisia* and its relatives prove the existence of an area mostly deprived of arboreal taxa, while *Selaginella* implies the existence of high peat bogs. In terms of paleoclimatic modification a visible change toward more sensibly deteriorating conditions has taken place.

Conclusions

A prime inference ensuing from this study is the fact that continental palynomorphs of Pliocene age, though inadequate for bringing about proper stratigraphic characterizations, may nevertheless offer a reliable background of research even though restricted to local scale.

In terms of vegetation growing, it may be said that during the Parscovian a range of successive phases has developed, making up, on the whole, a more diversified spectrum out of which some taxa show strong Caspian and even Far East influences. In marked contrast, the following succession appears more limited and includes shrubs and trees only at the beginning of the Romanian, a period of time during which some Mediterranean species have found propitious ambiency to develop. Both are the consequence of a mixed development of paleosubtropical and arcto-Tertiary species. Whereas the Parscovian is characterized by all types of vegetation compatible with a variety of environments and controls, during the Romanian especially wild-growing herbs have characterized the inhabiting vegetation.

References

Demetrescu, E., (1993) Palynostratigraphic levels in the Dacian stage from Romania. *Rev.Roum. Géol.*, 37, p. 95-99.

— (1995) Studiul palino-sedimentologic şi palino-stratigrafic. Potential şi aplicabilitate. Cazul sedimentelor pliocene din avanfosa Carpaţilor Meridionali. Doctorate thesis (in Romanian), Univ. Bucharest, 386 p., unpublished.

Erdtman, G. (1969) Handbook of palynology, Morphology-Taxonomy-ecology. Munksgaard.

Genx. J., (1987) Correlations biochronologiques et associations unitaires. Univ. Lausanne, 249 p.

Jacobson, G. L. (1979) The palaeoecology of White Pine (*P. strobus*) in Minnesota. *Jour. Ecol.*, 67, p. 697-726.

An. Inst. Geol. Rom., 72, part. II, p. 9-27, Bucureşti, 2000

L'ANALYSE DU STRAIN ET SES IMPLICATIONS POUR L'ETABLISSEMENT DES TRACÉS DE LA DÉFORMATION DANS LES MÉTACONGLOMÉRATS PALÉOZOIQUES DES MONTS APUSENI DU NORD

Mihaela DIMITRESCU

Institutul Geologic al României, str. Caransebeş nr. 1, RO-79678 Bucureşti 32

Key words: Metaconglomerates. R_f/ϕ technique. Plane strain. Coaxial deformation.

Abstract: *Strain analysis and its implications for the determination of deformation paths in the Paleozoic metaconglomerates of the Apuseni Mountains.* In the Northern Apuseni Mountains, the presence of stretching lineations of pebbles in metaconglomerates and the angle between the schistosity and the boundaries of the nappes suggest that, during the deformation, a component of the shearing strain was active. The strain rate (R) and its orientations (Θ') in the bi-dimensional planes were determined only on the basis of measures in the metaconglomerates. The data of the three principal perpendicular planes were combined in order to determine the finite strain ellipsoidal in 10 localities. The finite strain was decomposed into two components, the simple shear one (γ), and the pure shear one (λ), which were determined directly on the Θ'/R diagram. The collected data show that the observed deformation cannot be explained exclusively by simple shear, but rather by an association of simple shear with longitudinal strain. The combination of finite deformation with the time necessary for its accomplishment leads to the approximation of the mean strain rate at values comprised between 0.32 and $2.19X10^{-14}$ s^{-1}.

Introduction

Les Monts Apuseni du Nord ont comme caractéristique la structure en nappes de charriage constituées par des formations cristallines précambriennes-cambriennes recouvertes par des dépôts sédimentaires permiens-mésozoïques.

Pour connaître plus en détail les mécanismes des charriages il est nécéssaire de rassembler des données quantitatives concernant les modifications internes éprouvées par les nappes.

Dans la région étudiée, les repères du strain (de la contrainte) peuvent être trouvés dans les roches métasédimentaires (conglomérats, grès, argiles) ou dans les brèches tectoniques. Nous n'avons pris en considération que les conglomérats métamorphisés des nappes de Gârda, Poiana, Biharia et Highiş. Ils ont été étudiés en 10 points d'observation situés dans les zones d'affleurement aussi bien de la Formation des Conglomérats Laminés de la Nappe de Gârda que de ses équivalents dans les autres nappes, notamment la Série de Poiana pour la Nappe de Poiana et la Série de Păiuşeni pour les Nappes de Biharia et de Highiş (Olaru, Dimitrescu, 1994).

Les roches soumises à l'observation sont d'âge Carbonifère supérieur-Permien inférieur et ont soufert une déformation faible a moyenne, visible grâce au contraste de viscosité qui a généré le comportement à la contrainte nettement différent des galets par rapport à la matrice.

Le but du présent travail consiste en la détérmination des effets du charriage de l'accumulation de nappes pendant le Turonien, à l'aide de l'analyse du strain des galets dans les conditions de la modification de leur forme mais non pas de leur volume et en l'absence de la dissolution sous pression.

Nous avons aussi cherché a détérminer le taux du strain, quelques éléments de cinématique des zones de charriage, la variation du strain dans les nappes étudiées ainsi que les tracés parcourus au temps de la déformation par les repères choisis.

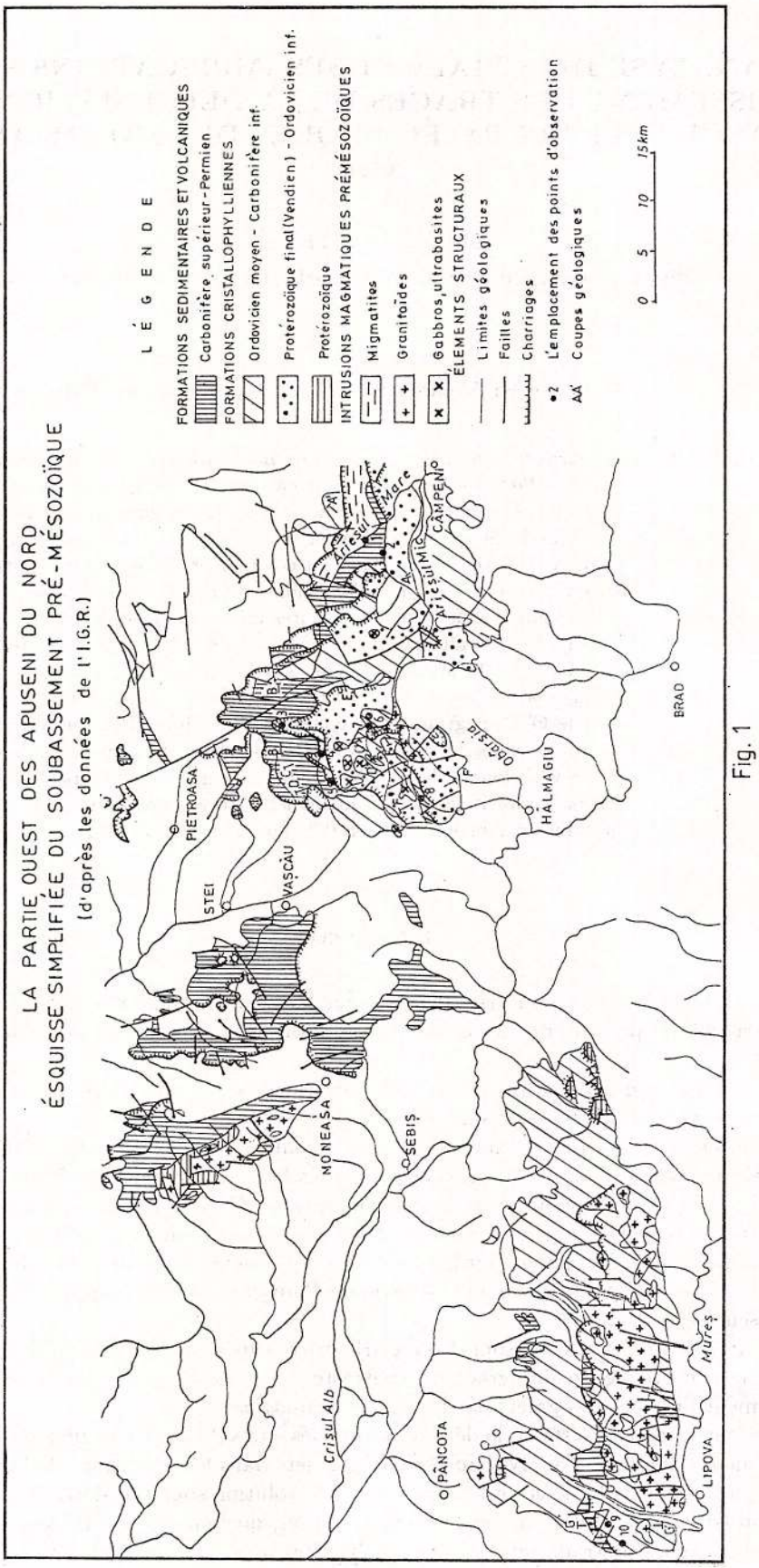

Fig. 1

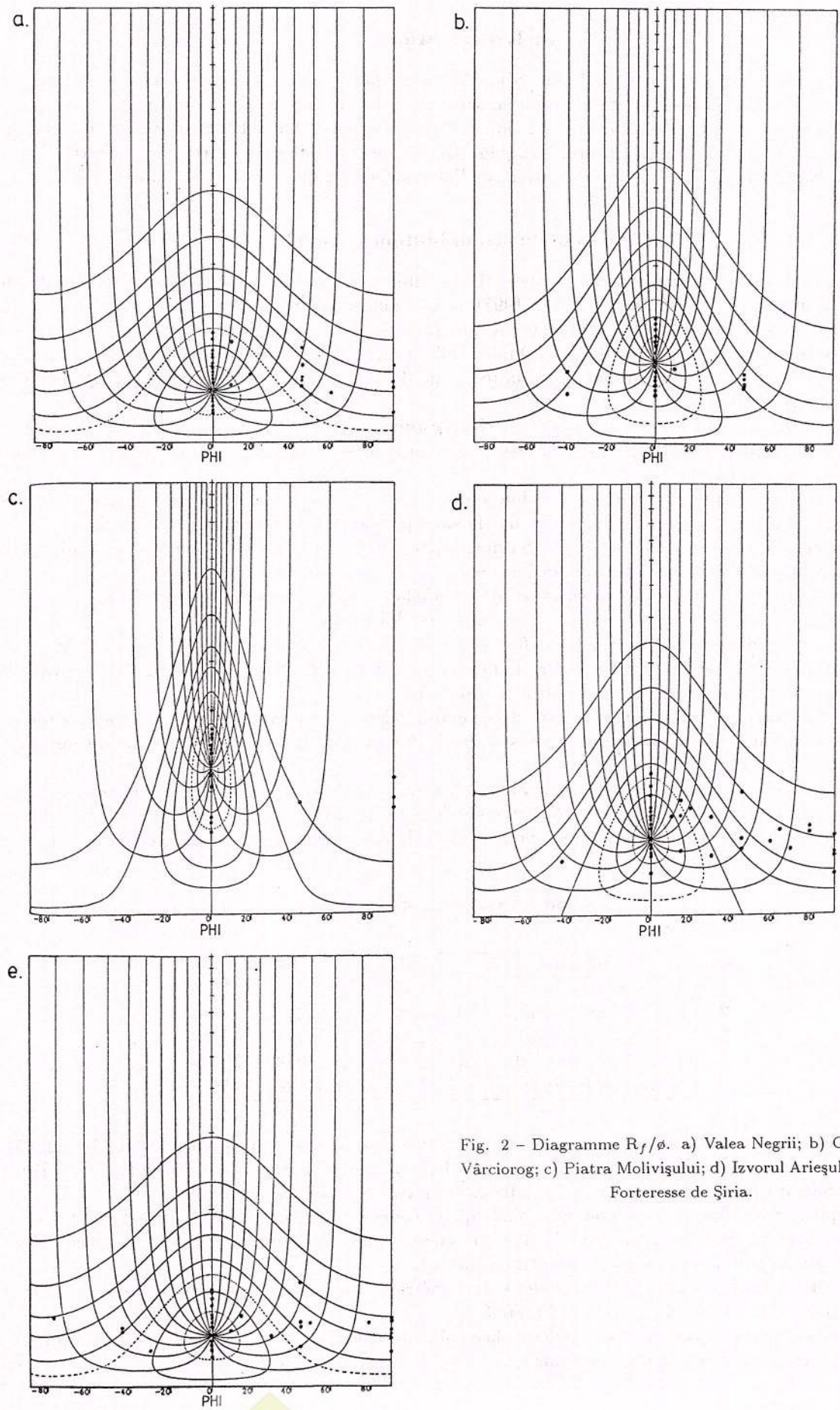

Fig. 2 – Diagramme R_f/ϕ. a) Valea Negrii; b) Cascade du Vârciorog; c) Piatra Molivişului; d) Izvorul Arieşului Mic; e) Forteresse de Şiria.

Analyse du strain

Les mesures des rapports axiaux et de l'orientation des galets dans les métaconglomérats ont été éffectuées en 10 points d'observation ayant la distribution suivante dans les différentes unités tectoniques: Briceşti, Valea Negrii (Nappe de Gârda); Cascade du Vârciorog, Pârâul Corbului, Valea Plaiului (Nappe de Poiana); Piatra Molivişului, Valea Bucegiţa, Izvorul Arieşului Mic (Nappe de Biharia); Forteresse de Şiria, Valea Sălăndaşului (Nappe de Highiş). Leur localisation sur l'esquisse géologique est montrée dans la Figure 1.

1. Analyse du strain bi-dimensionnel

La technique de travail adoptée pour l'analyse 2D (bi-dimensionnelle) de la contrainte a été décrite en détail dans d'autres travaux (Dimitrescu, 1995, 1997), nous n'allons plus insister sur elle.

Nous considérons toutefois nécessaire de faire quelques remarques sur la méthode R_f/ϕ.

Dénommée initialement méthode Ramsay-Dunnet, elle a été modifiée par les améliorations proposées par Lisle (1977), en arrivant aujourd'hui à être la technique la plus utilisée, avec plus de cent applications décrites dans la littérature.

Des études comparatives entre les diverses méthodes d'estimation du strain tectonique (Hanna, Fry, 1979; Siddans, 1980; Paterson, 1983; Lisle, 1985) il résulte que en dehors de sa large applicabilité, la technique R_f/Φ est aussi une des plus précises.

Le principe de la méthode consiste en l'évaluation des distributions initiales des galets par le retour à l'état antérieur au strain mesuré, en procédant par la superposition d'une contrainte coaxiale à l'axe long à 90^0 de l'orientation préférentielle des galets. Sa magnitude est réduite successivement, en calculant après chaque pas combien aléatoires sont les orientations des galets de moins en moins déformés.

Si initialement il n'a existé aucune orientation préférentielle, on peut calculer la valeur du strain fini (R_s) nécéssaire à la réalisation de la distribution la plus uniforme des galets.

Les données recueillies dans le terrain ont été opérées à l'aide du programme THETA pour ordinateur, élaboré par Ratschbacher et al. (1994) d'après le modèle plus ancien de Peach et Lisle (1979), les valeurs des paramètres déterminés étant présentées dans le Tableau 1.

Nous devons préciser que la mesure de la fluctuation des galets n'a pas été possible dans tous les points d'observation (ϕ ayant parfois des valeurs voisines de zéro), et en conséquence le calcul n'a été fait que pour cinq affleurements.

En comparant les diagrammes R_f/ϕ de la Figure 2, nous avons constaté que ceux correspondant aux points Valea Negrii, Izvorul Arieşului Mic et Forteresse de Şiria présentent une légère symétrie. Cet aspect pourrait être dû à l'existence d'une orientation préférentielle des axes longs des galets générée par la symetrie des distributions pré-tectoniques.

Tableau 1. Données du strain 2D

Nr.	Localisation	N.	Rf	Ri	Rs	V
1	Valea Negrii	46	1,79	1,34	1,64	1,50
2	Cascade du Vârciog	31	1,87	1,53	2,07	0,80
3	Piatra Molivişului	21	2,52	1,74	2,97	1,00
4	Izvorul Arieşului Mic	46	1,97	1,80	2,02	2,00
5	Forteresse de Şiria	60	1,72	1,46	1,62	0,50

Pour approfondir ce problème nous avons utilisé une autre série de diagrammes concus par Lisle (1985), qui montrent les tracés suivis par les galets au temps de leur transformation de l'état initial (R_i, Θ) à l'état final (R_f, ϕ) quand entre les galets et la matrice il existe un contraste de viscosité.

Afin d'expliciter les diagrammes, nous précisions qu'au cours de la déformation, les galets sont soumis à une rotation vers la direction principale d'extension, chaque galet se mouvant le long d'un tracé propre (ligne à Θ constant) vers la gauche (vers de petits angles ϕ).

En général les formes des distributions finales sont symétriques, ainsi qu'on peut le constater en suivant les contours tracés sur les diagrammes de la Figure 3.

Théoriquement, dans les conditions spéciales de la combinaison des variables strain et distribution initiale, la symétrie des projections R_f/ϕ peut provenir de:

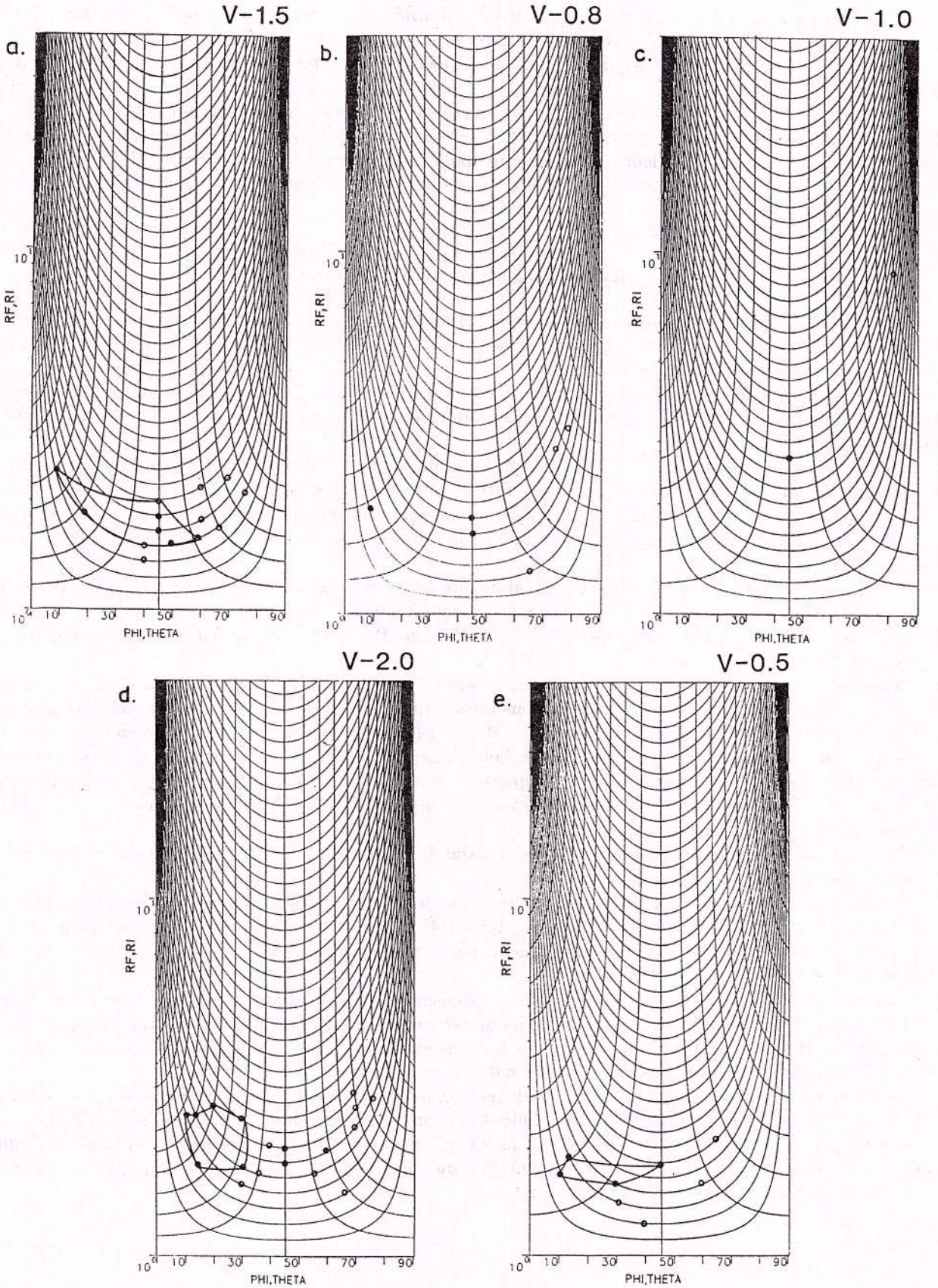

Fig. 3 – Tracés de la déformation par cisaillement pur pour divers contrastes de viscosité. a) Valea Negrii; b) Cascade du Vârciorog; c) Piatra Molivişului; d) Izvorul Arieşului Mic; e) Forteresse de Şiria.

1. distributions initiales symétriques, qui ont été déformées par une contrainte superposée symétrique, comme dans le cas des points Valea Negrii et Forteresse de Şiria;

2. distributions initialement asymétriques, sur lesquelles s'est superposé un strain oblique, situation possible à Izvorul Arieşului Mic.

Malgré nos efforts de déchiffrer les causes théoriques de la symétrie des diagrammes R_f/ϕ, il faut reconnaître que nous ne détenons pas encore toutes les observations de terrain nécéssaires à une étude sur la rotation des galets rigides dans leur matrice ductile, pour pouvoir établir avec précision si l'orientation des galets peut être attribuée aux procés primaires de déposition, au strain ou à un mécanisme de rotation des clastes dans la roche non lithifiée.

2. Analyse du strain tri-dimensionnel

La meilleure géométrie pour la détermination de l'ellipsoïde du strain à partir de trois sections se présente lorsque celle-ci coincident avec les trois plans principaux de l'ellipsoïde. On peut alors affirmer que les axes principaux sont mesurés directement.

En tenant compte de ces éxigences, pour obtenir les valeurs et les directions du strain fini en trois dimensions (3D), nous avons combiné les données de trois sections planes perpendiculaires ou quasi-perpendiculaires entre elles.

L'ellipsoïde du strain a été calculé à l'aide du programme pour ordinateur conçu par Milton (1980) et repris plus récemment sous la dénomination de TRISEC par Ratschbacher et al. (1994).

Les données primaires demandées par le programme sont: l'orientation des trois plans, la fluctuation moyenne des ellipses mesurées sur chaque section et le rapport axial final moyen calculé séparément pour chaque plan.

L'annexe 1 comprend les résultats de l'analyse effectuée pour la détermination de la longueur et de l'orientation des axes principaux de l'ellipsoïde de déformation dans les points d'observation: Briceşti, Valea Negrii, Cascade du Vârciorog, Pârâul Corbului, Valea Plaiului, Piatra Molivişului, Valea Bucegiţa, Forteresse de Şiria et Valea Sălăndaşului.

A la base de la méthode proposée par Milton réside l'observation suivante: dans le cas d'une contrainte homogène, les ellipses mesurées sur trois sections quelconques doivent idéalement être compatibles si celle-ci appartiennent au même ellipsoïde de strain. Mais quelques inconsistances, comme seraient les erreurs d'observation, l'inhomogénéité de la contrainte dans l'affleurement ainsi que la variation de la position des sections planes en rapport avec les axes principaux du strain, font obligatoire la correction des ellipses du strain à l'aide d'un facteur d'ajustement pour les rendre compatibles (c'est à dire pour pouvoir les considerer comme appartenant au même ellipsoïde).

Le facteur d'ajustement correspond au rapport axial de l'ellipse du strain d'ajustement qui se superpose au strain mesuré (Milton, 1980).

En revenant à l'analyse effectuée, nous constatons que les valeurs les plus élevées du facteur d'ajustement ont été calculées pour les points Piatra Molivişului (4,14) et Pârâul Corbului (1,72). On est même arrivé à la situation que à Valea Negrii les trois surfaces mesurées n'appartiennent pas à un ellipsoïde mais à un hyperboloïde (Annexe 1).

En échange, les valeurs réduites du facteur d'ajustement pour tous les autres points d'observation montrent le fait que, d'une part, les ellipses mesurées appartiennent au même ellipsoïde, le strain d'ajustement nécésaire à la réalisation de la compatibilité des sections étant de magnitude réduite, et que d'aute part, le plan XY coïncide avec ou est très approché de la direction X du strain.

Les directions principales du strain et les valeurs X/Z de l'ellipsoïde de la déformation sont projetées sur les coupes géologiques de la Figure 4 qui présentent la géométrie à moyenne échelle de la région étudiée.

L'explication que nous acceptons à présent dans le cas des points Piatra Molivişului et Pârâul Corbului où la direction de la contrainte diffère de l'orientation du plan XY, est que dans les affleurements respectifs la déformation a eu un caractère non homogène.

En conclusion, l'orientation des ellipses du strain de la plus grande partie des coupes géologiques présentées dans la Figure 4, reflète le strain fini produit par la même phase de déformation, commune à tous les points d'observation.

Résultats du strain fini

Tout strain fini résulte de l'accumulation de ses accroissements dûs aux phases de déformation qui se sont succédées.

Ramsay (1967) a montré que pour effectuer l'analyse de la déformation il est nécessaire de la décomposer en deux composants liés au strain non-rotationnel (produit par cisaillement pur) et au strain rotationnel (produit par cisaillement simple).

En ce qui suit nous allons essayer d'établir les relations entre la variation du strain de cisaillement et les mouvements des nappes de charriage.

Toutes les données du strain fini ont été projetées sur un diagramme logarithmique de la déformation (Fig. 5) pour suivre la variation de la forme de l'ellipsoïde du strain.

Les ellipsoïdes de type aplatissement et allongement sont séparés de ceux du strain plan par la ligne E_1-E_2=E_2-E_3+ln (1+Δ), ou Δ est la modification du volume et $E_{1,2,3}$ représentent les contraintes principales finies logarythmiques (Ramsay, Wood, 1973). Les valeurs du paramètre k=(E_1-E_2)/(E_2-E_3) se trouvent dans le Tableau 2.

Tableau 2. Paramètres de la forme des galets

Nr.	Localisation	E_1	E_2	E_3	K
1	Briceşti	0,67	- 0,16	- 0,55	2,07
2	Valea Negrii	0,80	0,23	- 0,92	- 0,50
3	Cascada Vârciogului	0,64	- 0,04	- 0,59	1,25
4	Pârâul Corbului	0,22	0,05	- 0,46	0,33
5	Valea Plaiului	0,95	0,04	- 0,83	1,04
6	Piatra Molivişului	0,86	- 0,20	- 0,70	2,08
7	Izv. Arieşului Mic	0,70	- 0,07	- 0,63	1,37
8	Valea Bucegiţa	1,12	0,01	- 1,01	1,10
9	Cetatea Şiria	0,47	- 0,14	- 0,35	2,86
10	Valeă Sălăndaşului	0,51	- 0,16	- 0,48	2,06

La plupart des projections se situe dans le champ de l'allongement, mais seulement les points Briceşti, Piatra Molivişului et Forteresse de Şiria s'éloignent de la ligne du strain plan. Dans l'autre champ sont emplacés les points Valea Negrii et Pârâul Corbului. Leur position par rapport à la ligne du strain plan peut être expliquée comme résultat des deux suivants processus différents: 1. allongement physique en direction d'Y; 2. superposition d'une contrainte homogène sur une contrainte plane (Ramsay, 1980).

Si l'éloignement de la ligne k=1 (et Δ=0) est dû entièrement a l'extension suivant Y, des modifications considérables de l'axe Y, entre 50 % et 250 %, sont à attendre. Comme tels allongements n'ont pas été mis en évidence ni dans le terrain, ni par calcul (Dimitrescu, 1997), l'examen de l'autre hypothèse s'impose.

La déviation à partir du strain plan peut résulter d'un cisaillement simple ou d'une combination entre un cisaillement simple et un strain longitudinal (Ramsay, 1980). Pour le cisaillement simple on peut établir une relation entre l'orientation de l'axe principal de l'ellipse du strain (Θ') par rapport avec la marge de la zone de cisaillement et le rapport du strain (R_s), relation décrite par une courbe du type reproduit en Figure 6.

L'appréciation des angles entre les grands axes des ellipses du strain et les fronts des nappes n'a été possible que dans 6 points d'observation, ainsi qu'il résulte du Tableau 3.

Nos données projetées sur le diagramme de la Figure 3 ne se posent pas sur la courbe, et on peut donc tirer la conclusion que le strain fini observé n'est pas dû exclusivement au cisaillement simple, ni à l'allongement parallèle à l'axe principal X, mais à la combinaison des deux déformations.

Tableau 3. Paramètres du strain de cissaillement

Nr.	Localisation	Θ'(o)	Rs	λ	γ
1	Briceşti	5	2,09	2,00	0,25
2	Valea Negrii	20	2,15	1,50	0,75
3	Cascada Vârciogului	5	1,88	1,85	0,25
4	Pârâul Corbului	10	2,08	1,85	0,50
5	Valea Plaiului	17	1,28	1,25	0,25
6	Piatra Molivişului	5	2,13	2,10	0,25

Mathews et al. (1971) ont montré que la contrainte finie peut être décomposée en un strain de cisaillement (γ) en direction du cisaillement et un strain longitudinal (λ) en direction de l'axe principal X.

A l'aide du diagramme conçu par Coward et Kim (1981), reproduit en Figure 7, on peut déterminer les paramètres γ et λ en fonction de R_s et Θ', sans prendre en calcul la diminution de volume (Δ).

Toutes les valeurs du strain longitudinal determinées graphiquement (Tab. 3) sont supraunitaires, ce qui conformément aux observations de Coward (1976) et Kligfield et al. (1981) reflèterait un amincissement des zones de cisaillement.

En faveur de cette idée plaiderait aussi la distribution des points sur le diagramme Flinn (la plupart dans le champ de l'extension), qui d'après l'opinion de Ramsay et Allison (1979) indiquerait la présence d'une partie terminale des zones de cisaillement.

Du groupement evident des points d'observation dans le champ du cisaillement pur (Fig. 7), on peut déduire le fait que, bien que des nappes de charriage différentes ont été étudiées, la déformation produite sur leur entière aire de développement a eu un caractère homogène, exprimé par l'allongement de l'axe principal X de l'ellipsoïde du strain dans la direction d'avancement des nappes.

Une autre hypothèse ayant trait aux valeurs très basses du strain de cisaillement (Tab. 3) serait aussi possible, valeurs qui suggèrent le rôle réduit du cisaillement simple par rapport au cisaillement pur.

Sans tenter une séparation nette entre les domaines de manifestation des cisaillements simple et pur, mains, au contraire, en les traitant toujours ensemble, nous avons illustré dans la Figure 8 les nombreuses sequences intermédiaires. Bien que nos points se projettent dans le domaine du strain longitudinal, l'aspect de continuité ne peut pas être ignoré dans le champ delimité par les courbes à accroissement de la rotation (ω) à partir de 0,00 (cisaillement pur) jusqu'à 5,45 (cisaillement simple).

L'obtention du nombre le plus élevé possible de données concernant l'histoire du strain rend inévitable une réponse à la question si le strain sectionnel a un caractère coaxial ou non-coaxial.

Lisle (1986) a démontré mathémathiquement le mode de détermination du caractère du strain sectionnel dans le cas ou les plans mesurés sont choisis rigoureusement parallèles aux plans principaux de l'ellipsoïde de déformation.

Tableau 4. Données de la déformation combinée coaxiale et non-coaxiale

Nr.	Localisation	E_1	E_2	E_3	K
1	Briceşti	2,60	0,57	2,58	2,40
2	Valea Negrii	2,17	0,65	3,42	1,80
3	Cascada Vârciogului	4,71	0,29	2,43	2,53
4	Pârâul Corbului	2,19	0,36	1,27	4,43
5	Valea Plaiului	7,93	0,18	3,52	1,30
6	Piatra Molivişului	2,75	0,59	3,93	1,60
7	Izv. Arieşului Mic	3,81	0,38	2,77	2,23
8	Valea Bucegiţa	14,38	0,12	7,92	1,00
9	Cetatea Şiria	2,13	0,65	1,80	3,33
10	Valea Sălăndaşului	2,17	0,60	1,93	2,43

Etant donné que cette condition est remplie (Dimitrescu, 1997), nous avons projeté les 10 points d'observation sur le diagramme realisé par Lisle (1986), dans lequel les axes de coordonnées sont notées de la manière sui-

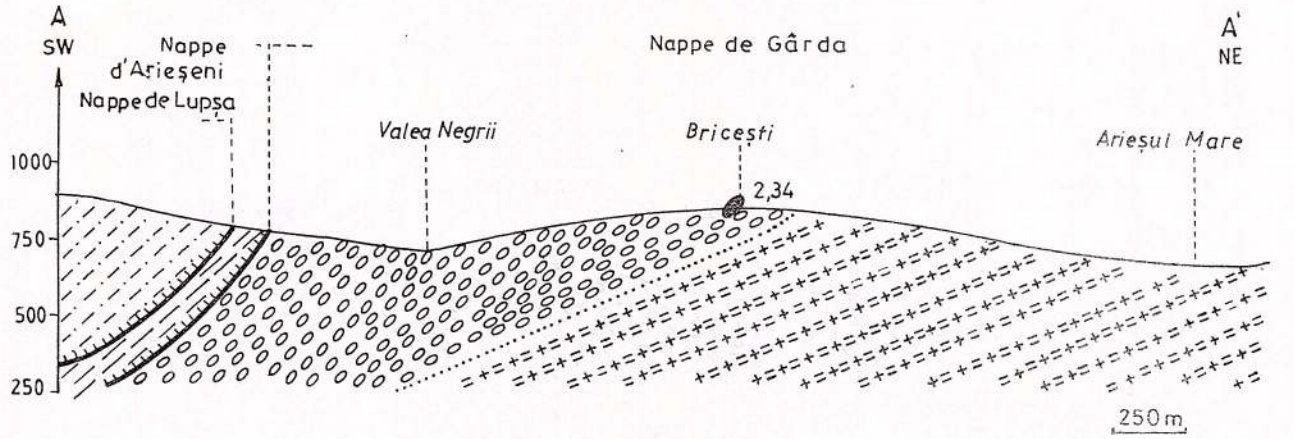

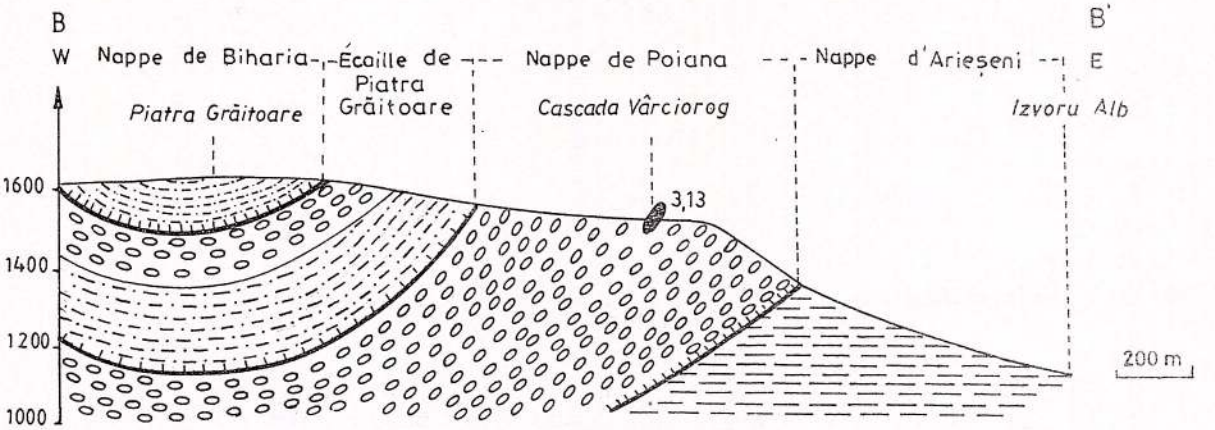

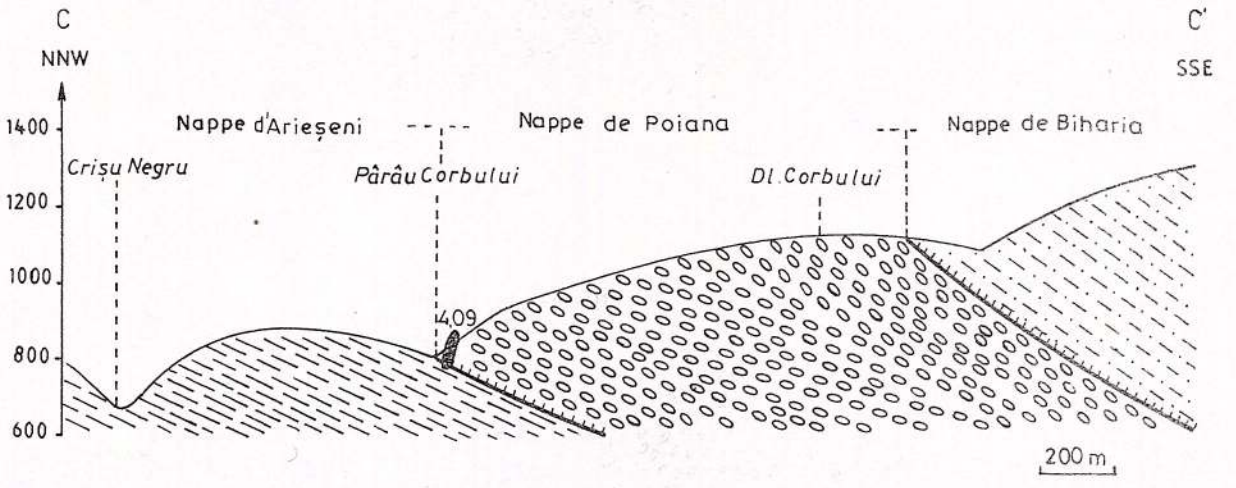

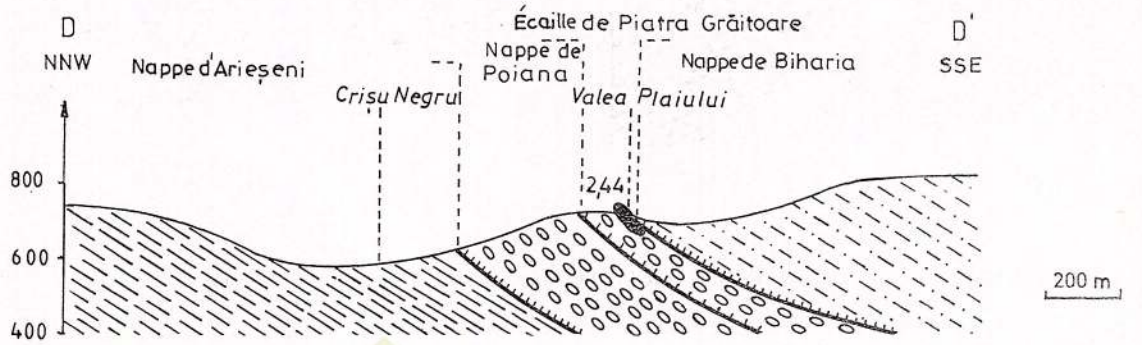

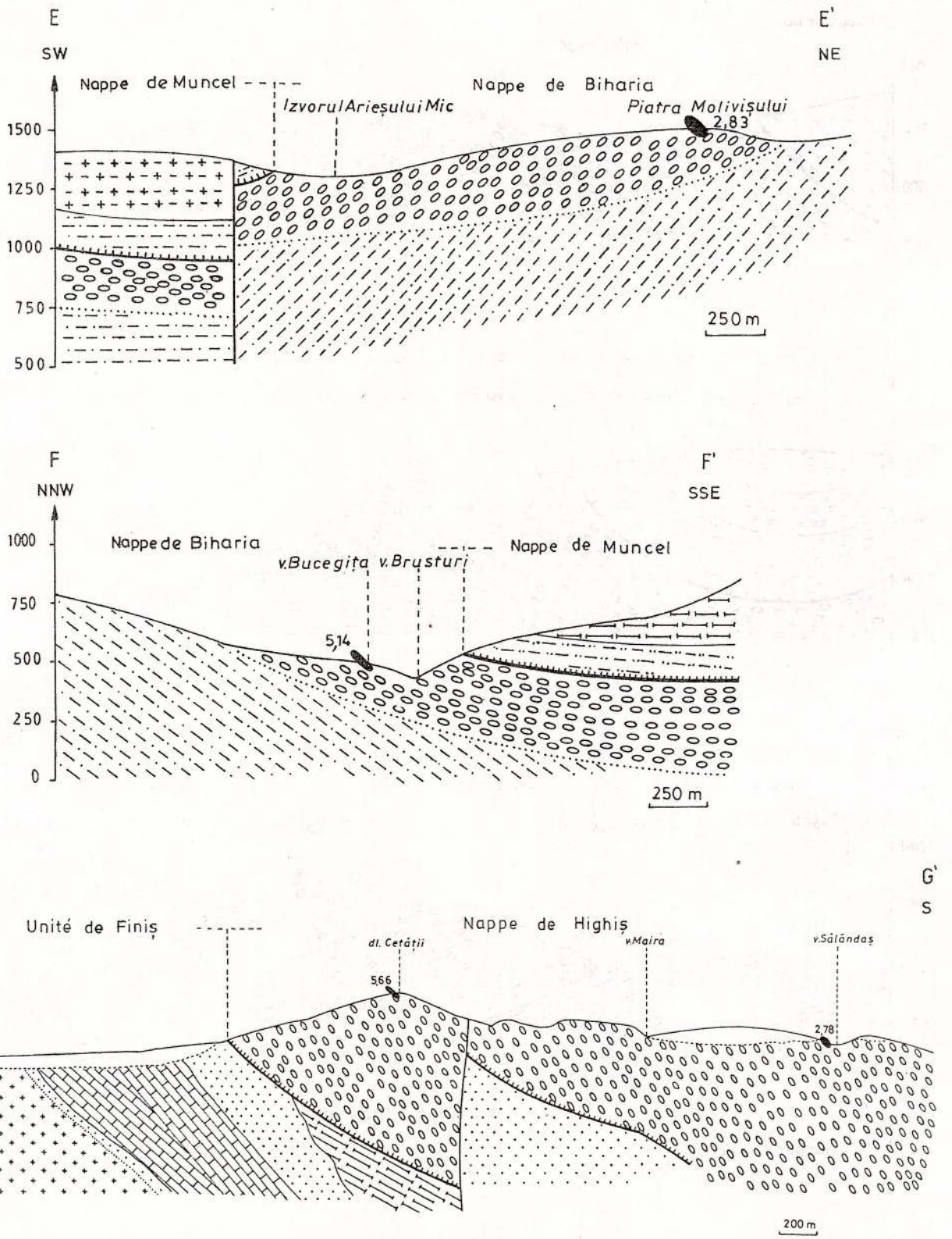

Fig. 4 – Coupes géologiques dans la région étudiée avec l'indication des rapports X/Z des ellipsoïdes de strain.

L É G E N D E - Fig. 4

Dépôts quaternaires

Système des nappes de Biharia

Nappe de Muncel-Lupșa

Porphiroïdes

Schists sériciteux

Métagranites gneissiques

Schists chloriteux à porphyroblastes d'albite

Nappe de Biharia

Métaconglomérats

Schists chloriteux à porphyroblastes d'albite

Écaille de Piatra Grăitoare

Métaconglomérats

Schists chloriteux à porphyroblastes d'albite

Nappe de Highiș-Poiana

Métaconglomérats et schists quartzo-sériciteux

Système des nappes de Codru

Nappe d'Arieșeni

Phyllites sériciteuses, grès

Nappe de Finiș-Gârda

Dolomies

Quartzites

Porphyres

Conglomérats laminés

Granites

Migmatites de Codru

Signes conventionnels

Limite géologique

Limite de discordance

Limite du Quaternaire

Nappe de charriage

Écaille

Faille

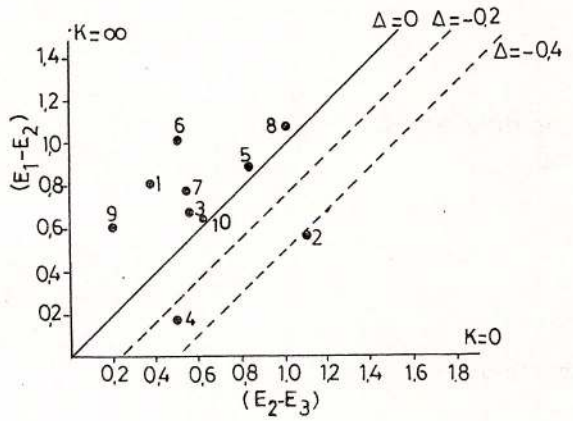

Fig. 5 – Diagramme Flinn des valeurs du strain des métaconglomérats des Monts Apuseni du Nord.

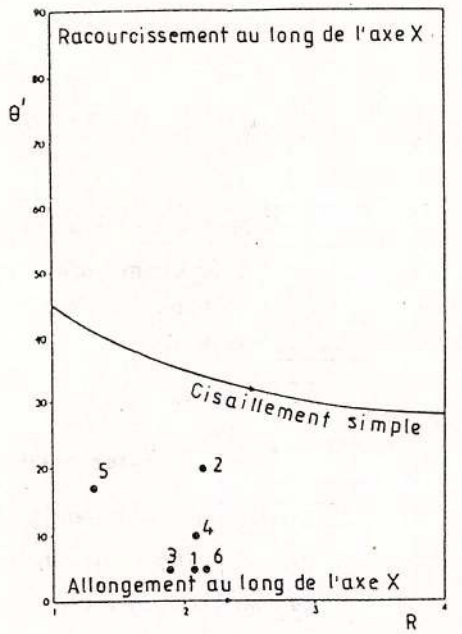

Fig. 6 – Projection du rapport du strain (R) versus l'angle (Θ') fait par le plan principal XY avec la surface frontale de la nappe (d'après Coward et Kim, 1981).

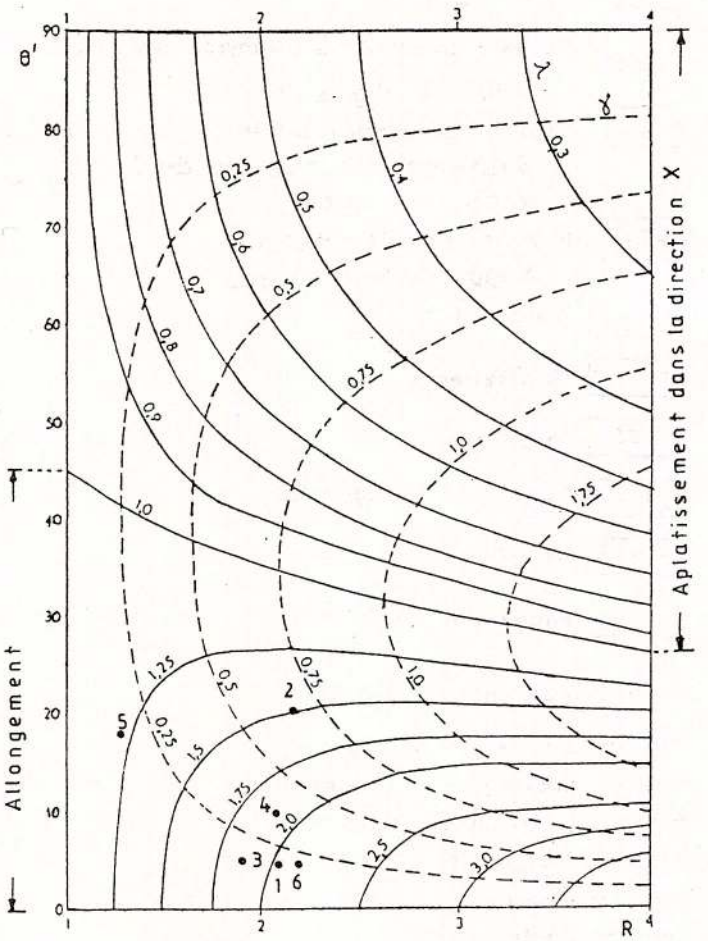

Fig. 7 – Valeurs du cisaillement simple (lignes interrompues) et du cisaillement pur (lignes continues) projetées sur la carte de la déformation pour divers rapports (R) et orientations (Θ') du strain (d'après Coward et Kim, 1981).

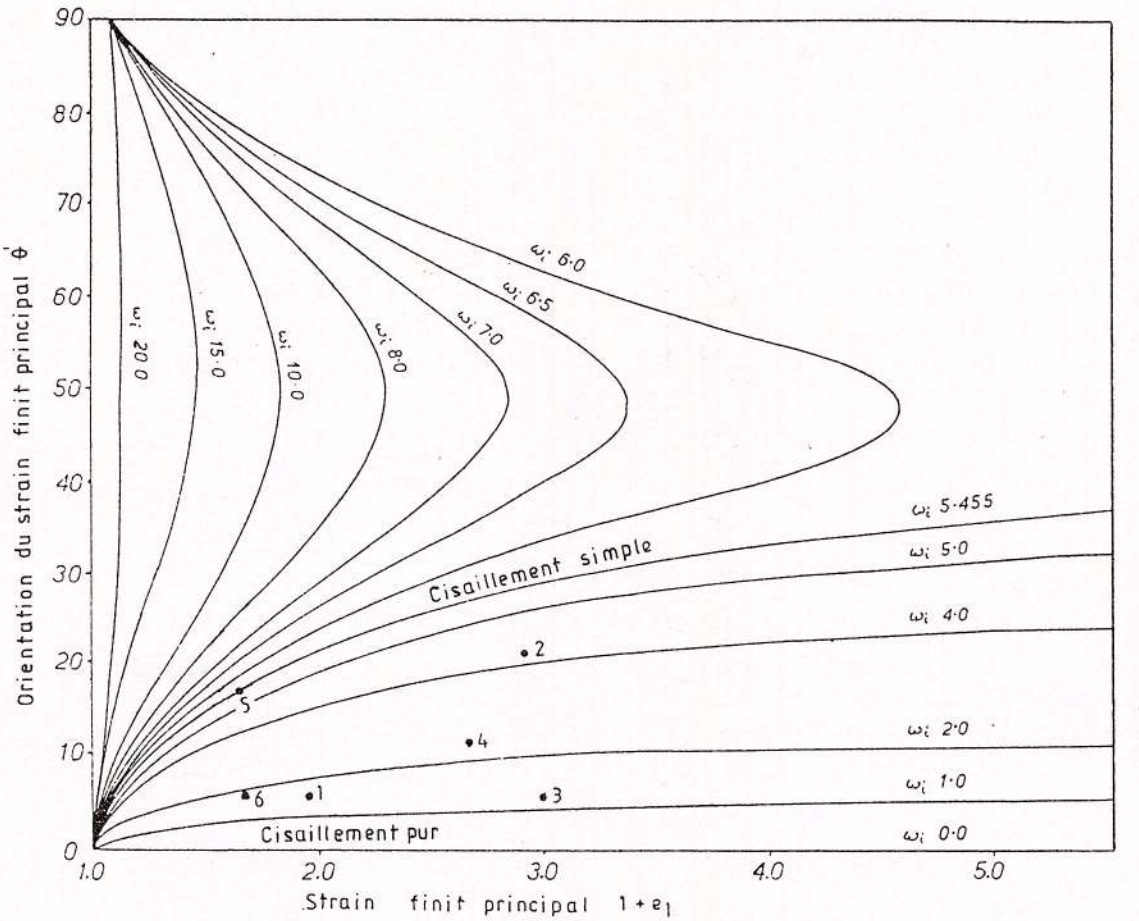

Fig. 8 – Courbes théoriques du strain fini en fonction de la rotation (d'après Pfiffner et Ramsay, 1982).

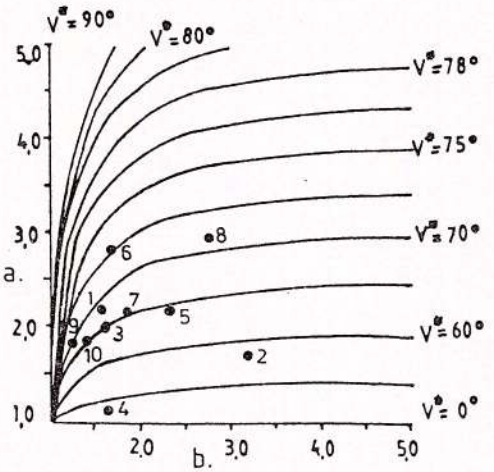

Fig. 9 – Tracés du strain en fonction des courbes V* (d'après Lisle, 1986).

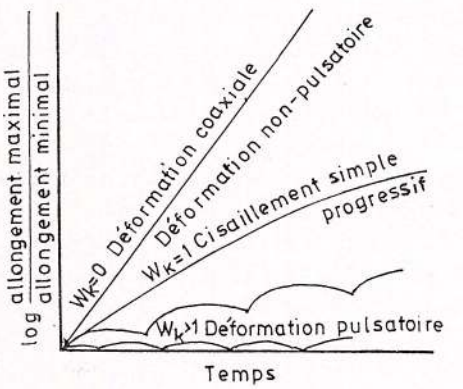

Fig. 10 – Diagramme des histoires possibles de la déformation (d'après Means et al., 1980).

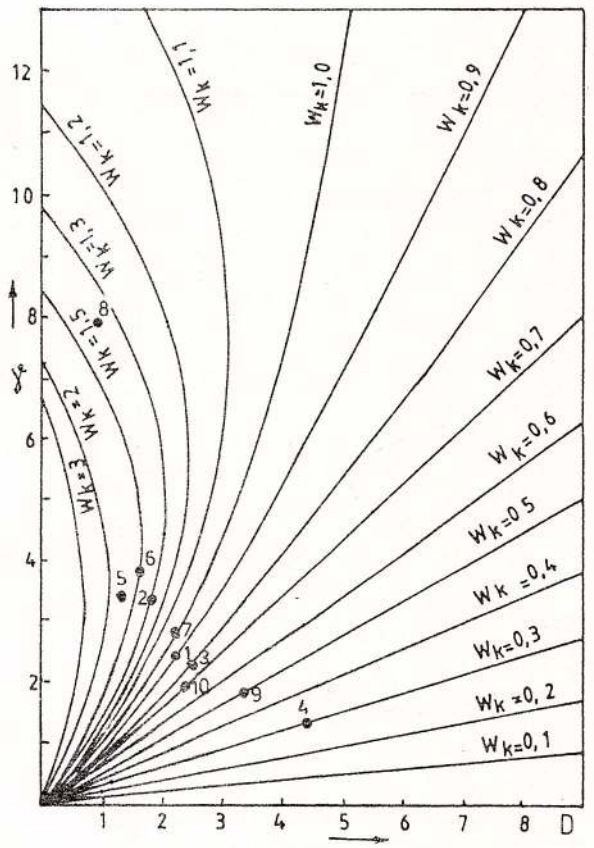

Fig. 11 – Variation du strain de cisaillement avec le strain naturel le long de l'axe X (d'après Ghosh, 1987).

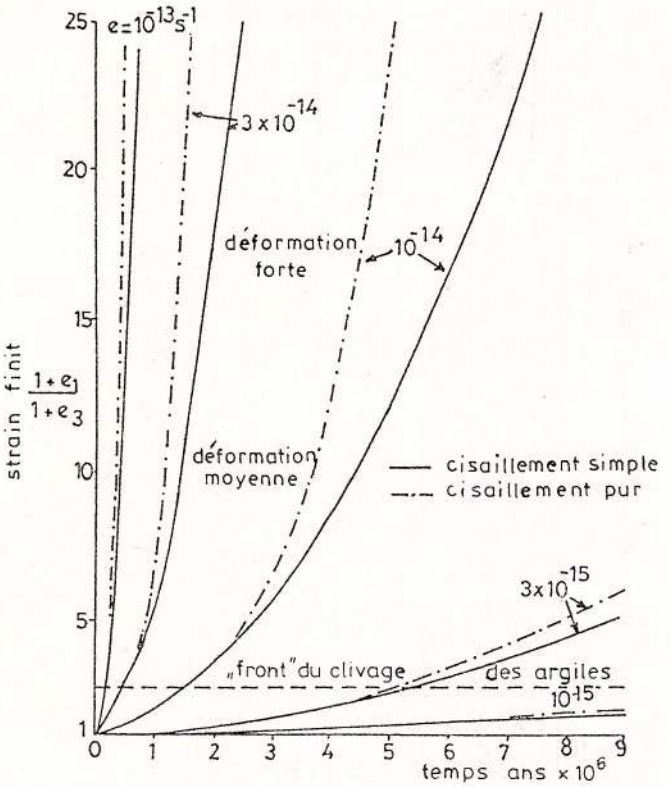

Fig. 12 – Les taux du strain de cisaillement (simple et pur) correspondant à certains intervalles de temps (d'après Pfiffner et Ramsay, 1982).

vante: abscisse $b=(l_2/l_3)^{1/2}$ et ordonnée $a=(l_1/l_2)^{1/2}$, où $l_{1,2,3}$ sont les allongements des axes principaux des galets (Tab. 4).

Les points situés sur les courbes-standard du paramètre V* (l'équivalent de l'angle V de l'ellipsoïde de déformation pour l'ellipsoïde réciproque de la déformation), respectivement Cascade du Vârciorog, Valea Plaiului, Piatra Molivişului, Izvorul Arieşul Mic, Forteresse de Şiria et Valea Sălăndaşului reflètent le caractère coaxial du strain sectionnel, tandis que les autres, notamment Briceşti, Valea Negrii, Pârâul Corbului et Valea Bucegiţa, reflètent le caractère non-coaxial de la déformation (Fig. 9).

En partant de l'ouvrage de référence de Ramberg (1975), Means et al. (1980) ont détaillé la classification des déformations progressives (imaginées comme superpositions simultanées de cisaillements purs sur des cisaillements simples) et ont établi pour chaque type d'histoire du strain un tracé caractéristique des particules en fonction du nombre de la vorticité cinématique (W_k) (Fig. 10).

En accord avec la théorie élaborée par les auteurs cités, Ghosh (1987) a réalisé un diagramme à courbes-standard qui peut être utilisé de manière orientative à la détermination du nombre de la vorticité cinématique et implicitement du type de déformation. Ce diagramme n'est valable que pour les données qui, après calcul, ont indiqué la manifestation d'une contrainte plane en conditions isochores.

Les projections des points d'observation sur le diagramme de la Figure 11 ont été faites à la suite du calcul des paramètres nécessaires à la représentation graphique (Tab. 4), conformément aux équations indiquées par l'auteur:

$D=2e_1$ et $e_1=\sinh^{-1}(\gamma/2)$ où D est le strain naturel le long de l'axe X et γ est la quantité de cisaillement simple.

Par leurs valeurs-standard, les courbes sur lesquelles se projètent les points peuvent indiquer si la déformation dévie de manière significative du tracé du cisaillement simple defini par la relation $W_k=1$. De ce point de vue, les valeurs calculées couvrent presque entièrement le champ des déformations pulsatoires pour lesquelles $1>W_k>0$ et qui correspondent aux déformations les plus fréquentes de la géologie structurale.

Ramberg (1975) a montré qu'à la base des nappes, à cause de la friction avec le soubassement, apparaissent des cisaillements simples parallèles à la surface de charriage, la déformation à la partie inférieure des nappes étant donc plus correctement décrite comme une combinaison entre le cisaillement pur avec un cisaillement simple.

En accord avec ce qui a été écrit plus haut concernant les tracés de la déformation, en base des résultats que nous détenons jusqu'à présent, nous considérons que les galets de métaconglomérats analysés constituent les repères d'un strain plan provoqué aussi bien par le poids propre des nappes que par leur propre mouvement.

En ce qui concerne la relation entre le strain fini et le temps (le taux du strain) au cours du processus tectonique étudié, nous considérons comme d'interêt les observations suivantes.

Pour l'estimation du taux moyen du strain nous avons recouru à la combinaison des données du Tableau 2 avec le temps de 3 Ma (durée du Turonien) nécessaire à la génération des déformations étudiées. En appliquant les formules de calcul indiquées par Pfiffner et Ramsay (1982) nous avons établi que le strain d'extension (e_1) varie entre 2,07 et 0,24, tandis que le strain de raccourcissement (e_3) varie entre 0,64 et -0,30. Conformément à ces valeurs, le taux du strain (é) pour extension est compris entre $2{,}19X10^{-14}s^{-1}$ et $0{,}25X10^{-14}s^{-1}$ et celui pour raccourcissement oscille entre $0{,}32X10^{-14}s^{-1}$ et $0{,}67X10^{-14}s^{-1}$. Selon Pfiffner et Ramsay (1982) il est à attendre que des taux plus rapides que $10^{-13}s^{-1}$ produisent des contraintes de grande intensité tandis que des taux sous $10^{-15}s^{-1}$ vont conduire à des déformations très réduites (roches aparemment non déformées).

A l'aide du diagramme de la Figure 12, en connaissant le taux du strain, on peut déduire graphiquement l'intensité de la déformation à un moment donné de l'histoire géologique. En ce qui concerne nos données, elles se situent entre les courbes du taux du strain de $10^{-14}s^{-1}$ et $10^{-15}s^{-1}$ et correspondent à des déformations d'intensité réduite ou modérée. Cette observation vient à confirmer nos resultats antérieurs obtenus toutefois par d'autres méthodes (Dimitrescu, 1995).

Conclusions

1. L'analyse du strain bi-dimensionnel effectuée par la méthode R_f/ϕ a mis en évidence la symetrie des distributions initiales des galets.

2. L'analyse tri-dimensionnelle du strain a montré que celui-ci est le produit d'une seule phase de déformation, commune a toutes les nappes de charriage étudiées.

3. Le strain plan conservé par les galets des métaconglomérats s'éloigne en certains points d'observation de la ligne k=1, en se situant dans le champ de l'extension, ce que nous pouvons interpréter comme dû à la superposition simultanée d'un cisaillement pur dominant sur un cisaillement simple de petite intensité.

4. Le calcul du taux du strain a permis la détermination de l'intensité de la déformation provoquée par le charriage des nappes des Monts Apuseni du Nord au temps du Turonien.

Bibliographie

Coward, M. P. (1976) Strain within ductile shear zones. *Tectonophysics*, 34, p. 184-197, Amsterdam.

— , Kim, J. H. (1981) Strain within thrust sheets. In: Thrust and nappe tectonics. *Spec. Publ. geol. Soc. London*, 9, p. 275-292, London.

Dimitrescu, M. (1995) Variaţia formei galeţilor metaconglomeratelor paleozoice din Bihorul de Sud. *Stud. cerc. geol.*, 40, p. 3-18, Bucureşti.

— (1997) Studiul petrologic al metaconglomeratelor paleozoice din Munţii Bihor. Teză nepublicată, Univ. Bucureşti.

Dunnet, D. (1969) A technique of finite strain analysis using elliptical particles. *Tectonophysics*, 7/2, p. 117-136, Amsterdam.

— , Siddans, A.W.B. (1971) Non random sedimentary fabrics and their modification by strain. *Tectonophysics*, 12/4, p. 307-325, Amsterdam.

Ghosh, Y. K. (1978) Measure of non-cooaxiality. *J. Struct. Geol.*, 9/1, p. 111-113, Oxford.

Hanna, S., Fry, N. (1979) A comparison of methods of strain determination in rocks from southwest Dyfed (Pembrokeshire). *J. Struct. Geol.*, 1/2, p. 155-162, Oxford.

Kligfield, R., Carmignani, L., Owens, W. H. (1981) Strain analysis of a Northern Apennine shear zone using deformed marble breccias. *J. Struct. Geol.*, 3/4, p. 421-436, Oxford.

Lisle, R. J. (1977) Clastic grain shape and orientation in relation to cleavage from the Aberystwyth Grits, Wales. *Tectonophysics*, 39, p. 381-395, Amsterdam.

— (1985) Geological strain analysis. A manual for the Rf/ø technique. Pergamon Press, 1-100, London.

— (1986) The sectional strain ellipse during progressive cooaxial deformations. *J. Struct. Geol.*, 8/7, p. 809-817, Oxford.

Mathews, P. E., Bond, R., Van den Berg, J. (1974) An algebraic method of strain analysis using elliptical markers. *Tectonophysics*, 24/1-2, p. 31-67, Amsterdam.

Means, W. D., Hobbs, B. E., Lister, G. S., Wiliams, P. F. (1980) Vorticity and non-cooaxiality in progressive deformations. *J. Struct. Geol.*, 2/3, p. 371-378, Oxford.

Milton, N. J. (1980) Determination of the strain ellipsoid from measurements on any three sections. *Tectonophysics*, 64, T19-T27, Amsterdam.

Olaru, L., Dimitrescu, R. (1994) Contribuţii preliminare la cunoaşterea vârstei Seriei de Păiuşeni din masivul Highiş. *Rom. J. Stratigraphy*, 76, p. 1-5, Bucureşti.

Paterson, S.R. (1983) A comparison of methods used in measuring finite strain from ellipsoidal objects. *J. Struct. Geol.*, 5/6, p. 611-618, Oxford.

Peach, C., Lisle, R. J. (1979) A FORTRAN IV program for the analysis of tectonic strain using deformed elliptical markers. *Comp. & Geosci.*, 5, p. 323-334, Oxford.

Pfiffner, O. A., Ramsay, J. G. (1982) Constraints on geological strain rates: arguments from finite strain states of naturally deformed rocks. *Journ. of Geophys Res.*, 87/B1, p. 311-321, Washington.

Ramberg, H. (1975) Particle paths, displacement and progressive strain applicable to rocks. *Tectonophysics*, 28/1-2, p. 1-37, Amsterdam.

Ramsay, J. G. (1967) The folding and fracturing of rocks. Mc Graw-Hill, New York.

— (1980) Shear zone geometry: a review. *J. Struct. Geol.*, 2/1-2, p. 83-99, Oxford.

— , Allison, I. (1979) Structural analysis of shear zones in an alpinished Hercynian granite (Maggia Lappen, Pennine Zone, Central Alps). *Schweiz. Miner. Petrogr. Mitt.*, 59, p. 251-279.

— , Wood, D. Y. (1973) The geometric effects of volume change during deformation processes. *Tectonophysics*, 16/3-4, p. 263-277, Amsterdam.

Ratschbacher, L., Sperner, B., Meschede, M., Frisch, W. (1994) Computer techniques and applications: a program library for quantitative structural analysis. Tübinger Geowissenschaftliche Arbeiten, Reihe A, Band 21.

Siddans, A. (1980) Analysis of 3-D homogeneous finite strain using elliptical objects. *Tectonophysiscs*, 64, p. 1-16, Amsterdam.

Annexe 1. Les valeurs des paramètres du strain obtenues par la mèthode TRISEC pour les points d'observation des Monts Apuseni

1. Bricesti

SECTION 1 DIP 85 STRIKE 305 PITCH OF ELLIPSE LONG AXIS 90 ELLIPSE RATIO 1.870
SECTION 2 DIP 35 STRIKE 76 PITCH OF ELLIPSE LONG AXIS 90 ELLIPSE RATIO 1.820
SECTION 3 DIP 85 STRIKE 210 PITCH OF ELLIPSE LONG AXIS 45 ELLIPSE RATIO 2.100
2.2095530
2.3004168
1.0083502
PRODUCT OF ADJUSTMENT FACTORS 0.3822
SECTION 1 ADJUSTMENT ELLIPSE RATIO 0.713
SECTION 2 ADJUSTMENT ELLIPSE RATIO 0.712
SECTION 3 ADJUSTMENT ELLIPSE RATIO 0.713
MATRIX REPRESENTING ELLIPSOID
0.694 -0.048 0.337
-0.048 1.152 0.085
0.337 0.085 0.463
AXIS NUMBER 1 TREND 190 PLUNGE 54 LENGHT 2.169
AXIS NUMBER 2 TREND 357 PLUNGE 35 LENGHT 1.035
AXIS NUMBER 3 TREND 91 PLUNGE 6 LENGHT 0.927
X:Y:Z = 2.339: 1.116: 1.000 LODES PARAMETER = -0.742
ES VALUE = 0.860
TECTONIC CLEAVAGE AS DEFINED BY X:Y PLANE HAS STRIKE 181 AND DIP 84

2.Valea Negrii

SECTION 1 DIP 85 STRIKE 310 PITCH OF ELLIPSE LONG AXIS 90 ELLIPSE RATIO 2.160
SECTION 2 DIP 55 STRIKE 150 PITCH OF ELLIPSE LONG AXIS 81 ELLIPSE RATIO 1.820
SECTION 3 DIP 65 STRIKE 180 PITCH OF ELLIPSE LONG AXIS 45 ELLIPSE RATIO 2.640
2.4981923
1.2525140
1.2136556
PRODUCT OF ADJUSTMENT FACTORS 0.6173
SECTION 1 ADJUSTMENT ELLIPSE RATIO 0.813
SECTION 2 ADJUSTMENT ELLIPSE RATIO 0.807
SECTION 3 ADJUSTMENT ELLIPSE RATIO 0.809
MATRIX REPRESENTING ELLIPSOID
0.334 -0.786 -0.104
-0.786 -0.023 -0.180
-0.104 -0.180 0.333
3D FIGURE IS NOT AN ELLIPSOID
AXIS NUMBER 2 TREND 217 PLUNGE 78 LENGHT 1.638
AXIS NUMBER 3 TREND 321 PLUNGE 3 LENGHT 1.019

3. Cascada Vârciorogului

SECTION 1 DIP 80 STRIKE 315 PITCH OF ELLIPSE LONG AXIS 90 ELLIPSE RATIO 2.690
SECTION 2 DIP 40 STRIKE 135 PITCH OF ELLIPSE LONG AXIS 90 ELLIPSE RATIO 1.920
SECTION 3 DIP 85 STRIKE 225 PITCH OF ELLIPSE LONG AXIS 45 ELLIPSE RATIO 2.740
1.4142136
1.5581819
1.0191886
PRODUCT OF ADJUSTMENT FACTORS 0.3212
SECTION 1 ADJUSTMENT ELLIPSE RATIO 0.670
SECTION 2 ADJUSTMENT ELLIPSE RATIO 0.670
SECTION 3 ADJUSTMENT ELLIPSE RATIO 0.674
MATRIX REPRESENTING ELLIPSOID
0.727 -0.327 0.156
-0.327 0.620 0.104
0.156 0.104 0.242
AXIS NUMBER 1 TREND 225 PLUNGE 53 LENGHT 3.119
AXIS NUMBER 2 TREND 54 PLUNGE 37 LENGHT 1.446
AXIS NUMBER 3 TREND 321 PLUNGE 4 LENGHT 0.996
X:Y:Z = 3.131: 1.452: 1.000 LODES PARAMETER = -0.347
ES VALUE = 0.938
TECTONIC CLEAVAGE AS DEFINED BY X:Y PLANE HAS STRIKE 51 AND DIP 86

4. Pârâul Corbului

SECTION 1 DIP 0 STRIKE 270 PITCH OF ELLIPSE LONG AXIS 90 ELLIPSE RATIO 1.840
SECTION 2 DIP 85 STRIKE 310 PITCH OF ELLIPSE LONG AXIS 90 ELLIPSE RATIO 1.580
SECTION 3 DIP 85 STRIKE 238 PITCH OF ELLIPSE LONG AXIS 45 ELLIPSE RATIO 1.630
1.5557238
1.0058303
1.8870799
PRODUCT OF ADJUSTMENT FACTORS 1.7230
SECTION 1 ADJUSTMENT ELLIPSE RATIO 1.204
SECTION 2 ADJUSTMENT ELLIPSE RATIO 1.202
SECTION 3 ADJUSTMENT ELLIPSE RATIO 1.202
MATRIX REPRESENTING ELLIPSOID
0.266 -0.116 0.217
-0.116 0.826 0.140
0.217 0.140 0.366
AXIS NUMBER 1 TREND 197 PLUNGE 38 LENGHT 4.392
AXIS NUMBER 2 TREND 351 PLUNGE 49 LENGHT 1.368
AXIS NUMBER 3 TREND 96 PLUNGE 13 LENGHT 1.072
X:Y:Z = 4.099: 1.276: 1.000 LODES PARAMETER = -0.654
ES VALUE = 1.362
TECTONIC CLEAVAGE AS DEFINED BY X:Y PLANE HAS STRIKE 186 AND DIP 77

5. Valea Plaiului

SECTION 1 DIP 85 STRIKE 270 PITCH OF ELLIPSE LONG AXIS 90 ELLIPSE RATIO 2.150
SECTION 2 DIP 15 STRIKE 45 PITCH OF ELLIPSE LONG AXIS 90 ELLIPSE RATIO 1.690
SECTION 3 DIP 85 STRIKE 225 PITCH OF ELLIPSE LONG AXIS 45 ELLIPSE RATIO 1.270
62.3909494
1.4142136
1.0044738
PRODUCT OF ADJUSTMENT FACTORS 0.3848
SECTION 1 ADJUSTMENT ELLIPSE RATIO 0.698
SECTION 2 ADJUSTMENT ELLIPSE RATIO 0.707
SECTION 3 ADJUSTMENT ELLIPSE RATIO 0.698
MATRIX REPRESENTING ELLIPSOID
0.558 0.109 0.274
0.109 1.008 -0.051
0.274 -0.051 0.389
AXIS NUMBER 1 TREND 168 PLUNGE 52 LENGHT 2.405
AXIS NUMBER 2 TREND 345 PLUNGE 38 LENGHT 1.156
AXIS NUMBER 3 TREND 76 PLUNGE 1 LENGHT 0.984
X:Y:Z = 2.445: 1.175: 1.000 LODES PARAMETER = -0.640
ES VALUE = 0.856
TECTONIC CLEAVAGE AS DEFINED BY X:Y PLANE HAS STRIKE 166 AND DIP 89

6. Piatra Molivişului

SECTION 1 DIP 85 STRIKE 310 PITCH OF ELLIPSE LONG AXIS 45 ELLIPSE RATIO 2.270
SECTION 2 DIP 25 STRIKE 130 PITCH OF ELLIPSE LONG AXIS 88 ELLIPSE RATIO 2.520
SECTION 3 DIP 85 STRIKE 215 PITCH OF ELLIPSE LONG AXIS 90 ELLIPSE RATIO 1.910
1.5557238
2.3683052
1.0083502
PRODUCT OF ADJUSTMENT FACTORS 4.1415
SECTION 1 ADJUSTMENT ELLIPSE RATIO 1.620
SECTION 2 ADJUSTMENT ELLIPSE RATIO 1.619
SECTION 3 ADJUSTMENT ELLIPSE RATIO 1.636
MATRIX REPRESENTING ELLIPSOID
0.275 -0.102 -0.101
-0.102 0.653 0.250
-0.101 0.250 0.232
AXIS NUMBER 1 TREND 313 PLUNGE 62 LENGHT 3.164
AXIS NUMBER 2 TREND 201 PLUNGE 11 LENGHT 1.975
AXIS NUMBER 3 TREND 106 PLUNGE 25 LENGHT 1.115
X:Y:Z = 2.836: 1.771: 1.000 LODES PARAMETER = 0.096
ES VALUE = 0.717
TECTONIC CLEAVAGE AS DEFINED BY X:Y PLANE HAS STRIKE 196 AND DIP 65

7. Valea Bucegiţa

SECTION 1 DIP 85 STRIKE 318 PITCH OF ELLIPSE LONG AXIS 45 ELLIPSE RATIO 2.170
SECTION 2 DIP 50 STRIKE 70 PITCH OF ELLIPSE LONG AXIS 90 ELLIPSE RATIO 2.680
SECTION 3 DIP 85 STRIKE 208 PITCH OF ELLIPSE LONG AXIS 90 ELLIPSE RATIO 2.710
1.3754652
1.6832539
1.0115661
PRODUCT OF ADJUSTMENT FACTORS 1.0499
SECTION 1 ADJUSTMENT ELLIPSE RATIO 1.020
SECTION 2 ADJUSTMENT ELLIPSE RATIO 1.020
SECTION 3 ADJUSTMENT ELLIPSE RATIO 1.020
MATRIX REPRESENTING ELLIPSOID
1.216 1.736 -0.019
1.736 3.732 0.436
-0.019 0.436 0.508
AXIS NUMBER 1 TREND 329 PLUNGE 36 LENGHT 2.385
AXIS NUMBER 2 TREND 160 PLUNGE 54 LENGHT 1.263
AXIS NUMBER 3 TREND 63 PLUNGE 5 LENGHT 0.464
X:Y:Z = 5.144: 2.724: 1.000 LODES PARAMETER = 0.224
ES VALUE = 1.099
TECTONIC CLEAVAGE AS DEFINED BY X:Y PLANE HAS STRIKE 153 AND DIP 85

8. Cetatea Şiria

SECTION 1 DIP 85 STRIKE 310 PITCH OF ELLIPSE LONG AXIS 45 ELLIPSE RATIO 1.620
SECTION 2 DIP 35 STRIKE 90 PITCH OF ELLIPSE LONG AXIS 88 ELLIPSE RATIO 1.720
SECTION 3 DIP 85 STRIKE 240 PITCH OF ELLIPSE LONG AXIS 90 ELLIPSE RATIO 1.630
2.5334266
2.2202984
1.0056874
PRODUCT OF ADJUSTMENT FACTORS 1.1944
SECTION 1 ADJUSTMENT ELLIPSE RATIO 1.064
SECTION 2 ADJUSTMENT ELLIPSE RATIO 1.064
SECTION 3 ADJUSTMENT ELLIPSE RATIO 1.064
MATRIX REPRESENTING ELLIPSOID
0.173 0.243 -0.186
0.243 1.484 0.171
-0.186 0.171 0.622
AXIS NUMBER 1 TREND 348 PLUNGE 21 LENGHT 4.556
AXIS NUMBER 2 TREND 192 PLUNGE 67 LENGHT 1.210
AXIS NUMBER 3 TREND 81 PLUNGE 9 LENGHT 0.804
X:Y:Z = 5.669: 1.506: 1.000 LODES PARAMETER = -0.528
ES VALUE = 1.567
TECTONIC CLEAVAGE AS DEFINED BY X:Y PLANE HAS STRIKE 171 AND DIP 81

9. Valea Sălăndaş

SECTION 1 DIP 5 STRIKE 275 PITCH OF ELLIPSE LONG AXIS 90 ELLIPSE RATIO 1.760
SECTION 2 DIP 85 STRIKE 300 PITCH OF ELLIPSE LONG AXIS 45 ELLIPSE RATIO 1.930
SECTION 3 DIP 85 STRIKE 230 PITCH OF ELLIPSE LONG AXIS 90 ELLIPSE RATIO 1.880
26.8769401
1.0056874
16.1083541
PRODUCT OF ADJUSTMENT FACTORS 0.4698
SECTION 1 ADJUSTMENT ELLIPSE RATIO 0.773
SECTION 2 ADJUSTMENT ELLIPSE RATIO 0.772
SECTION 3 ADJUSTMENT ELLIPSE RATIO 0.772
MATRIX REPRESENTING ELLIPSOID
0.492 0.149 -0.270
0.149 1.219 0.285
-0.270 0.285 0.573
AXIS NUMBER 1 TREND 338 PLUNGE 42 LENGHT 2.411
AXIS NUMBER 2 TREND 195 PLUNGE 42 LENGHT 1.131
AXIS NUMBER 3 TREND 86 PLUNGE 19 LENGHT 0.867
X:Y:Z = 2.779: 1.304: 1.000 LODES PARAMETER = -0.481
ES VALUE = 0.901
TECTONIC CLEAVAGE AS DEFINED BY X:Y PLANE HAS STRIKE 176 AND DIP 71

An. Inst. Geol. Rom., 72, part. II, p. 29-35, Bucureşti, 2000

^{40}Ar -^{39}Ar LASER PROBE DATING ON SINGLE CRYSTALS FROM TRONDHJEMITIC DIKES – SEBEŞ-CIBIN MOUNTAINS (SOUTH CARPATHIANS) – ROMANIA

Anca DOBRESCU[1], Patrick SMITH[2]

[1] Geological Institute of Romania, 1 Caransebes St., RO-79678 Bucharest 32, Romania

[2] Depart. of Physics, University of Toronto, Toronto, Ontario M5S 1A7, Canada

Key words: Trondhjemites. $^{40}Ar/^{39}Ar$ method of dating. Getic-Supragetic Domains. South Carpathians.

Abstract: Single biotite, plagioclase and quartz crystals from porphyritic trondhjemites have been analyzed for $^{40}Ar/^{39}Ar$ isotopes. The dike system occurs along and within a shearing belt of almost 90/2 km in the north Sebes-Cibin Mts. (South Carpathians), which separates the Getic and the so-called Supragetic Realm. Structurally, the trondhjemitic dikes are variably deformed to undeformed, suggesting either a heterochroneous emplacement or a differential response to the brittle shearing associated with the Alpine metamorphic event. LASER step-heating $^{40}Ar/^{39}Ar$ age determinations on three different minerals (biotite, plagioclase and quartz) are discussed here. A plateau age of 108.4+0.5 Ma from biotite from an undeformed rock is identical to its integrated age, indicating negligible Ar loss since rapid cooling of the mineral through its closure temperature. Another biotite from a different trondhjemitic dike shows small amounts of Ar loss in low temperature gas fractions. Its plateau age of 109.3+0.5 Ma is almost concordant to that one from the previous dated rock. Consequently, the $^{40}Ar/^{39}Ar$ data on biotites show the igneous cooling age of the trondhjemitic magma from two different dikes, meaning that this age represents the coeval intrusion of these bodies, responding differently to the brittle shearing stage, probably related to the Austrian phase. Most of the plagioclase phenocrysts are slightly altered and their age-spectra are problematic, indicating both excess Ar and younger ages relative to biotite. These effects may be attributed to an event at 96 - 95 Ma. Similar ages appear to be registered by inclusions within quartz crystals. The coincidence between the Albian-Aptian age of the trondhjemitic dikes and the supposed age of the overthrust precludes the idea of the overthrust position of the Getic - Supragetic Domains, at least on the outcropping area of the swarm of dikes. Considering the main geochemical characteristics of the low-K magmatism related to some tectonic and geochronological data, the genesis of these dikes could be related to the subduction of an oceanic crust of Severin Nappe type beneath the Getic Domain.

Introduction

The scarcity of geochronological data in the South Carpathians, but moreover the significance of a low-K granitoidic (trondhjemitic) magmatism along an important shearing zone, was a stimulating motif to perform the $^{40}Ar/^{39}Ar$ incremental heating method of dating on individual crystals from trondhjemitic dykes. Dating K-bearing minerals (biotite, plagioclase and quartz(!)) from deformed to undeformed rocks, we demonstrate the feasibility of using $^{40}Ar/^{39}Ar$ single-crystal LASER-probe method to separate the effects of deformation induced by a tectonic event, from the cooling age of the trondhjemitic dikes.

Geological setting and geochemical constrains

The shearing zone (90Km/2 km) (Fig. 1) along and within which the swarm of over 300 trondhjemitic dikes occurs, has a quite controversial significance in the tectonic models of the northern South Carpathians:

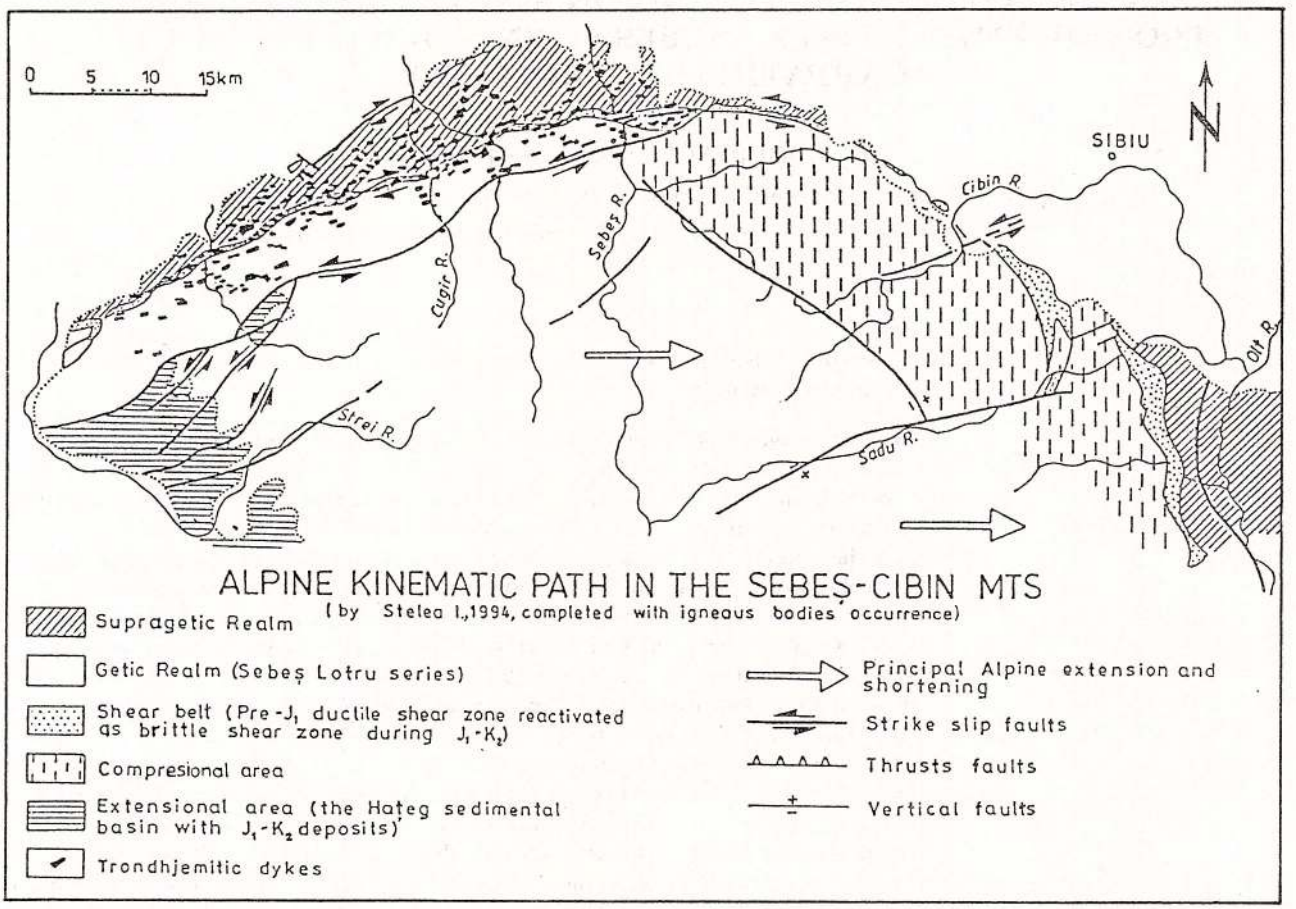

Fig. 1 – Sketch-map of the northern part of the Sebeş-Cibin Mts.

A - reverse fault (Chivu, 1968; Savu, 1978) cross-cutting the Sibişel series;

B - thrust fault (Balintoni et al, 1989), separating the Getic Domain from the overlying Supragetic Domain (or even conversely the Getic Domain thrust over the Supragetic Domain (Iancu & Mărunţiu, 1994). The shortening event is considered either Austrian (quite contemporaneous to the main tectogenesis affecting the Central East and South Carpathians Nappes (Săndulescu, 1984) in the first hypothesis, or Pre-Alpine (related to the M2 dynamo-thermal metamorphic event) in the second one;

C - strike-slip fault (Stelea, 1994) (at least on the SW-NE segment) initiated probably in Lower Jurassic. The trondhjemitic dikes (Dobrescu & Stoian, 1994, Dobrescu, 1995) have been characterized as belonging to a CA low-K (almost exclusively trondhjemitic) magmatism. The main geochemical features are: low Rb, Ba, Zr abundance, moderate Sr contents; low REE contents, low Yb values, moderate to high (La/Yb)n ratios and increasing Sr/Y with decreasing Y (indicating a partial melting process of metabasaltic rocks - Drummond & Defant, 1990); low 87Sr/86Sr (0.702 - 0.704) (typical of mantle derived magmas or of crustal-derived magmas with a metabasic source);

These geochemical features both with several other considerations (see the above mentioned papers) could be explained by deep-seated dehydration partial melting of a metabasic source. This could be appropriate for convergent margin setting (confirmed by plots on Pearce's et al., 1984 diagrams – in Dobrescu, 1998) where convergence-related imbrication places mafic terranes in deep crustal environments.

Analytical technique

We present here an example of $^{40}Ar/^{39}Ar$ age spectra for biotite, plagioclase and quartz crystals derived by LASER step-heating on individual grains. It was used the LASER fusion system at the University of

Toronto which consists of a Spectra-Physics 171-18 (18 Watt) continuous argon-ion laser and a VG 1200S mass spectrometer with a Baur-Signer ion source and an electrón multiplier. For comparison it was used a hornblende Hb3gr spectrum standard (Zartman, 1964 in Layer et al., 1987), a widely used Precambrian standard with an assumed age of 1071 m.y.

Sample description

This study presents analytical data from LASER incremental-heating experiments on 6 single grain samples. The crystals (biotite, plagioclase and quartz phenocrysts) were separated from three porphyritic trondhjemitic bodies, situated in different places vs. the shearing zone.

Sample S79c

The biotite, plagioclase and quartz grain samples belong to the most basic trondhjemitic sill which was mapped in the area (SiO2 = 62.95 %). The sill lies concordant between low metamorphic crystalline schists and crystalline limestones, downstream Cetăţelei Brook, in the central part of the area. It has a "high-porphyritic" (large and dense phenocrysts), almost *undeformed structure*. Plagioclase, quartz, biotite and random altered hornblende phenocrysts are widespread in a microcrystalline matrix.

The sample, taken from the core of the sill, exhibits very well defined, sometimes zoned or twinned plagioclase (An_{15}-An_{29}) laths, slightly sericized mainly in the middle of the phenocrysts. The fine biotite crystals are slightly chloritized, but the bigger ones (0.8 mm in length), which were used in our experiments, are mostly unaltered. The quartz phenocrysts, which sometimes are paramorphs of β-quartz on α-quartz, are rather undeformed.

Sample S80

The dike occurs on the Sebeş valley, near Căpâlna. It is high-silicic (73.61 %), high-porphyritic, with coarser crystallized matrix than sample S79c and fairly *undeformed*. Large plagioclase phenocrysts are sometimes twinned, rarely zoned. Biotites are long-shaped, a little more altered than the biotites in sample S79c.

Sample 6182

The sample was taken from a trondhjemitic dike from the Râuşoru valley, western part of the area. It is a remarkable fresh rock, "low-medium porphyritic" with a fine microcrystalline matrix and a slightly oriented structure with aligned and sometimes long kink-waved biotite crystals. The quartz (sometimes dipyramidal) and plagioclase phenocrysts have waved extinction and sometimes biotite inclusions.

Results

The Ar-Ar data for step-heating analyses of 6 mineral crystals are summarized in Table 1. Significant gas fractions from the biotite sample S79c give concordant ages, resulting in a plateau age of 108.4+0.5 Ma that is identical to the integrated age of 108.1±0.5 Ma (Fig. 2A). The undisturbed age spectrum for this sample indicates negligible Ar loss since rapid cooling of the mineral through its closure temperature. The age-spectrum for S80 biotite from another trondhjemitic dike shows small amounts (less than 20 %) of Ar loss in low temperature gas fractions. However, age plateau at 109.3+0.5 Ma for the remaining gas fractions is indistinguishable from the age of sample S79c. Thus, the ages of biotite from both dikes are the same within uncertainties.

The age spectra for the plagioclase crystals are more complex compared to their associated biotite. There are also geochemical differences between the feldspars indicated by a Ca/K of 18.3 for S80, which is significantly higher than the ratio of 5.8 for S79c. The spectrum of plagioclase S80 shows the effects of excess Ar in the low-temperature fractions 1-4, which is reflected in its high integrated age of 124.4+2.0 Ma. These effects can be circumvented by the use of an isotope correlation plot of $^{39}Ar/^{40}Ar$ vs. $36Ar/^{40}Ar$. On this plot fractions 7-12 are co-linear within experimental uncertainties and yield an age of 111.3±4.5 Ma. This isochron age is within the uncertainties of the biotite age of 108 Ma. Plagioclase from samples S79 gives an integrated age of 96.2±0.8, significantly younger than that of S80. An isochron fit through points 4 to 11 gives an indistinguishable estimate of 96.5±2.3 Ma (Fig. 2C).

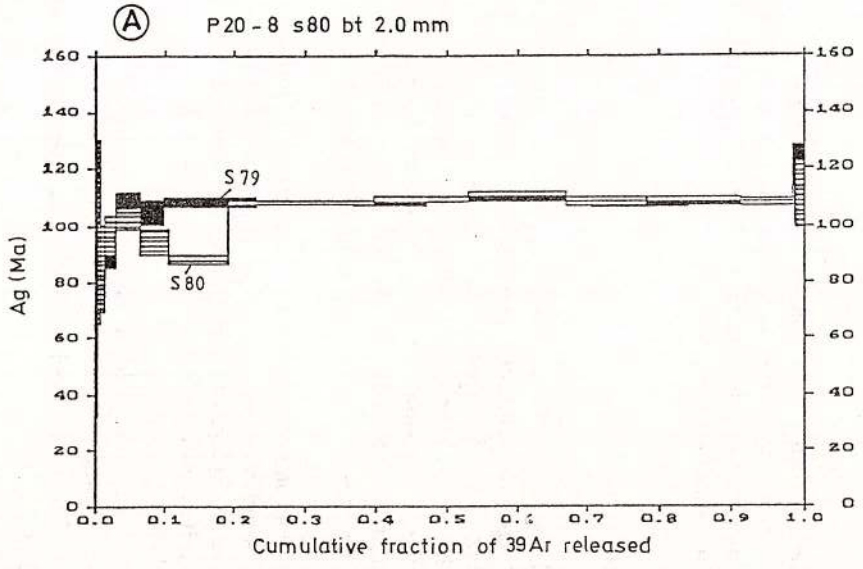

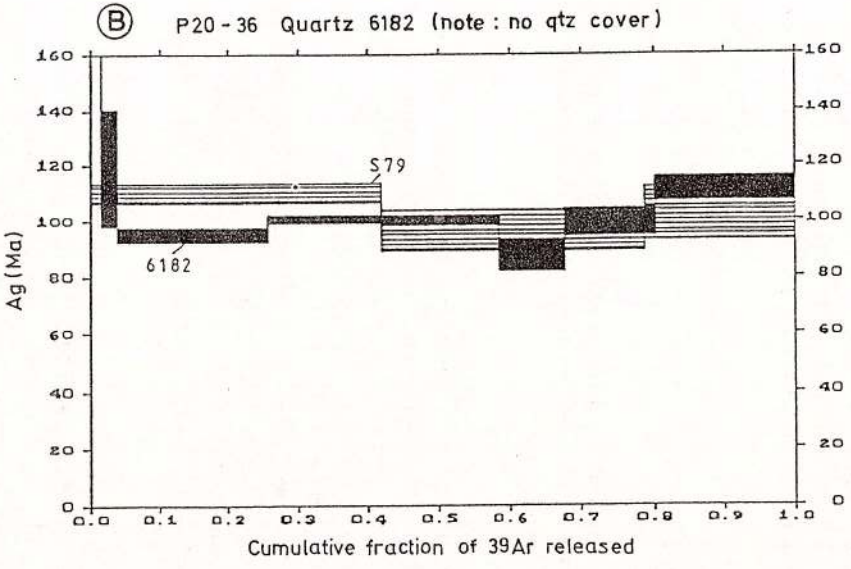

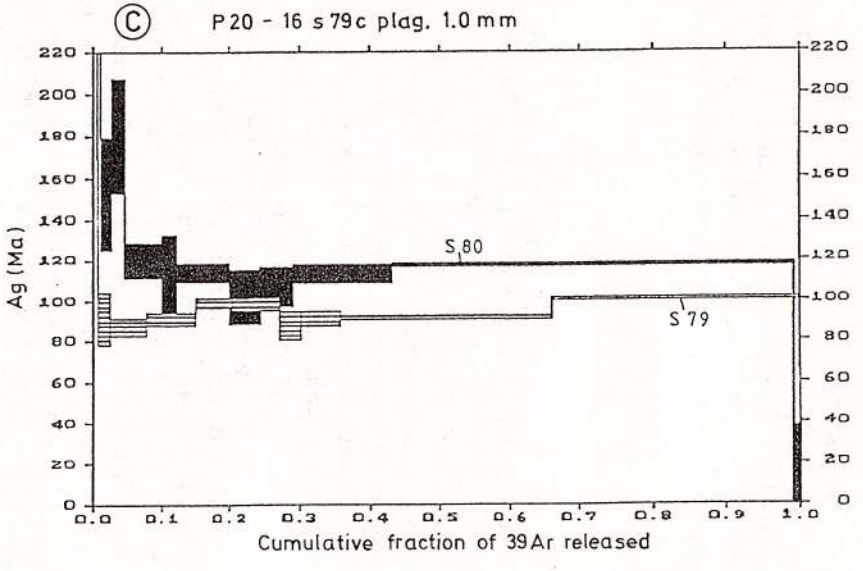

Fig. 2. – A. $^{40}Ar/^{39}Ar$ age spectra for biotite samples S79c and S80.
B. $^{40}Ar/^{39}Ar$ age spectra of quartz samples S79c and 6182.
C. $^{40}Ar/^{39}Ar$ age spectra of plagioclase samples S79c and S80.

Table
Summary of results of $^{40}Ar/^{39}Ar$ incremental heating experiments
on undisturbed and disturbed minerals

Sample	Description	n	Plateau			Isochron			Integrated		
			Age	N	%	Age	Initial	SumS/ (n-2)	Age	vol ^{39}Ar 10^{-12}	$^{37}Ar/^{39}Ar$
s79c											
p20-15	0.8 mm biotite	11	108.4±0.5	9	96				108.1±0.5	23.6	0.01±0.01
p20-16	1.0 mm plagioclase	13							96.2±0.8	13.7	3.18±0.02
p20-31	quartz	3	~96±7	1	37						0.35±0.02
s80											
p20-8	2.0 mm biotite	14	109.3±0.5	7	81	107.8±1.6	385±96	0.75	106.1±0.6	20.8	0.067 ±0.004
p20-9	1.5 mm plagioclase	14	115.1±1.5	6	90				124.4±2.0	4.9	9.98±0.05
6182											
p20-36	quartz	8				95±3	484±85	1.52	103.7±1.7	4.4	0.13±0.01

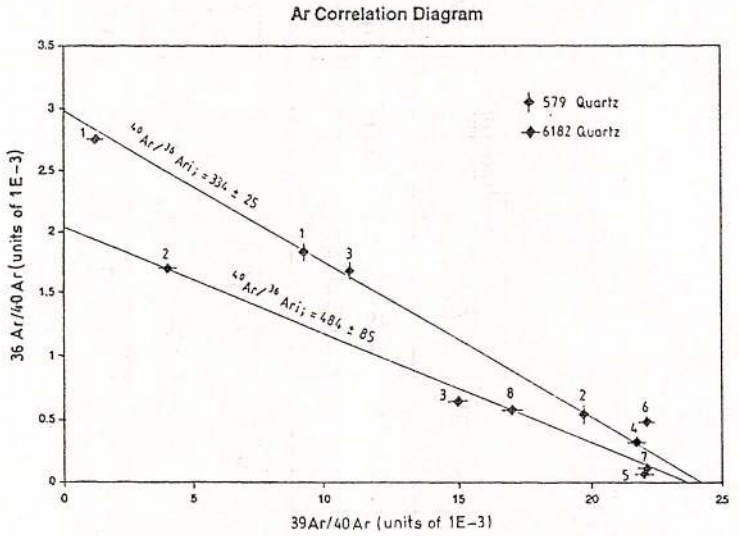

Fig. 3 – Ar correlation diagram on quartz crystals.

Two quartz grains were analyzed from two different dikes. The source of K generating ^{39}Ar is believed to come from minute inclusions. A preliminary experiment to test for ^{39}Ar on a sample from S79 was divided into only 3 steps. Steps 1 and 3 contain Ar that is only 50 % radiogenic. The second step contains 83 % radiogenic Ar and thus its calculated age is less dependent on the choice of initial ratio. This fraction gives an age of 96±7 Ma, the same as 96 Ma for associated S79 plagioclase. An isochron plot of the 3 points (Fig. 3) gives 93+10 Ma with an initial $^{40}Ar/^{36}Ar$ of 334±25. This ratio is marginally higher than the modern atmospheric value of 296, suggesting that the mineral trapped some radiogenic Ar. A quartz sample from dike 6182 was run in more detail. Seven step-heated fractions are co-linear (S/(n-2) =1.52) giving an initial $^{40}Ar/^{36}Ar$ value of 484±8.5 Ma, confirming that the quartz grains trapped radiogenic Ar (Fig. 2B, 3, the first fraction may have been contaminated by modern atmospheric Ar and has been omitted). The x-intercept of this isochron corresponds to an age of 95±3 Ma. Thus, although the two quartz crystals appear to have crystallized with distinct initial ratios, their ages are the same. Quartz crystals may have incorporated variable amounts of radiogenic Ar either at the quartz/matrix interface or from biotite inclusions.

Conclusions

Our study shows that the trondhjemitic dikes from the North Sebeş-Cibin Mts. can be successfully dated by the $^{40}Ar/^{39}Ar$ LASER step-heating method. Biotite samples from different dikes display fairly undisturbed (concordant) plateau age, almost identical to its integrated age of 108.4±0.5 to 109.3±0.5 Ma. Flat spectra of both biotite samples could reflect either rapid cooling through its closure temperature, or complete and rapid resetting. According to Maluski (1978), under tectonic influence, all domains suffer a partial loss of radiogenic argon, and the magnitude of the loss increases with the degree of deformation. Moreover, recent $^{40}Ar/^{39}Ar$ analyses on medium-grade metamorphic rocks of the Sebeş-Lotru series and on low-grade metamorphics belonging to the Sibişel series (Dallmeyer et al., 1994) yielded results of 294 to 309 Ma, and 200 to 118 Ma, respectively. These data hint that the last medium-grade metamorphic overprint is Variscan and show that penetrative Alpine tectonics that affected at least some areas must be accommodated in regional interpretation (Pană & Erdmer, 1994).

We may conclude that the $^{40}Ar/^{39}Ar$ data on biotite show the igneous cooling age of the trondhjemitic magma from two different dikes, meaning that this age represents the coeval intrusion of these bodies. The data obtained on other K-bearing minerals reveal that disturbed age spectra may discriminate tectonic events at 95-96.2 Ma., while almost perfect plateau age spectra seem to reflect the cooling age of the trondhjemitic dikes at 108-109 Ma.

The described magmatism seems to coincide with the end of the brittle shearing stage (J1-K2) described by Stelea (1994), occuring probably in a calm period. The different response to the shearing is revealed from the age spectra of dikes S79 and S80.

Following the idea of the Getic/Supragetic overthrust relationship, we can notice the coincidence between Aptian-Albian age obtained on the trondhjemitic rocks and the supposed age of the overthrust. This coincidence precludes the superposed position of the two domains, at least on the outcropping area of the swarm of dikes, moreover as the dikes are aligned quite symmetrically along the faulting (shearing) zone.

Taking into account the geochemical features together with the tectonic and chronological data, the trondhjemitic magmatism from north Sebeş-Cibin Mts. could be related to the subduction of an oceanic crust of Severin Nappe-type beneath the Getic Domain (Săndulescu, oral information).

Acknowledgements

Financial support from the Romanian Academy of Science (GAR 3855/1997) and the Romanian Ministry of Research (GR 3023/1997) is gratefully acknowledged.

Dr. H. Savu, Dr. I. Stelea and prof. J.-P. Liegeois are thanked for useful comments.

References

Balintoni, I., Berza, T., Hann, H. P., Iancu, V., Kräutner, H. G., Udubaşa, G. (1989) Precambrian metamorphics in the South Carpathians. Probl. Comm.IX, Guide to Excursions, Bucharest.

Chivu, C. (1968) Date noi asupra geologiei şi petrografiei părţii de Nord a munţilor Sebeş. *D.S. Inst. Geol. Geofiz.* LIII/3, 23-37, Bucureşti.

Dallmayer, R. D., Neubauer, F., Mocanu, V., Fritz, H. (1993) $^{40}Ar/^{39}Ar$ mineral age controls for the Pre-Alpine and Alpine tectonic evolution of nappe complexes in the Southern Carpathians. Alcapa II. *Rom. J. Tect. Reg. Geol.*, 75, Supplement 2, p. 77-86, Bucharest.

Dobrescu, A., Stoian, T. (1994) New data concerning the origin of the igneous leucocratic rocks in the northern Sebeş Mts. – South Carpathians. Geochemical evidence. *Rom. J. Petrol.*, 76, p. 41-50, Bucharest.

— **(1995)** Trondhjemitic magmas related to a pre-alpine shear zone in the central South Carpathians. *Geol. Soc. Greece Sp. Publ.*, No. 4, p. 506-511, Atena.

Drummond, M. S., Defant, M. J. (1990) A model for trondhjemitite-tonalite-dacite genesis and crustal growth via slab melting: Archean to modern comparisons. *J. Geophys. Res.*, v. 95, no. B13, p. 21.503-21.521.

Iancu, V., Mărunţiu, M. (1994) Pre-Alpine litho-tectonic units and related shear zones in the basement of the Getic-Supragetic Nappes (South Carpathians). Overview on Rom. Geol.- Alcapa II. *Rom. J. Tect. Reg. Geol.*, 75, Supplement 2, p. , Bucharest.

Layer, P. W., Hall. D., York, D. (1987) The derivation of $^{40}Ar/^{39}Ar$ age spectra of single grains of hornblende and biotite by LASER step-heating. *Geophys. Res. Lett.*, 14, 7, p. 757-760.

Maluski, H. (1978) Behaviour of biotites, amphiboles, plagioclases and K-feldspars in response to tectonic events with the ^{40}Ar-^{39}Ar radiometric method. Example of Corsican granite. *Geochim. Cosmochim. Acta*, 42, p. 1619-1633. Pergamon Press. Printed in Great Britain.

Pană, D., Erdmer, P. (1994) Alpine crustal shear zones and pre-Alpine basement terranes in the Romanian Carpathians and Apuseni Mountains. *Geology*, 22, p. 807-810.

Pearce, J. A., Harris, N. B. W., Tindle, A. G. (1984) Trace element discrimination diagrams for the tectonic interpretation of granitic rocks. *J. Petrol.*, 25, part 4, p. 956-983.

Richardson S. M., Mc Sween, H.Y. (1989) Geochemical pathways and processes., p. 396-398. Prentice Hall Inc., Englewood Clifs, New Jersey.

Savu, H. (1978) Dalslandian metamorphosed formations in the Southern Carpathians. *Rev. Roum. Geol. Geophys. et Geogr., Geologie*, 22, p. 7-17, Bucharest.

Săndulescu, M. (1984) Geotectonica României. Ed. Tehnică, 334 p., Bucureşti.

Săndulescu, M. (1994) Overview on Romanian Geology, Alcapa II, Field Guidebook - *Rom. J. Tect. Reg. Geol.*, vol. 75. Supplement 2, p. 3-16, Bucharest.

Stelea, I. (1994) Pre-alpine shear zone in the Central South Carpathians. *Rom. J. Tect. Reg. Geol.*, 75, Supplement 1, p. 58-59, Bucharest.

An. Inst. Geol. Rom., 72, part. II, p. 37-45, Bucureşti, 2000

KIMMERIDGIAN AND LOWER TITHONIAN SEQUENCES FROM EAST AND SOUTH CARPATHIANS – ROMANIA

Dan GRIGORE

Geological Institute of Romania, 1 Caransebeş St., RO-79678 Bucharest 32

Key words: Biostratigraphy. Ammonites. Kimmeridgian. Lower Tithonian. East Carpathians. South Carpathians.

Abstract: This paper presents some sequences from the Greben Formation and, for the first time, from the Valea Cetăţii Formation and Acanthicum Formation. The biostratigraphy of the Kimmeridgian - Lower Tithonian Carpathian deposits and the ammonite zones: Platynota, Hypselocyclum, Divisum, Acanthicum, Cavouri, Beckeri, interval Hybonotum-Albertinum, Verruciferum and Richteri, is presented in detail.

Introduction

In the last five years, detailed biostratigraphic studies on the Kimmeridgian and Lower Tithonian deposits were carried out in three areas of the Carpathians: two of them, namely the Lacu Rosu (Ghilcoş) and Sviniţa, were explored by previous authors, as Neumayr (1873), Herbich (1878), and Răileanu (!960) respectively; the third one - Raşnov, is new.

The studied Upper Jurassic deposits belong to three different major geostructural units (Figs. 1 and 2).

In the Sviniţa area (SW of the South Carpathians), the outcrop is located 1 km north of the Sviniţa locality, in the western slope of the Vodiniciki Valley (Fig. 1a). The Upper Kimmeridgian-Lower Tithonian deposits belong to the lower member of the Greben Formation (Pop, 1996), of the Marginal Dacides (Săndulescu, 1984). The sequence (the interval Acanthicum - Richteri), of 20 m thick, starts up by nodular limestones with subordinate marly interbeds, less frequent to the upper part of this formation; at certain levels some cherty nodules or lenses occur (Fig. 3 and 4).

In the Raşnov area (Postăvaru Mt., East Carpathians) the outcrop is located near to the source of the Cetăţii Rivulet (in the proximity of the Râşnov-Poiana Braşov road, at the km 6). Here are exposed the Kimmeridgian deposits (the interval Hypselocyclum-Beckeri); they belong to the Valea Cetatii Formation (Pop & Grigore, in progress) - of the Braşov Unit (Median Dacid .; Săndulescu, 1984). The studied sequence (the basal interval of 7 m thick) is made up of nodular limestones and calcarenites with thin marly interbeds (Fig. 5).

The Upper Jurassic deposits from the Lacu Roşu area (west of the Ghilcoş Mt.-Hăghimaş Massif) belong to the Acanthicum Formation (Grigore, in progress), the basal term of the Hăghimaş Nappe (Transylvanids; Săndulescu, 1984). There are studied two types of outcrops, located in the western and northwestern side of the Ghilcoş Mountain; one type is represented by the western walls of the mountain (affected by transversal faults) and the other type, by the slipped blocks (big ones), full of ammonites and more accessible (the location of all sections is presented in Fig. 1c). In this region, the Lower Kimmeridgian is constituted by nodular limestones, calcarenites and thin marly interbeds, while the Upper Kimmeridgian - Lower Tithonian rock sequence is mainly detrital: built up of calcarenites, sandstones, marls and, subsequently, calcilutites; the terrigene fraction increases at the upper part of this interval (Figs. 6 and 7). In both these rock sequences (the interval Platynota - Hybonotum) lateral variations of facies and thickness (of a maximum 30 m) were observed.

The correlation of the Upper Jurassic deposits between those three Carpathian formations is presented in Figure 2.

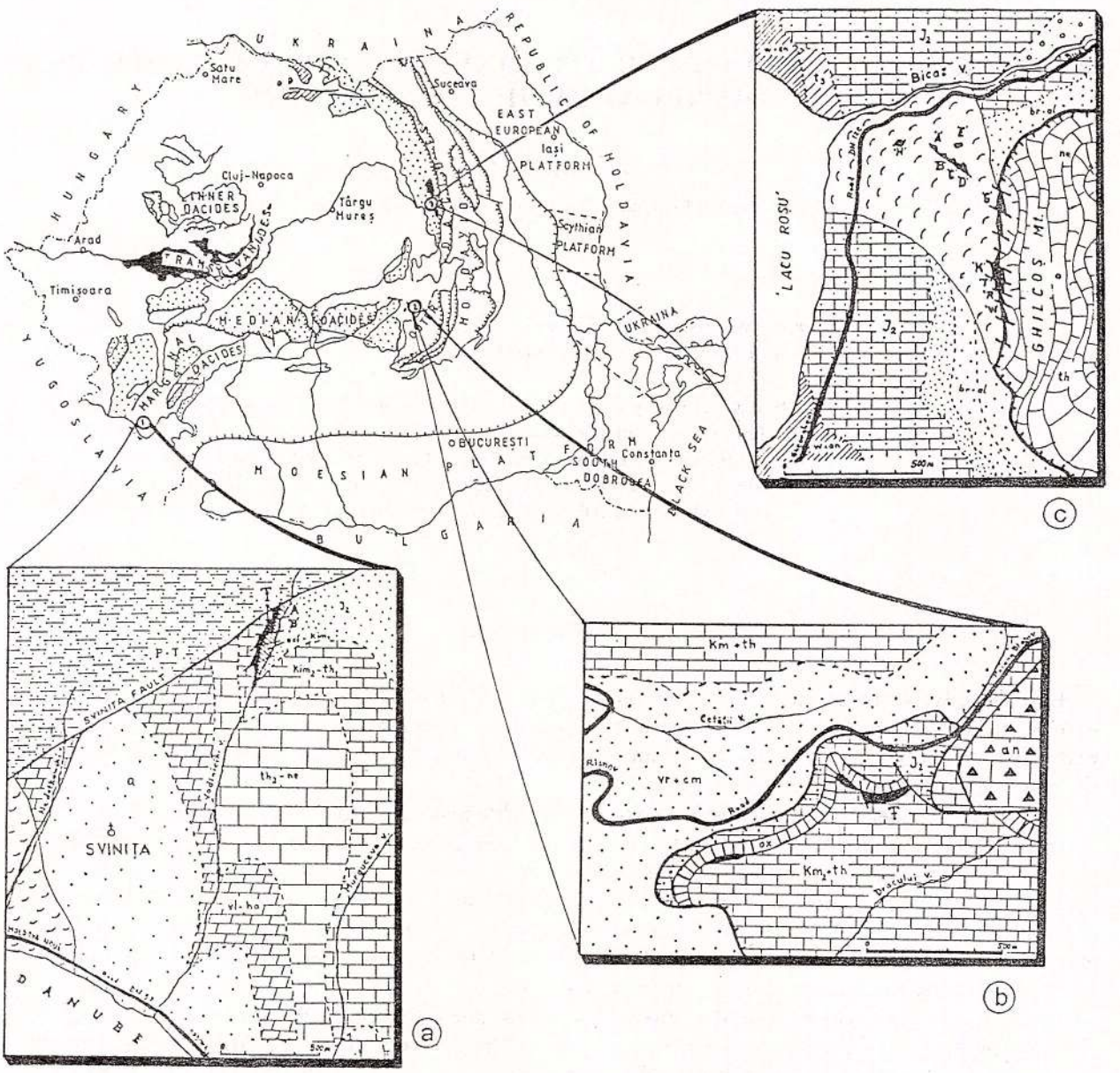

Fig. 1 – The location of the studied areas on the Romanian geostructural map. Details from the windows: a) location of the studied sequences ("A" and "B") from the Greben Formation - Sviniţa area; b) location of the studied sequence from the Valea Cetăţii Formation - Râşnov area; c) location of the studied sequences ("A", "B", "C", "D", "E", "G", "H", "K", "T", "R" and "W") from the Acanthicum Formation - Lacu Roşu area (a, b and c are sketches of map after the maps sc. 1: 50,000, modified).

Biostratigraphy

A general biostratigraphic view (zones and ammonites distribution), as a result of the correlation of the entire ammonite fauna from the studied sequences, is presented in Figure 8.

The Lower Kimmeridgian is known only from the Lacu Roşu and Râşnov areas. The Platynota Zone was recognized only in the former of these areas; there is possible to be defined as Taxon Range Zone on the ground of the high frequency of *Sutneria platynota* in the whole interval, of 60 cm thick. The lower boundary is unknown and its upper one is marked by the LAD of the index species. The interval is full of ammonites, the phylloceratids being dominant - with an acme of *Sowerbyceras silenum*. The assemblage of this zone comprises some characteristic taxa, such as: *Taramelliceras (T.) hauffianum, T. (T.)* cf. *greenakeri, Epa-*

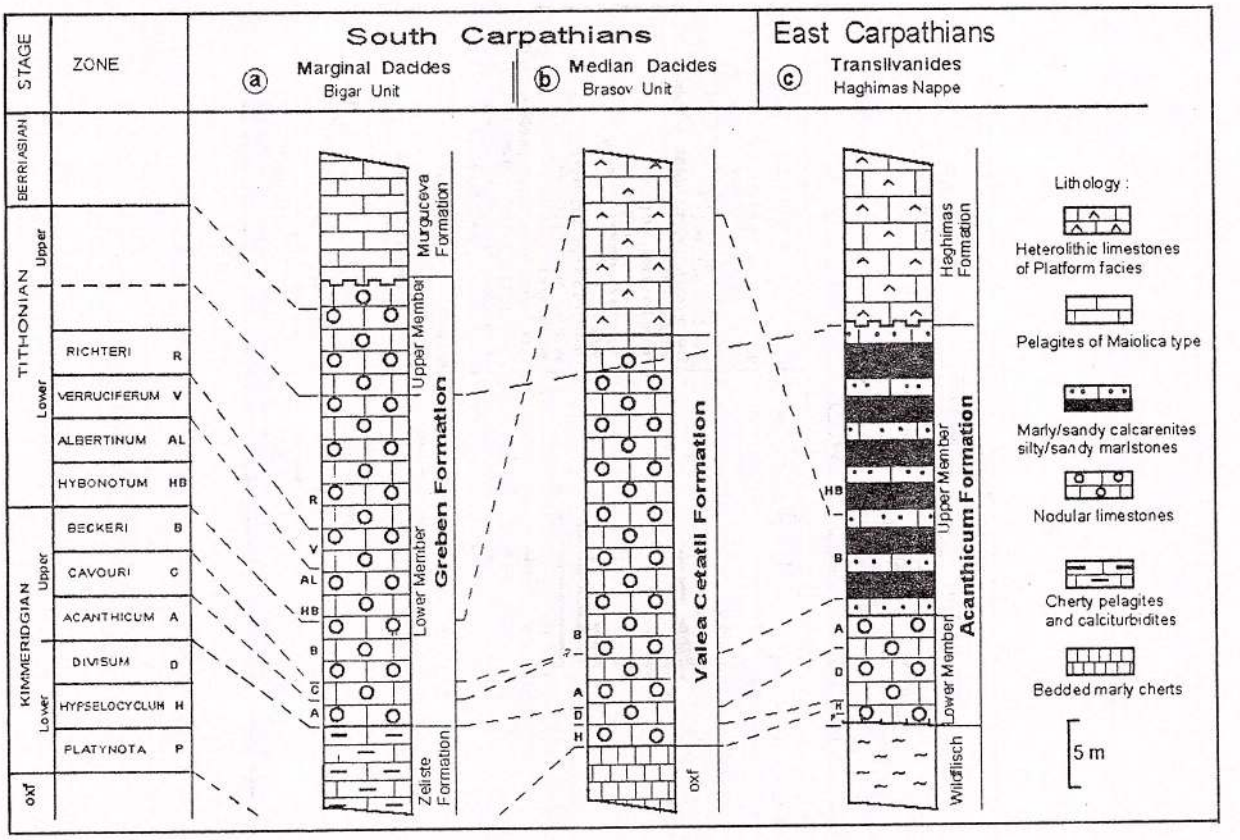

Fig. 2 – Correlation of the Upper Jurassic deposits of the studied formation from the East and South Carpathians.

spidoceras ruppelensis, Benetticeras vaii, Physodoceras wolfi morpha *wolfi, Sutneria* cf. *pedinopleura, Sutneria spinata* n.sp., *Progeronia breviceps, Progeronia* sp. aff. *P. lictor, Lithacosphinctes* cf. *evolutus, Lithacosphinctes* cf. *callomoni, Ataxioceras (Parataxioceras) inconditum.* In the upper part of the zone the occurrence of the *Trenerites* group and the FADs of *Progeronia progeron, Taramelliceras (Metahaploceras) strombecki* and *T. (M.) nodosiusculum* is obvious. The assemblage is completed by some other taxa (with their FADs in this interval) as: *Holcophylloceras mediterraneum, H. polyolcum, Calliphylloceras manfredi, Aspidoceras binodum, A. sesquinodosum, A. linaresi, Physodoceras altenense, Orthosphinctes polygyratus, Lytoceras polycyclum.*

The Hypselocyclum Zone has not been well argued until now; it is possible to be recognised on the ground of its assemblage, in both areas (Lacu Roşu and Râşnov). Its lower boundary is considered only in the Lacu Roşu area at the LAD of *Sutneria platynota*, while its upper boundary is marked in the Râşnov area only, at the FAD of *Crussoliceras divisum.* The fauna recorded by the previous authors (Neumayr, 1873; Herbich, 1878), with *Ataxioceras (A.) lothari, A. (A.) fasciferum, A. (A.) polyplocum*, makes possible to presume the existence of *Ataxioceras hypselocyclum* in this interval. In both these regions the assemblage is poor, represented by few characteristic taxa, as follows: *Taramelliceras (Metahaploceras) strombecki, T. (M.) nodosiusculum, Aspidoceras uninodosum, A. sesquinodosum, A. linaresi, Nebrodites hospes hospes, Lessiniceras ptychodes, Orthosphinctes polygyratus, Progeronia* cf. *triplex, Ataxioceras cf. metamorphus* and *Lytoceras polycyclum.* In this interval the phylloceratids are in decrease. The maximum thickness, of 60 cm, is registered in the Râşnov area.

The Divisum Zone is better argued in Râşnov area, where the lower boundary is marked at the FAD of *Crussoliceras divisum.* The upper boundary is traced at the LADs of *Orthaspidoceras uhlandi* and *Sowerbyceras silenum*, in both regions. It is defined as Assemblage Zone, because the index species is frequent only in a short interval, in the base of the zone. In this interval we have the occurrence of all the Presimoceras and Crussoliceras. Some of the characteristic species are there encountered: *Taramelliceras (T.) trachinotum, Streblites tenuilobatus, S.* cf. *levipictus, Physodoceras wolfi* morpha *montisprimi, Orthaspidoceras uhlandi, Crussoliceras divisum, C. geyeri, C. tenuicostatum, C.* cf. *acre, Garnierisphinctes* cf. *championeti, Presimoceras fucinii, P. avrami* n.sp., *P.* cf. *herbichi, P.* cf. *planulacinctum, P.* aff. *ludovici, Nebrodites agrigentinus*

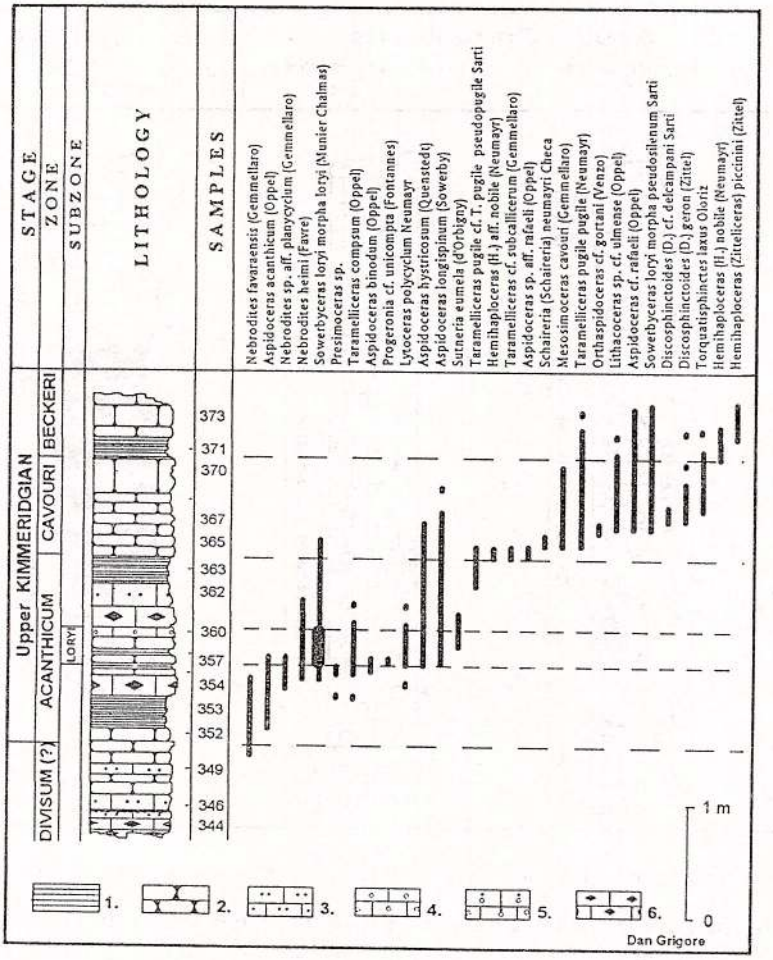

Fig. 3 – Greben Formation - section N Sviniţa ("A"). Lithology, ammonites distribution and Zones. Lithology: 1. marls; 2. nodular limestones; 3. calcarenites; 4. calcirudites; 5. sorted ruditic - arrenitic limestones; 6. cherts.

agrigentinus, N. favaraensis morpha *favaraensis, N. peltoideus, N. rhodanensis, N.* cf. *doublieri, Progeronia unicompta, P.* cf. *pseudolictor*. It is possible to identify the Divisum Subzone (sensu Sarti, 1993) in the lower part of this interval only in the Râşnov area; the Uhladi Subzone is well argued in both regions. The maximum thickness of this interval is of 3 m.

The Upper Kimmeridgian is developed in all the areas we focused on, but is well argued only in Sviniţa. The Acanthicum Zone is defined as Assemblage Zone. In the Râşnov area only the lower boundary of the Acanthicum Zone was observed; there, as in the Lacu Roşu area, it is marked by the LAD of Orthaspidoceras uhlandi. The upper boundary is marked only in the Lacu Roşu and Sviniţa at the LADs of the Nebrodites taxa (*N. contortus, N. heimi*). The assemblage is characterized by the occurrence of *Phylloceras consanguineum, Glochiceras fialar, Taramelliceras (T.) compsum compsum, T. (T.) mikoi, T. (T.)* cf. *franciscanum, T. (T.) pseudoflexuosum, T. (T.) oculatiforme, T. (T.)* cf. *subpugile, Aspidoceras acanthicum, A. longispinum, A. hystricosum, Pseudowaagenia micropla, Orthaspidoceras liparum, O. lallerianus, Schaireria (S.) neumayri, Sutneria eumela, S. hoelderi, S. lorioli, Nebrodites favaraensis* morpha *pasubiensis, N. agrigentinus agrigentinus, N. agrigentinus contortus, N. heimi, N.* aff. *planycyclum* and *Progeronia ernesti*. As we can see, the assemblage is dominated by aspidoceratids, oppelids and some species of the Nebrodites group, which extinct in the top. In the Sviniţa area, *Sowerbyceras loryi* morpha *loryi* displays its maximum abundance at the mid interval of the zone, marking the Loryi Horizon (sensu Sarti, 1993). The maximum thickness of this interval is about 3 m (in the Lacu Roşu area).

The Cavouri Zone is well argued only in the Sviniţa area (in the Lacu Roşu this interval has not been argued until now, because of the scarce ammonite faunas and is possible to be replaced with the Eudoxus

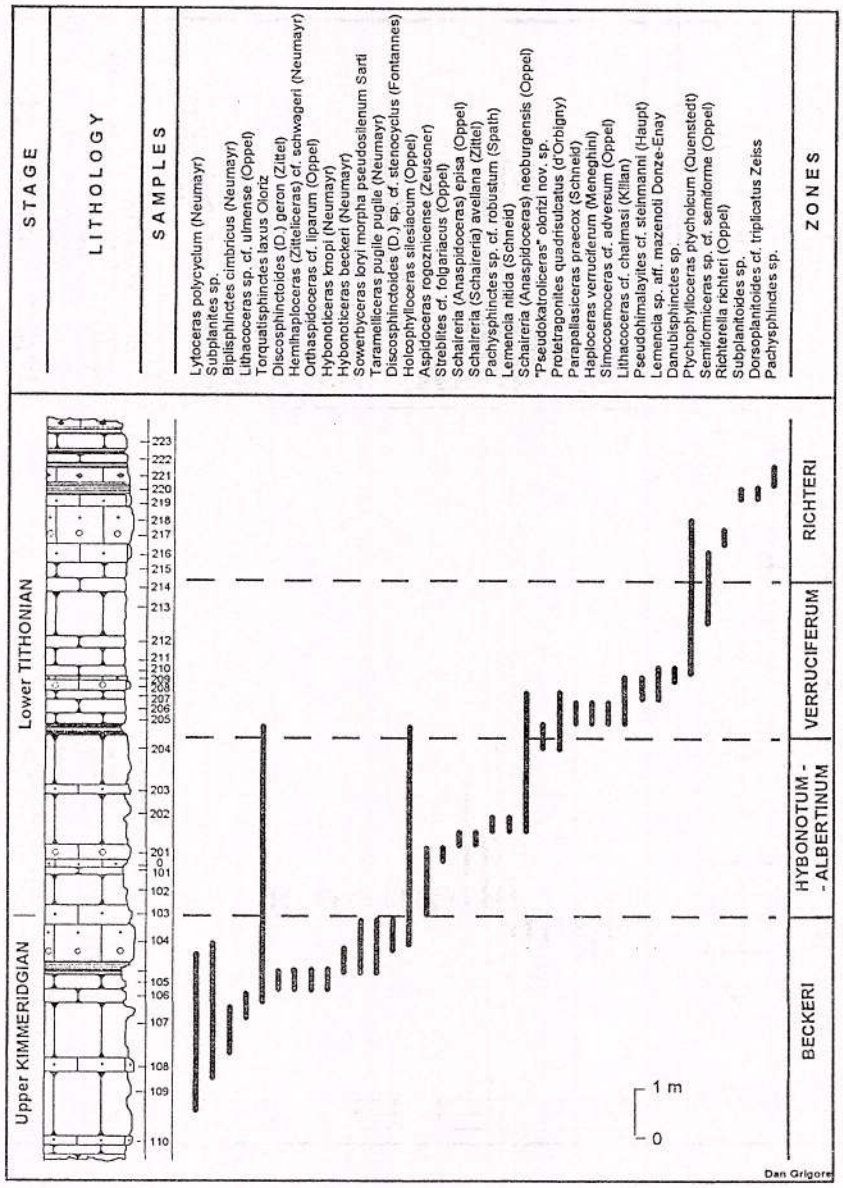

Fig. 4 – Greben Formation - section N Sviniţa ("B"). Lithology, ammonites distribution and Zones. (The lithology legend in Fig. 3).

Zone); its boundaries are marked by the FAD and LAD of Mesosimoceras cavouri. The Eudoxus Zone cannot be recognised until now, by the absence of Aulacostephanus group. The assemblage is dominated in the lower part of its interval by aspidoceratids *(Aspidoceras longispinum, A. hystricosum, A.* aff. *rafaeli, Orthaspidoceras* cf. *gortani, Schaireria (S.) neumayri*) and oppelids (*Hemihaploceras (H.)* aff. *nobile, Taramelliceras (T.) subcallicerum, T. (T.) pugile pseudopugile, T. (T.) pugile pugile)*, while the ataxioceratids (*Discosphinctoides (D.) geron, D. (D.)* cf. *delcampani, Lithacoceras* cf. *ulmense, Torquatisphinctes laxus*) become abundant in the upper part. Among the phylloceratids, *Sowerbyceras loryi* morpha *pseudosilenum* replaces the morphotype *loryi* at the mid of the zone. The interval is of 1 m thick.

The Beckeri Zone is defined as Assemblage Zone (sensu Sarti, 1993) and is argued only in the Lacu Roşu and Sviniţa areas, until now. In the Lacu Roşu area, the lower boundary is marked at the FAD of *Hybonoticeras harpephorum*, the first representative of this group. In the Sviniţa region, the lower boundary is considered at the LAD of *Mesosimoceras cavouri* or the FADs of *Hemihaploceras (Zitteliceras)* taxa; the upper one is marked by the LADs of *Hybonoticeras beckeri* and *Sowerbyceras loryi* morpha *pseudosilenum*

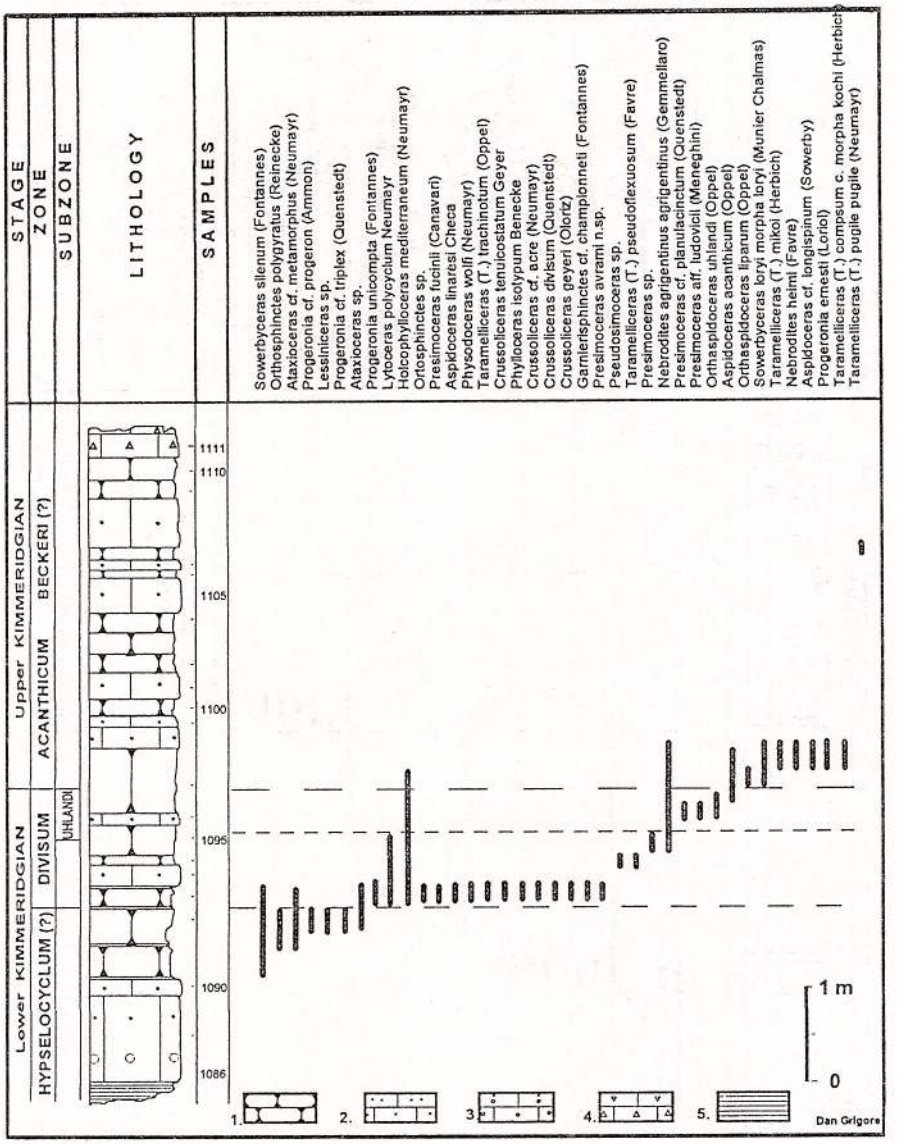

Fig. 5 – Section from the Valea Cetăţii Formation. Lithology, ammonites distribution and Zones. Lithology: 1. nodular limestones; 2. calcarenites; 3. calcirudites; 4. calcareous breccias; 5. marls.

(in both regions). Besides, the assemblage includes: *Hybonoticeras beckeri, H. harpephorum, H. knopi, H.* cf. *pressulum, Hybonoticeras* sp., *Taramelliceras pugile pugile, Hemihaploceras (H.) nobile, H. (Zitteliceras) piccinini, H. (Z.)* cf. *schwageri, Lithacoceras* cf. *ulmense, Discosphinctoides (D.) geron, D. (D.)* cf. *stenocyclus, Biplisphinctes cimbricus, Subplanites* sp. and *Lytoceras polycyclum*. The thickness of this interval is of 3 m.

Up to now, the Lower Tithonian is proved by some pure assemblages, recorded exclussively in the Sviniţa area. The interval corresponding to the Hybonotum - Albertinum Zones, reaching 3.50 m in thickness, is yielded only by common species, such as: *Holcophylloceras silesiacum, Streblites* cf. *folgariacus, Aspidoceras rogoznicense, Schaireria (S.) avellana, S. (Anaspidoceras) episa, S. (A.) neoburgensis, Lemencia nitida, Pachysphinctes* sp. cf. *robustum* and *Torquatisphinctes laxus*; its lower boundary is traced at the LAD of *H. beckeri* and the upper one - below the FAD of *Haploceras verruciferum*.

Owing to the low frequency of the index species, the Verruciferum Zone is mainly accepted on the ground of other species from its ammonite assemblage. Its lower boundary is marked by the FAD of the Haploceras

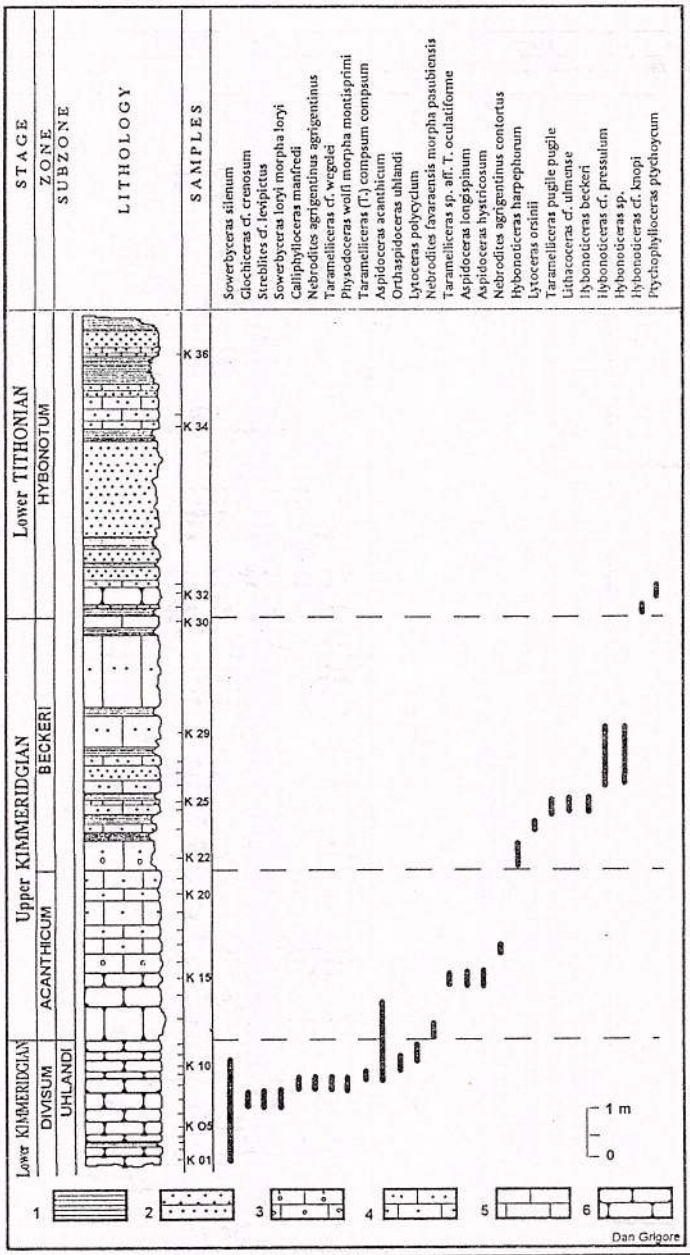

Fig. 6 - Acanthicum Formation - the section "K" from the western walls of Ghilcoş Mt. Lithology, ammonites distribution and Zones. Lithology: 1. marls; 2. sandstones; 3. calcirudites; 4. calcarenites; 5. marly limestones; 6. nodular limestones.

Fig. 7 – Acanthicum Formation - the section in the sliped block "E". Lithology, ammonites distribution and Zones. (The lithology legend in the Fig. 6).

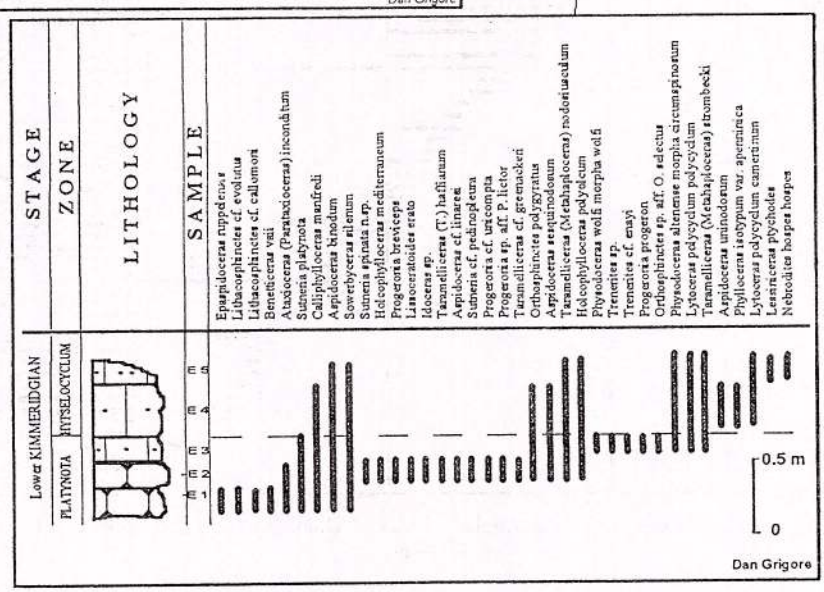

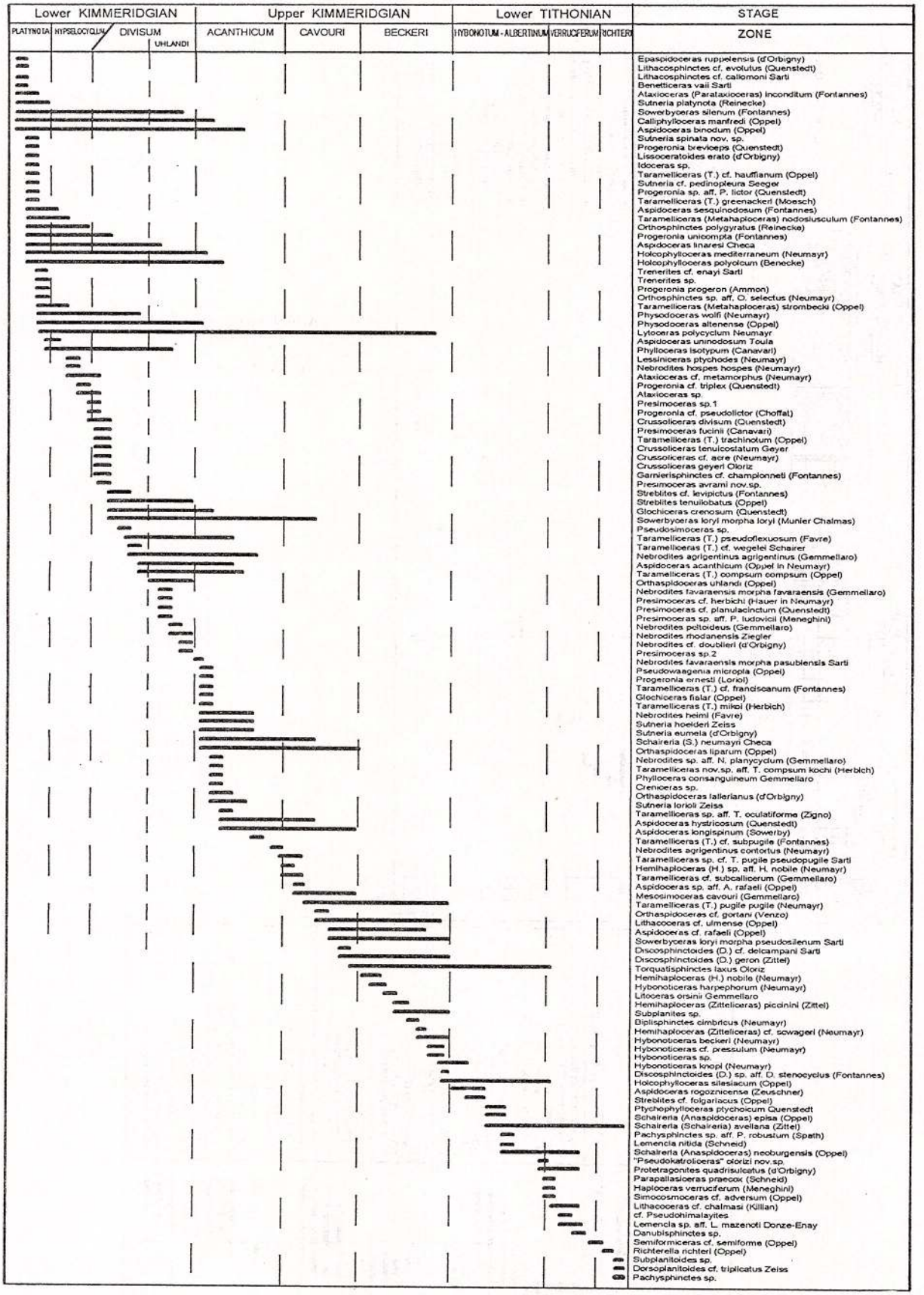

Fig. 8 – General biostratigraphic view of Kimmeridgian - Lower Tithonian ammonites fauna from the studied Carpathians sequences.

verruciferum and the upper one - below the FAD of *Richterella richteri* (interval of 3 m thick). The assemblage comprises some characteristic species, such as *Simocosmoceras* cf. *adversum, Parapallasiceras praecox, Lithacoceras* cf. *chalmasi, Lemencia* aff. *mazenoti, Danubisphinctes* sp. and a new species, *Pseudokatroliceras olorizi.*

The Richteri Zone is until now only purely argued because of the scarce ammonite faunas recorded in the upper part (3 m thick) of the Greben Formation. In this site, only its lower boundary could be recognised. Its pure assemblage still comprises some ataxioceratid species, such as *Richterella richteri, Dorsoplanitoides* cf. *triplicatus, Pachysphinctes* sp. and *Subplanitoides* sp.

As a conclusion, the Kimmeridgian is better developed and richer in fauna than the Lower Tithonian in those sequences which are considered (until now) the best sites of the Carpathians (for these stages).

References

Herbich, F. (1878) Das Szeklerland mit Berücksichtigung der angrenzenden Landesteile, geologisch und paläontologisch beschrieben. *Mitt. Jahresb. kgl. ungar. geol. Anstalt.*, V/2, p. 17-363, Budapest.

Neumayr, M. (1873) Die Fauna der Schichten mit *Aspidoceras acanthicum. Abh.K.K. Geol.R.*,V/6, p. 141-257, Viena.

Oloriz, F. (1978) Kimmeridgiense-Tithonico inferior en el sector central de las Cordilleras beticas (zona subbetica). *Paleontologia. Bioestratigrafia.* Tesis Doctorales Univ. Granada, 758 p, Granada.

Pop, Gr. (1996) Noi apariţii ale Unităţii de Severin in Munţii Almajului (Carpaţii Meridionali). *An. Inst. Geol. Rom.*, 69/1, p. 37-40, Bucureşti.

Răileanu, Gr., Năstăseanu, A. (1960) Contribuţii la cunoaşterea faunei de amoniţi din Jurasicul superior de la Sviniţa. *Stud. cerc. geol.*, Acad.R.P.R., V/1, p. 7-38, Bucureşti.

Sarti, C. (1993) Il Kimmeridgiano delle Prealpi Veneto-Trentine: fauna e biostratigrafia. Mem. *Mus. St. Nat. Verona*, Seria II, Ses. Sc. Terra, 5, 140 p., Verona.

Săndulescu, M. (1984) Geotectonica României. Ed.Tehn., 336 p., Bucureşti.

Plate I

Fig. 1 — *Sowerbyceras silenum* (FONTANNES) (x 1); Râşnov area, Hypselocyclum Zone, level 1091

Fig. 2 — *Aspidoceras sesquinodosum* (FONTANNES) (x 1); Lacu Roşu area, Hypselocyclum Zone, level E 2

Fig. 3 — *Taramelliceras (Taramelliceras)* cf. *hauffianum* (OPPEL) (x 1); Lacu Roşu area, Platynota Zone, level E 2

Fig. 4 — *Streblites tenuilobatus* (OPPEL) (x 1); Lacu Roşu area, Divisum Zone, level G 12

Fig. 5 — *Sutneria (Sutneria) cyclodorsata* (MOESCH) (x 1.7); Lacu Roşu area, Divisum Zone, level A 4

Fig. 6 — *Sutneria (Sutneria) platynota* (REINECKE) (x 1.7); Lacu Roşu area, Platynota Zone, level E 1

Fig. 7 — *Glochiceras (Lingulaticeras) lingulatum* (QUENSTEDT) (x 1); Lacu Roşu area, Platynota Zone, level E 2

Fig. 8 — *Calliphylloceras manfredi* (OPPEL) (x 1); Lacu Roşu area, Platynota Zone, level E 3

Fig. 9 — *Taramelliceras (Taramelliceras) greenackeri* (MOESCH) (x 1); Lacu Roşu area, Platynota Zone, level E 2

Fig. 10 — *Sowerbyceras loryi morpha loryi* (MUNIER CHALMAS) (x 1); Lacu Roşu area, Acanthicum Zone, level A 9

Fig. 11 — *Crussoliceras tenuicostatum* GEYER (x 1); Rasnov area, Divisum Zone, level 1092

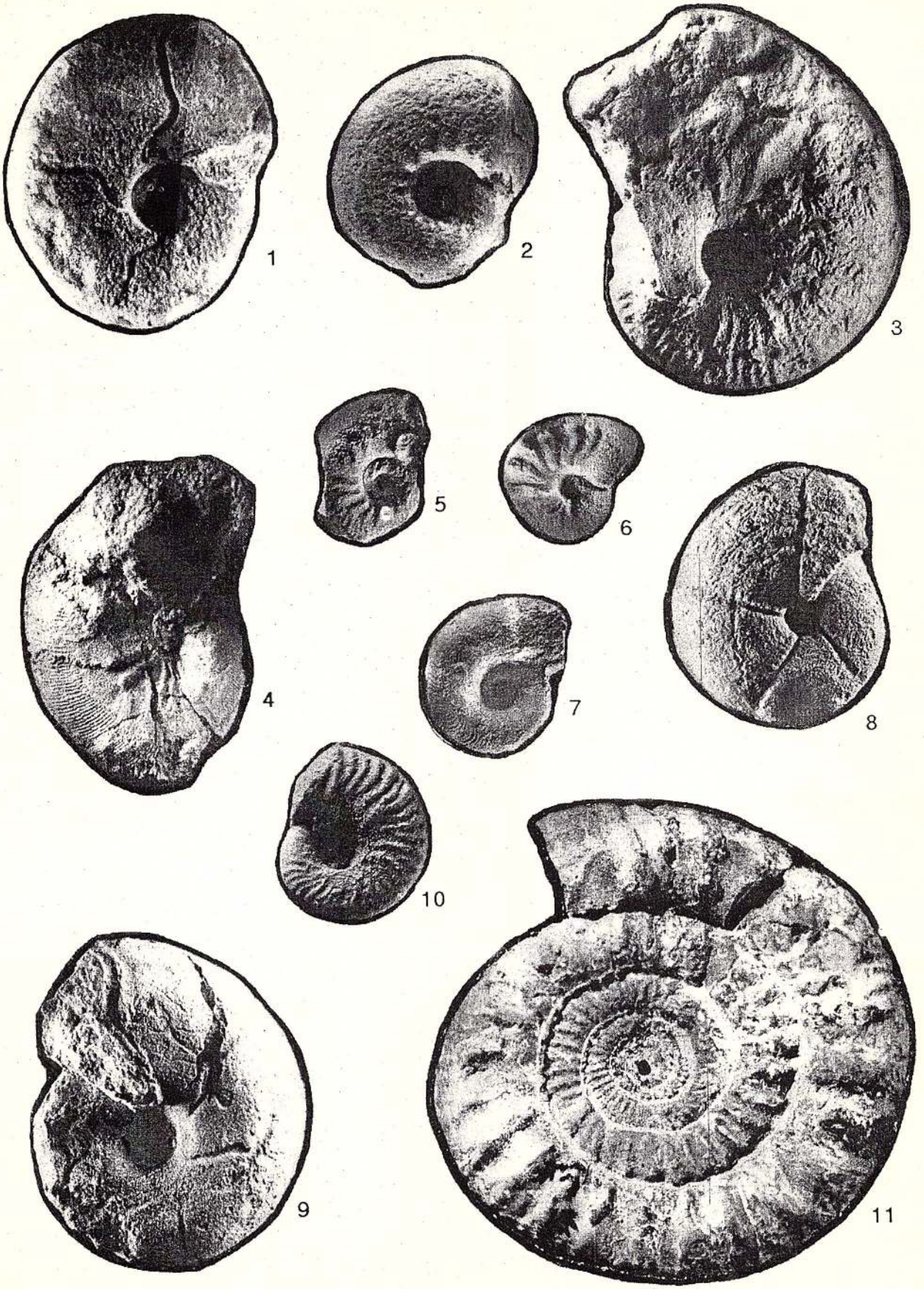

Plate II

Fig. 1 — *Presimoceras herbichi* (HAUER), Preda Colection (x 0.80); Lacu Roşu area, Divisum Zone

Fig. 2 — *Nebrodites agrigentinus contortus* (NEUMAYR) (x 1); Lacu Roşu area, Acanthicum Zone, level K 16

Fig. 3 — *Nebrodites peltoideus* (GEMMELLARO) (x 1); Lacu Roşu area, Divisum Zone, level A 4

Fig. 4 — *Orthosphinctes polygyratus* (REINECKE) (x 1); Lacu Roşu area, Platynota Zone, level E 2

Fig. 5 — *Nebrodites heimi* (FAVRE) (x 1); Lacu Roşu area, Acanthicum Zone, level A 7

Fig. 6 — *Progeronia progeron* (AMMON) (x 1); Lacu Roşu area, Platynota Zone, level E 3

Fig. 7 — *Progeronia unicompta* (FONTANNES) (x 1); Lacu Roşu area, Platynota Zone, level E 2

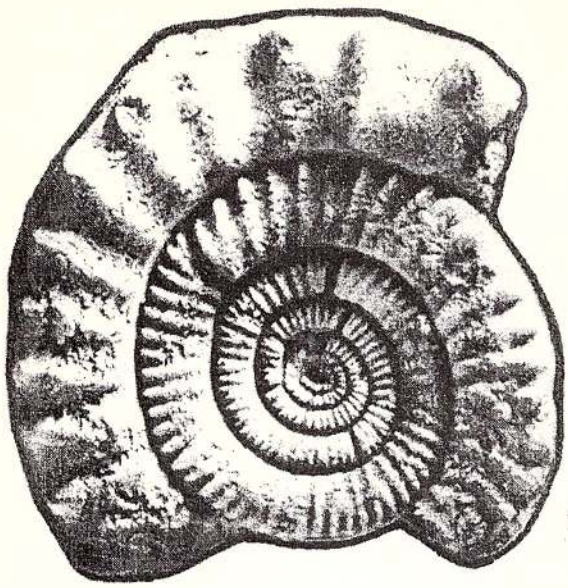
1


2

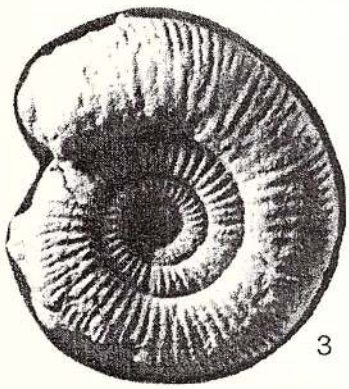
3

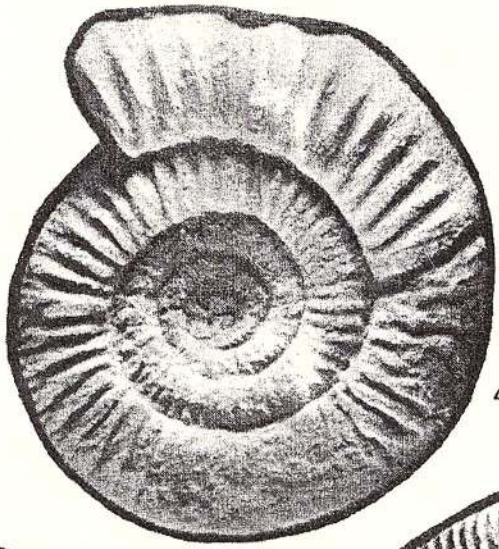
4

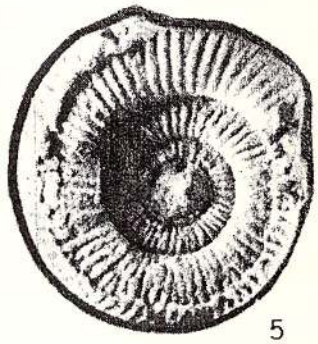
5

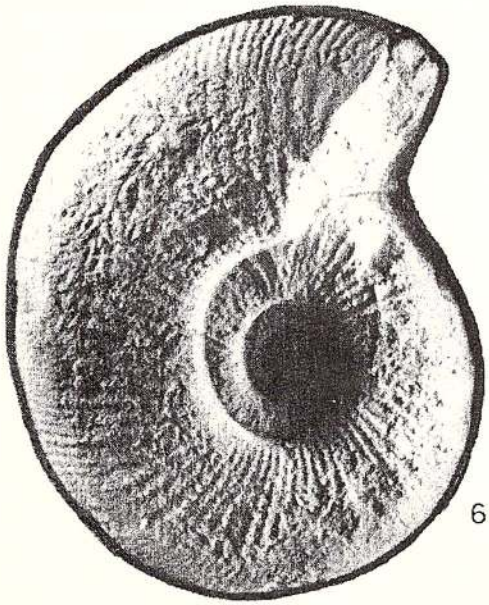
6

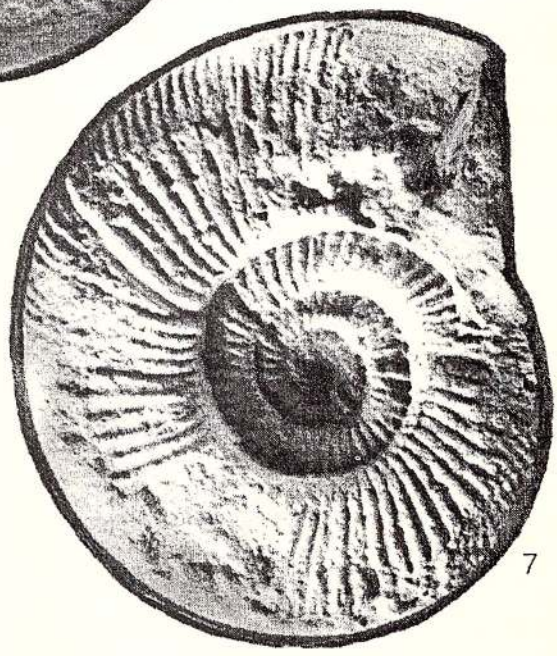
7

Plate III

Fig. 1 — *Hybonoticeras beckeri* (NEUMAYR), Preda Colection (x 1); Lacu Roşu area, Beckeri Zone

Fig. 2 — *Discosphinctoides* sp. aff. *D. stenocyclus* (FONTANNES) (x 1); Sviniţa area, Beckeri Zone, level B 104

Fig. 3 — *Richterella richteri* (OPPEL) (x 1); Sviniţa area, Richteri Zone, level B 216

Fig. 4 — *Subplanites* sp. (x 1); Sviniţa area, Beckeri Zone, level B 105

Fig. 5 — *Mesosimoceras cavouri* (GEMMELLARO) (x 1); Sviniţa area, Cavouri Zone, level A 366

Fig. 6 — *Discosphictoides (Discosphinctoides) geron* (ZITTEL) (x 1); Sviniţa area, Cavouri Zone, level A 369

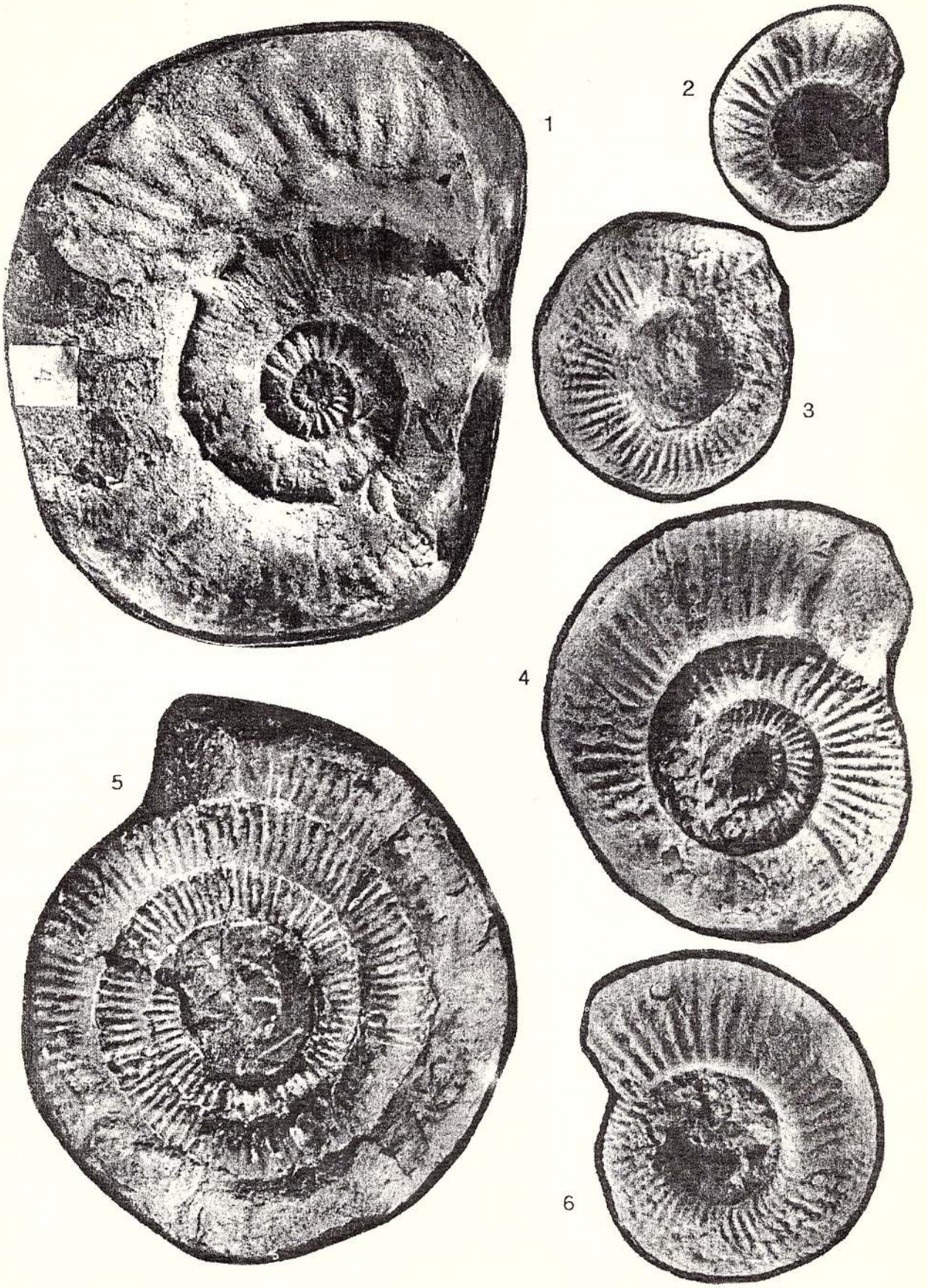

An. Inst. Geol. Rom., 72, part. II, p. 47-54, Bucureşti, 2000

REGIONAL TECTONICS AS INFERRED FROM GRAVITY & GEOIDAL ANOMALIES

Dumitru IOANE, Ligia ATANASIU

Geological Institute of Romania, 1 Caransebeş St., RO-79678 Bucharest 32

Key words: Gravimetric geoid. Gravity anomalies. Integrated interpretation. Regional tectonics. Romania.

Abstract: Lately, the rapid development of gravimetric geoid determination on continental areas offered geophysicists valuable information regarding deep seated density inhomogeneities within the Earth, besides earlier ones, obtained in the oceanic domain. The distribution of the geoidal undulations, closely analysed with better known gravity anomalies (both Bouguer and free-air), may offer new insights on the sub-surface evolution of the main crustal and lithospheric boundaries, as well as information on shallower sources, such as sedimentary basins or crystalline shields. The computation of the free-air and gravimetric geoid maps for the territory of Romania (having as input mean Bouguer gravity anomalies) and of several derived ones, as a result of processing the gravity and geoidal data, offers new possibilities of integrated interpretations on regional tectonics, a valuable additional information on deep-seated geological structures for deep seismics, seismology and MT.

Introduction

Due to the advent of the GPS technology, the urgent need for precise gravimetric geoids on continental areas involved geophysicists in determining gravimetric solutions in order to interpret the geoidal anomalies in connection with the gravity ones in terms of deep density inhomogeneities within the Earth.

The Geological Institute of Romania started a research project based on its national gravity database aimed at computing a gravimetric geoid for the territory of Romania and derive geophysical significances of the geoidal undulations as crustal or lithospheric mass distributions. Using the Bouguer gravity map of Romania, the "free-air" gravity anomalies have been calculated and used as input data to obtain a FFT gravimetric geoid solution, the longest wavelength components being extracted from the OSU91A global geopotential model.

The mean Bouguer values dataset, evaluated in a 5' x 7.5' grid and utilized in geoid computations, have been processed (filtering, total horizontal gradient) in order to provide additional information in an attempt to integrate gravity and geoidal anomalies for geophysical and geological interpretations.

Preliminary results of this study are briefly discussed in the following as "regional" considering the scale of the Romanian territory.

1. Gravity data for the territory of Romania

The Bouguer gravity map of Romania has been built based on the first order gravity network determined in 1976, following two previous attempts of such reference measurements performed by Socolescu (1941-1948) and Botezatu (1956-1960). The gravity observations which covered the whole territory have been carried out during 1961-1987, the resulted 1:200.000 scale map being related to the Potsdam absolute gravity reference value. The Bouguer map has been constructed for two density values (2.20 g/cm^3 and 2.67 g/cm^3) and contoured at 1 mgal interval (Gulie et al., 1992; Nicolescu, Rosca, 1993).

This gravity database, owned by the Geological Institute of Romania, offered the possibility of determinig gravimetric geoid solutions, a first step being represented by the preparation of a mean gravity values data set, evaluated in 5' x 7.5' blocks (Ioane, 1993; Ioane et al., 1996). This work has been done on the gravity

map sheets on the scale 1: 100.000, and produced a number of 2770 mean values assigned to the centre of the 5' x 7.5' blocks, having as maximum and minimum values 30.0 mgal, -136.5 mgal, respectively.

Using the corresponding mean elevations in the 5' x 7.5' blocks (NRB, 1979), whose values are ranging from -8 m in the vicinity of the Black Sea shoreline and 1850 m in the South Carpathians mountainous area, free-air or Faye (Forsberg, 1994) mean gravity anomalies for the Romanian territory have been computed.

2. Geoidal data for the territory of Romania

A paper dedicated to the status of geoid determination in Romania (Gulie et al., 1992) showed at the beginning of the '90 that the only geoid solution computed for the whole territory was the one calculated at the end of the '70 by the Military Topographic Department (Dragomir et al., 1977). Taking into account the normal heights system utilized in Romania and the great number of points with astronomical observations, an astro-gravimetric quasigeoid has been determined, the accuracy of the relative heights being evaluated as ± 0.4 - ± 0.5 m, with contour lines drawn at 0.5 m interval.

The activity dedicated to determine a gravimetric geoid for the territory of Romania started at the Geological Institute of Romania in 1993 as a consequence of the great interest shown by geophysicists, on a world wide scale, to interpret geoidal data in terms of geological deep structures. The gravity database owned by the Geological Institute of Romania has been considered suitable for obtaining information on the geoid undulations distribution on the national territory, considering that the accuracy required for geophysical purposes is considerably lower than for geodetic ones.

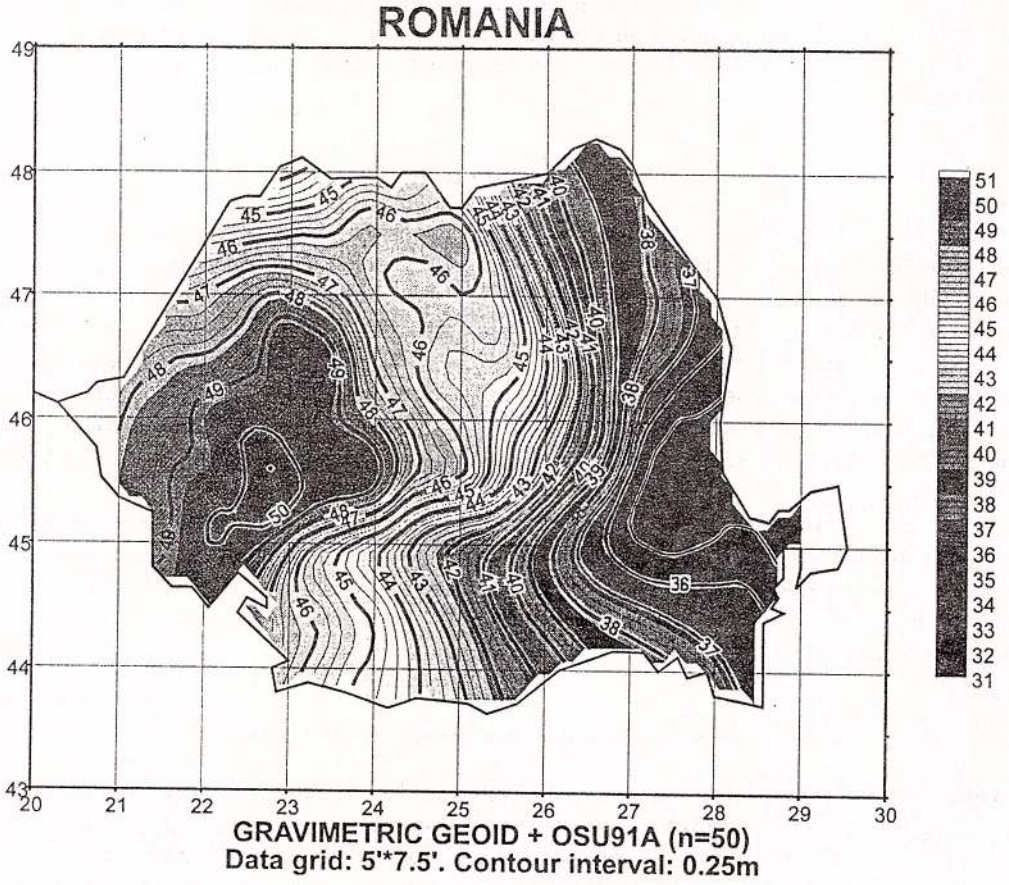

Fig. 1 - Gravimetric geoid for the territory of Romania

Since every method used for a gravimetric geoid determination evaluates the Stokes integral, an immediate consequence is the need of a global coverage with gravity anomalies. When such gravity information is not available, the restriction may be avoided in the presence of a global geopotential model which provides the

long wavelength components of the gravity field, the quality of the geopotential model in the studied region being of great importance for the accuracy of the final geoid solution. Due to the limited computing facilities and the possibility of having as input gridded gravity anomalies and as output gridded geoidal undulations, Fast Fourier Transform procedure has been used to evaluate the Stokes integral in planar approximation, the FFT gravimetric geoid being drawn at 0.25 m interval (Fig. 1).

OSU91A global geopotential model (Rapp et al., 1991), which provided the long wavelength components for this gravimetric geoid solution for the Romanian territory, combined 30' x 30' mean gravity anomalies derived from terrestrial and altimetric data with the GEM-T2 satellite-only solution, being complete to degree and order 360. In areas devoid of observational data, the authors used a gravitational model based on a combination of low-degree potential coefficients from the satellite model, augmented by high-frequency information implied by the topography and its isostatic compensation (Rapp, Pavlis, 1990).

Lately, an improved global geopotential model has been released, EGM96 including homogeneous terrestrial gravity data for the region where Romania is located. The new European Gravimetric Geoid (EGG97) used similar gravity information as those included in EGM96, offering a more detailed picture of the geoid undulations over the European continent.

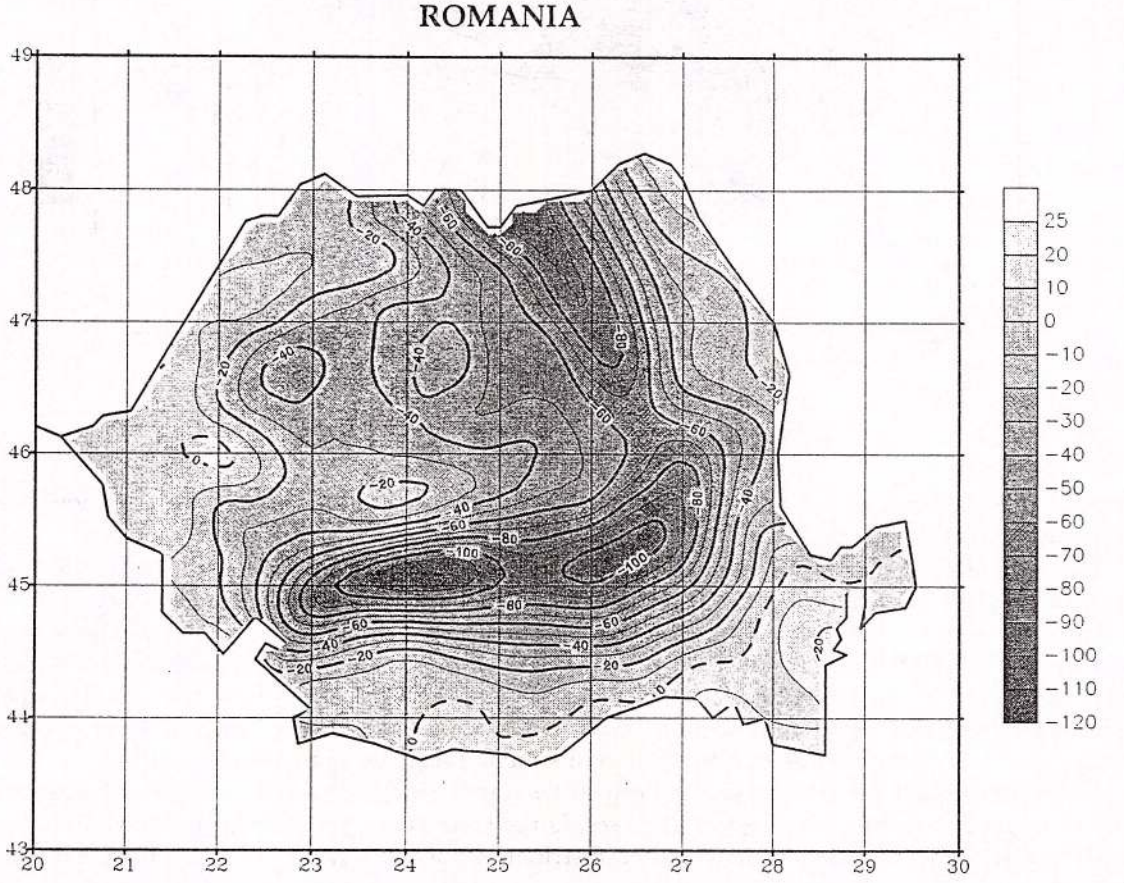

Fig. 2 – Filtered gravity Bouguer anomalies (L = 40 km)

3. Processing of the gravity and geoidal anomalies

In view of obtaining more geophysical information which might be related to the location of the major geological units and to regional tectonics, the Bouguer gravity data have been processed, benefiting of the 5' x 7.5' gridded mean values. Applying a traditional filtering procedure in Romanian geophysics called "running averages", two gravity maps over the Romanian territory have been derived: "filtered" Bouguer gravity anomalies (Fig. 2) and residual Bouguer gravity anomalies (Fig. 3). In an attempt to better emphasize particular geophysical features, which may be correlated with main geological structures due to the

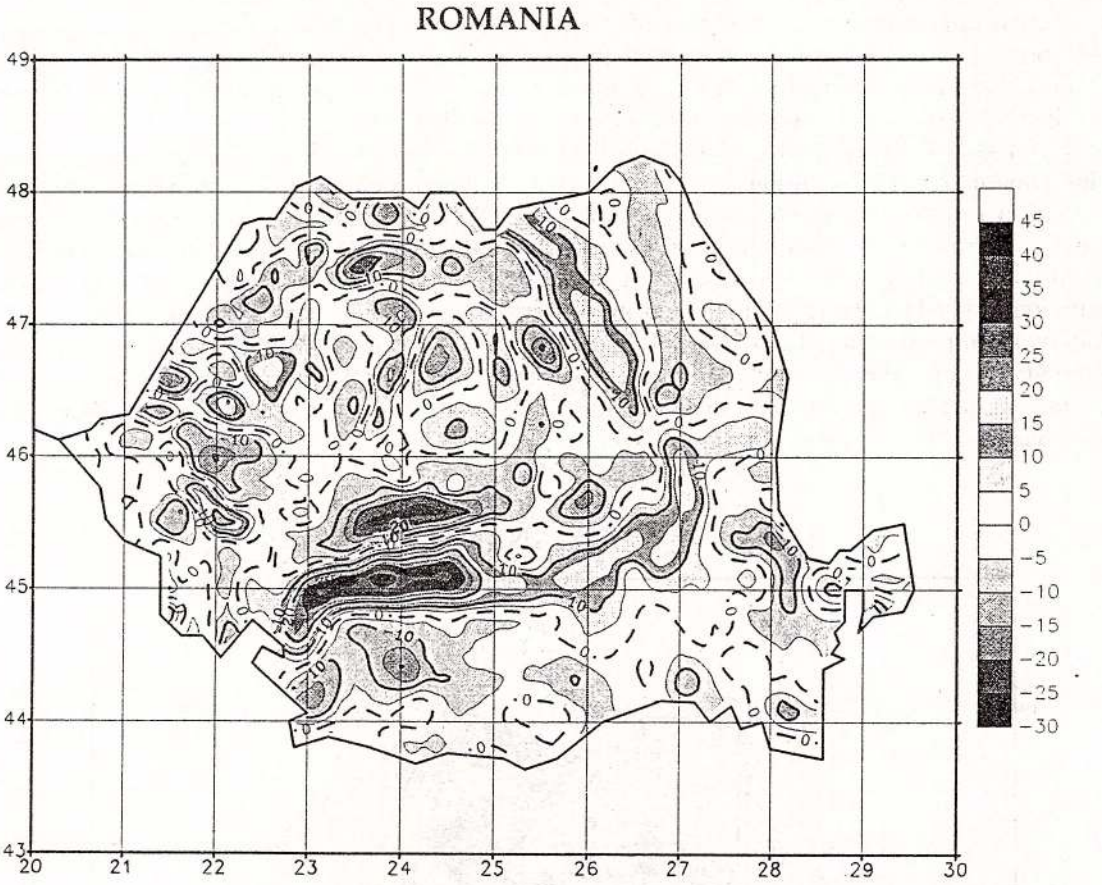

Fig. 3 – Residual gravity Bouguer anomalies (L = 80 km)

presence of significant density contrasts, the data array for computing the above mentioned maps was designed differently: L = 40 km for the filtered map and L = 80 km for the residual one.

The computation of the total horizontal gradient of the Bouguer anomalies over the Romanian territory, based on the gravity gridded mean values, represents a suitable way for revealing the location and direction of important density contrasts between geological units, such as major faults and/or contacts of magmatic, metamorphic or salt bodies, practical possibilities of calculating and interpreting such data in Romania being shown in Proca et al., 1993; Ioane, 1997; Ioane, 1999 . The map of the total horizontal gradient of the residual Bouguer anomalies, calculated at the scale of the territory of Romania is, in our opinion, a good example for illustrating the use of gravity data in studying regional tectonics (Fig. 4).

A useful technique for showing particular features contained by the gravity and geoidal anomalies, which may be of great interest for geological purposes, is the computation of the free-air/gravimetric geoid ratio (Bowin et al., 1986; Featherstone, 1992), its distribution on the territory of Romania being displayed in Figure 5.

4. Geoidal undulations and regional tectonics

The gravity anomalies (free-air, Bouguer, isostatic), some of the main geophysical features of the Earth, are for a long time analysed and geologically interpreted in view of deriving information on the geological structures, tectonics and geodynamics of the crust and lithosphere.

The geoidal undulations, which determine the figure of the Earth, represent the equipotential surface which best approximates the sea level. Similarly with the gravity anomalies, their amplitude and areal distribution reflect large-scale density inhomogeneities within the topography, crust and mantle; however, there are also significant differences (Ioane et al., 1993):

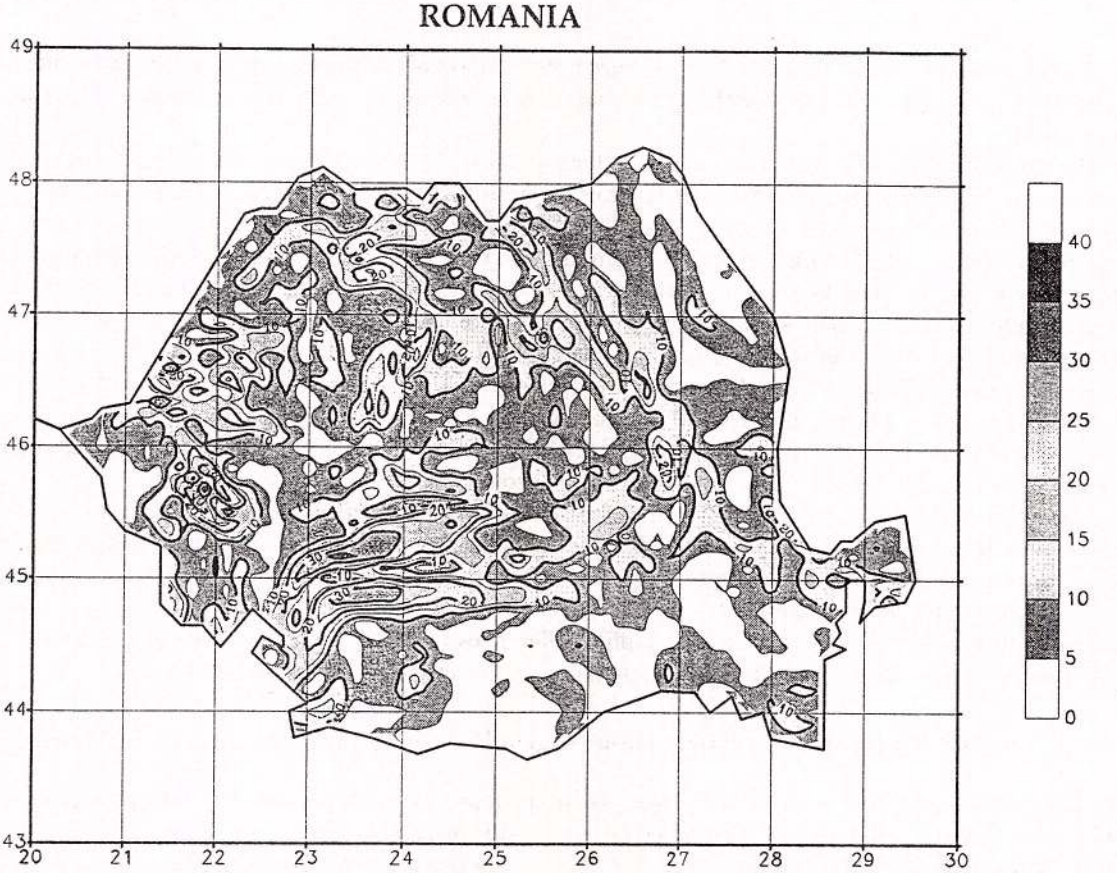

Fig. 4 – Total horizontal gradient of residual Bouguer gravity anomalies

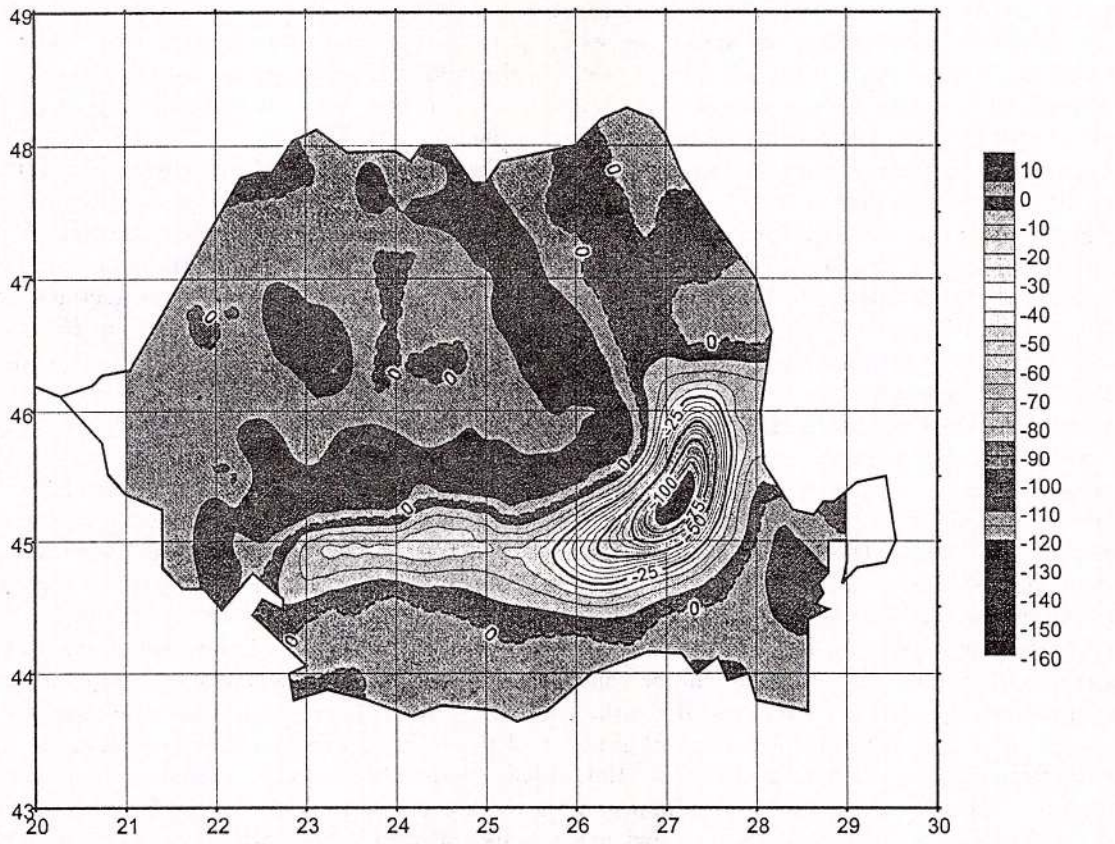

Fig. 5 - Map of free-air/gravimetric geoid ratio

- the dependence on the distance to the source of the anomaly is proportional with 1/r in the case of the geoidal anomalies and with $1/r^2$ for the gravity anomalies, implying much deeper density contrasts revealed by the geoid;
- the geoidal anomalies are smoother and larger than the gravity ones, showing effects of deep mass distributions, which may not be observed in gravity maps due to higher frequency components.

The geophysical interpretation of the geoidal anomalies (undulations) on continents started much later, comparing to those observed on the oceanic domain, due to difficulties in determining regional precise gravimetric geoids (confidentiality regime of the gravity terrestrial data) and to the higher complexity of the geological and tectonic features. For both oceanic and continental domains, it was stated that intermediate and short wavelengths in the geoid may originate in mass distributions within the lithospheric and crustal structures (Chase, 1985). In order to emphasize high frequency features of the geoidal anomalies (interesting for tectonics and geodynamics), the geoid height content assigned to the upper mantle may be removed by the "detrending" procedure, a high-pass filtering. The results of such a spectral study can be correlated with major density inhomogeneities or discontinuities, located at different depths. Considering the shortest wavelength anomalies which may be related to near-surface geological structures, geoidal high anomalies correspond to old and compacted rocks (continental shields), while low geoidal anomalies reflect large sedimentary basins or large acidic igneous intrusions (Featherstone, 1992). Rapid variations of the geoidal height values along alignments extended over several hundred kilometres may reveal major contacts of tectonic units (having important petrographic differences and corresponding density contrasts) or abrupt modifications on the chemical and mineralogical content of crustal or lithospheric blocks.

5. On the integrated interpretation of gravity and geoidal anomalies in Romania

A basic statement of geophysicists involved in the analysis and geophysical interpretation of geoidal anomalies is that such data must be studied in connection with the gravity ones, the information obtained from the geoid deriving from the Earth gravity field and being hence a complementary one. In the following we intend to show the usefulness of an integrated approach in analysing gravity derived quantities and to offer some preliminary interpretations referring to the Romanian territory.

Speaking first about the gravity anomalies, we are pointing out the particular importance of the available mean gravity values dataset (5' x 7.5' - Ioane, 1993) which allows different processing procedures to be more easily performed, enhancing this way the possibility of distinguishing mass distributions of geological interest within the topography, the Earth's crust and the lithosphere.

Inspecting the filtered Bouguer gravity anomalies (Fig. 2) one may deduce different crustal thickness over platforms (the higher gravity values over the Moesian Platform being associated with lower crustal thickness, comparing with the south-western end of the East European Platform, characterized by lower gravity values). The relatively high gravity values observed on the eastern end of the Pannonian Basin are to be also correlated with low crustal thickness, a well-known specific feature of this geotectonic unit.

The residual Bouguer gravity map (Fig. 3) shows a multitude of effects due to local (at the scale of the Romanian territory) and shallower sources, their analysis and geological interpretation being ascribed to "further work" intentions. Discussing briefly several residual gravity anomalies which might be of a certain importance at the regional scale, we should point out the elongated low anomalies, which accompany the East and South Carpathians, covering their eastern and southern extremities, respectively. Considering that the sources of such anomalies may have a near-surface location, we interpret that most of these gravity effects are explained by young, low density sedimentary deposits (including salt bodies), which develop along the Carpathians. Discontinuities and/or change of their strike are to be correlated with tectonics and geodynamics processes, most spectacular being, in our opinion, those outlined at the East Carpathians Bend Zone and western half of the South Carpathians.

Of particular interest for regional tectonics we consider the maps of total horizontal gradient of Bouguer anomalies, which are able to locate major contacts of important tectonic units and regional faults (the latter reaching many times transcrustal depths), due to sudden density contrasts generated by tectonic processes. The map of the total horizontal gradient of the residual Bouguer gravity anomalies, calculated over the Romanian territory (Fig. 4 - Ioane, 1997; Ioane, 1999), shows elongated high anomalies of regional significance especially in the East Carpathians and in the north-eastern region of the Moesian Platform, the mass distributions in the near-surface geological structures offering good possibilities of tracing for example the NNW development of the Peceneaga-Camena transcrustal fault.

The gravimetric geoid map determined for the territory of Romania (Fig. 1 - Ioane et al., 1996; Ioane, Atanasiu, 1998) displays as main features two major domains with specific characteristics: a region located on the eastern and southern parts of the territory, characterized by low values of the geoidal heights and a region situated in the western and south western parts of the territory, showing higher values of the geoidal heights. They are separated by an elongated zone of rapid variations, which crosses Romania from NE to SW. As "local" aspects, we may emphasize the geoidal low anomaly situated out of the East Carpathians Bend Zone and the geoidal high covering the Apuseni Mts and the western half of the South Carpathians, while the Transylvanian Basin shows small geoidal variations, in an area bordered by important alignments of "horizontal gradients" of height values variation.

A brief comment on the geophysical significance of the above-mentioned geoidal features states that the two major domains separated on the gravimetric geoid map correspond to either higher (lower geoidal heights) or lower (higher geoidal heights) crustal and lithospheric thickness, the intense "horizontal gradient" alignment which accompanies the East Carpathians representing the effect of a significant step of the Earth's crust and lithosphere, in close associatiation with the TTZ.

The map of the free-air gravity/gravimetric geoid ratio (Fig. 5), designed to emphasize shallow features of the mass distributions within the studied region, outlined very nicely the areal extent of the main sedimentary basins located out of the Carpathians. Considering magnetotelluric soundings results (Stănică, Stănică, 1998), the highest thickness of the sedimentary deposits reaches up to 18 km at the East Carpathians Bend Zone, within the well-known Focsani Depression. Even the Bouguer gravity map of Romania (Nicolescu, Roşca, 1993) located the lowest gravity values south of the western half of the South Carpathians (which would imply greatest depth of the sedimentary basin), the combined free-air gravity and geoidal information pointed out by means of the highest ratio values the Focsani Depression as deepest sedimentary pile out of the Carpathians, in good agreement with interpretations of seismic and MT data.

Acknowledgements: The authors wish to acknowledge that an important part of the data presented in this paper have been obtained during a scientific project financed by a Romanian Academy/Ministry of Research and Technology grant. Dr. J.G. Olliver from the University of Oxford is thanked for kindly offering the OSU91A global geopotential model.

References

Bowin, C., Scheer, E., Smith, W. (1986) Depth estimations from ratios of gravity, geoid and gravity gradient anomalies. *Geophysics*, 51, 1, p. 123-136.

Chase, C. G. (1985) The geological significance of the geoid. *Ann. Rev. Earth Planet. Sci.*, 13, p. 97-117.

Featherstone, W. E. (1992) A GPS controlled gravimetric determination of the geoid of the British Isles. Ph.D. Thesis, Univ. of Oxford, Oxford.

Forsberg, R. (1994) Terrain effects in geoid computations. *Lecture Notes*, Milano.

Dragomir, V., Ghitau, D., Mihailescu, M., Rotaru, M. (1977) Teoria figurii Pământului. Editura Tehnică, 664 p, Bucuresti.

Gulie, N., Popescu, I., Rosca, V., Ioane, D. (1992) The status of geoid determination in Romania. *Proceedings of the First Continental Workshop on the Geoid in Europe*, Prague.

Ioane, D. (1993) Actual developments of geoid determination in Romania. *Proceedings of the Second Workshop "GPS in Central Europe"*, Penc.

— **, Olliver, J., Radu, I., Atanasiu, L. (1993)** Geophysical significances of the geoidal anomalies. *Rev. Roum. Geophysique*, 37, p. 9-18.

— **, Atanasiu, L., Rogobete, M. (1996)** Gravimetric geoid for the territory of Romania. *Terra IV Vol.*, p. 70-85, Bucuresti.

— **(1997)** Contribuţii metodologice şi de interpretare la cercetarea gravimetrică, magnetometrică, spectrometrică gama şi mercurometrică a mineralizatiilor asociate eruptivului neogen din Romania. Teza de doctorat, Univ. Bucuresti, Bucuresti.

— **, Atanasiu, L. (1998)** Gravimetric geoids and geophysical significances in Romania. Mon. South Carpathians, Reports on Geodesy, 7 (37), p. 157-175, Warsaw.

— (1999) Posibilităţi actuale de utilizare a gradientului orizontal total al anomaliei gravităţii. *Studia (submitted)*, Cluj-Napoca.

Nicolescu, A., Rosca, V. (1993) Harta gravimetrică Bouguer, Romania, scara 1: 1.000.000. I.G.R., Bucuresti.

NRB (1979) Atlas von Karten mit mittleren gelandehohen nach trapezen mit den massen 5' x 7,5' und 10 x 10 für die Länder Europas und die teil von Asien und Afrika, Sofia.

Proca, A., Nicolau, V., Veliciu, S. (1993) Faults in the Miercurea Ciuc Basin Depicted by Gravity and Geothermics. *Rom. J. Geophys.*, 16, p. 45-52.

Rapp, R. H., Pavlis, N. K. (1990) The development and analysis of geopotential coefficient models to spherical harmonic degree 360. *J. Geophys. Res.*, 95, p. 21885-21911.

Rapp, R. H., Wang, Y. M., Pavlis, N. K. (1991) The Ohio State 1991 geopotential and sea surface topography harmonic coefficient model. *Rep. No. 410, Ohio State University*, Columbus.

Stănică, D., Stănică, M. (1998) 2D modelling of the geoelectrical structure in the area of the deep-focus Vrancea earthquakes. *Mon. South Carpathians, Reports on Geodesy*, 7 (37), p. 193-203, Warsaw.

An. Inst. Geol. Rom., 72, part. II, p. 55-58, Bucureşti, 2000

PIEMONTITE PORPHYROIDS FROM VALEA SEACĂ (TULGHEŞ GROUP, EAST CARPATHIANS ROMANIA) - EVIDENCE FOR A FAULT-RELATED METASOMATISM

Marian MUNTEANU, ŞTEFAN MARINCEA

Geological Institute of Romania, 1 Caransebeş St., RO-79678 Bucharest 32

Key words: Piemontite. Phengite geobarometry. East Carpathians. Romania

Abstract: Grossular-spessartine garnet formed locally in the metarhyolites from Valea Seacă, at the contact with Mn mineralizations. Subsequently, piemontite and clinozoisite formed on the garnet. The occurrence of the piemontite is assigned to the circulation of oxydizing fluids along the Valea Seacă fault system.

Introduction

The metamorphic terranes of the East Carpathians have a complex tectonics, implying Alpine and pre-Alpine thrust nappes. The piemontite porphyroids from Valea Seacă occur in the pre-Alpine Putna Nappe of the Alpine Bucovinian Nappe. Putna Nappe is built up by the rocks of the Tulgheş Group, Cambrian in age, metamorphosd under greenschist facies P-T conditions (quartz-sericite-chlorite schists±albite±graphite, black quartzites, carbonate-schists, porphyroids and a few actinolite amphibolites). The Tulgheş Group has been divided into four formations: Tg1 (quartzitic-phyllitic formation), Tg2 (graphitic formation± Mn), Tg3 (acidic metavolcanic formation with sulfides) and Tg4 (phyllitic-blastodetrital formation).

Porphyroids are common in Tg3 Formation of the Tulgheş Group. They have a rhyolitic composition (Tab. 1) and are build up essentially by quartz, plagioclase and alkali-feldspars as phenocrysts in a fine-grained matrix of the same composition. Muscovite is always present in the matrix.

Chemistry and Mineralogy

In the East Carpathians piemontite has been reported only in iron and manganese deposits. The piemontite porphyroids described in this study are abnormally Mn-rich over 1 % MnO_{Total}, while the ordinary porphyroids of the Tulgheş Group never reach 0.1 % MnO_{Total}. They have a CaO content fairly above the average (Tab. 1). Beside the piemontite they contain quartz, phengite, albite and garnet.

Table 1. Composition of piemontite porphyroids compared to the composition of common porphyroids

Rock Type	SiO_2	TiO_2	Al_2O_3	Fe_2O_3	FeO	MnO	MgO	CaO	Na_2O	K_2O	P_2O_5	H_2O	CO_2
Common porphyroids	76.10	0.10	11.92	0.93	0.16	0.00	0.91	0.26	3.04	3.04	0.02	1.13	0.00
Piemontite porphyroids	75.78	0.00	12.19	0.84	0.21	1.09	0.79	3.64	2.14	1.80	0.02	1.20	0.00

Piemontite occurs as tiny rounded to subhedral crystals. Its unit cell parameters (determined from 35 reflexions in the X-ray powder pattern, after 6 cycles of least-squares refinement) are: a = 8.903(7) Å, b = 5.671(3) Å, c = 10.132(7) Å, $\beta = 115.12(4)^0$. The piemontite from Valea Seacă (defined as recommended by Catti et al., 1989) contains 0.35-1 apfu Mn^{+3} and up to 0.27 apfu Fe^{+3}. Mn^{+2} replaces calcium at a concurrence of 0.28 apfu (Tab. 2).

Piemontite has grown on a garnet having an intermediary composition between spessartine and grossular: 57-75 % spessartine and 21-41 % grossular (Tab. 3).

A ferrian clinozoisite (0.29-0.38 apfu Fe^{3+}, 0.04-0.18 apfu Mn^{3+}) developed on piemontite, forming composite crystals with a core showing piemontite pleochroism and colorless rims. In the samples that preserved the porphyroid structure the epidote minerals are linearly disposed along the foliation. When the rocks are intensely transformed, the piemontite forms compact masses or intergrowths with phengite. The phengite has a celadonite content of 15-30 %. The albite (An up to 1 %, Or up to 0.5 %) has formed metasomatically on former K-feldspars (Or_{96-97}, Ab_{2-4}, $An_{0-0.16}$) which are preserved as very sparse relics.

Table 2 - Piemontite (piem) and clinozoisite (clz) compositions

Sample	H343	H344	H348	H349	B3461	B3463	B3464	H346	H345	H342	B3463	B3465
Mineral	clz	clz	clz	clz	piem	piem	piem	piem	piem	piem	piem	piem
SiO_2	38.60	38.38	37.59	38.16	37.08	40.63	37.85	39.61	36.97	39.30	38.20	36.61
TiO_2	0	0.07	0	0	0.11	0.11	0.25	0	0.12	0.21	0.11	0.21
Al_2O_3	27.35	27.92	29.16	28.49	26.63	25.04	26.22	23.53	20.77	19.62	23.39	23.28
Fe_2O_3	5.02	6.53	6.21	6.35	4.5	4.02	3.96	3.43	0.78	0.92	3.83	2.81
Mn_2O_3	2.97	1.18	0.62	1.06	5.85	6.99	5.84	9.96	15.78	17.05	9.22	11.45
MnO	0	0.18	0	0	1.27	0.54	1.25	0	4.02	0.85	3.16	2.30
CaO	23.97	23.86	24.56	24.05	22.85	20.66	22.76	21.51	19.72	20.07	20.15	21.52
Na_2O	0.18	0.005	0	0.005	0.02	0.009	0	0.3	0.01	0.04	0.05	0
H_2O	1.93	1.92	1.88	1.91	1.86	2.04	1.89	1.98	1.85	1.97	1.91	1.83
Total	100.02	100.05	100	100.03	100.17	100.04	100.02	100.3	100	100	100	100.01
Number of ions on the basis of 8 cations												
$\#Si^{+4}$	3.00	2.99	2.91	2.96	2.91	3.21	2.97	3.13	2.99	3.19	3.05	2.93
Al^{IV}	0	0.01	0.09	0.04	0.09	0	0.03	0	0.01	0	0	0.07
T site	3	3	3	3	3	3	3	3.13	3	3.19	3.05	3
Al^{VI}	2.49	2.55	2.60	2.57	2.37	2.33	2.40	2.20	1.96	1.88	2.20	2.12
$\#Ti^{+4}$	0	0	0	0	0.01	0.01	0.01	0	0.01	0.01	0.01	0.01
$\#Fe^{+3}$	0.29	0.38	0.36	0.37	0.27	0.24	0.23	0.20	0.05	0.06	0.23	0.17
$\#Mn^{+3}$	0.18	0.07	0.04	0.06	0.35	0.42	0.35	0.60	0.97	1.05	0.56	0.70
O site	2.96	3.00	3.00	3.00	3.00	3.00	3.00	3.00	3.00	3.00	3.00	3.00
$\#Mn^{+2}$	0.00	0.01	0.00	0.00	0.07	0.04	0.08	0.00	0.28	0.06	0.21	0.16
$\#Ca^{+2}$	2.00	1.99	2.04	2.00	1.93	1.75	1.92	1.82	1.72	1.75	1.73	1.84
$\#Na^{+1}$	0.04	0	0	0	0	0	0	0.05	0	0.01	0.01	0
A site	2.04	2.00	2.04	2.00	2.00	1.79	2.00	1.87	2.00	1.81	1.95	2.00
cations	8.00	8.00	8.00	8.00	8.00	8.00	8.00	8.00	8.00	8.00	8.00	8.00

Geothermobarometry

Tentative P and T determinations were based on the phengite barometry (Massonne and Schreyer, 1987), plagioclase-muscovite thermometry (Green and Usdansky, 1986) and two feldspar thermometry (Brown and Parsons, 1981). Taking into account that the Si content in phengite is of about 3.3 apfu [to 10 (O) and 2 OH pfu] a minimum pressure of about 7kb results for a temperature of at least 250°-300°C. Two feldspar thermometry suggests temperatures of about 300°C. Assuming the 7kb pressure, the plagioclase-muscovite thermometer indicates temperatures of 330°-360°C. These values may be doubty because plagioclase muscovite geothermometer has not been calibrated below 490°C.

The only data to compare with are the P-T determinations done by Roşu et al. (1998). The authors reported T=300°-370°C and P=3.6-4.4 kb using arsenopyrite thermometry and sphalerite barometry in the

sulfide deposits of the Tg3 Formation. The pressures determined by us are considerably higher. We take this as indicative for a tectonic factor that influenced the evolution of the piemontite porphyroids.

Table 3. The composition of garnets of the piemontite porphyroids from Valea Seacă

Sample	BR3461	BR3462	BR3463	BR3464	BR3465
SiO_2	37.16	36.99	37.55	36.38	36.44
TiO_2	0.14	0.22	0.13	0.15	0.18
Al_2O_3	20.75	20.86	20.43	20.59	21.03
Fe_2O_3 *	0.54	0.58	0.68	0.60	0.58
Mn_2O_3*	0.85	0.68	1.13	1.40	0.78
MnO	27.97	27.29	24.82	29.61	28.84
MgO	0.03	0.07	0.07	0.03	0.03
CaO	12.55	13.30	15.29	11.38	12.06
Total	99.98	100.00	100.09	100.14	99.94
Number of ions on the basis of 16 cations					
$\#Si^{+4}$	5.93	5.90	5.96	5.85	5.85
$\#Al^{IV}$	0.07	0.10	0.04	0.15	0.15
T site	6.00	6.00	6.00	6.00	6.00
$\#Al^{VI}$	3.83	3.83	3.78	3.76	3.82
$\#Ti^{VI}$	0.02	0.03	0.02	0.02	0.02
$\#Fe^{+3}$	0.05	0.06	0.07	0.05	0.06
$\#Mn^{+3}$	0.10	0.08	0.14	0.17	0.10
O site	4.00	4.00	4.00	4.00	4.00
$\#Mn^{+2}$	3.85	3.69	3.34	4.03	3.92
$\#Mg^{+2}$	0.01	0.02	0.02	0.01	0.01
$\#Ca^{+2}$	2.14	2.27	2.60	1.96	2.07
A site	6.00	5.98	5.95	6.00	6.00

Genesis

At least two mineral assemblages can be distinguished in the piemontite porphyroids: an older one, containing garnet+quartz+K-feldspar+plagioclase, and a younger one, with piemontite+clinozoisite+phengite+albite+quartz. The former resulted from the interaction between the Cambrian rhyolites of Tg3 Formation and the protoliths of the nowadays black quartzites of Tg2 Formation, containing a minor Mn mineralization. The Mn-Ca carbonates reacted with the acidic rocks to form Mn-Ca garnets. Subsequently, the garnet-bearing porphyroids have been affected by extended shearings that belong to the Valea Seacă fault system. Faulting-related mylonitization enabled circulation of oxidizing solutions. The oxidation of Mn^{2+} to Mn^{3+} instabilized the garnets that dissoluted in order to form piemontite. Concurrently, the plagioclase and K-feldspar were replaced by an almost pure albite. The released Ca participated to the formation of the epidote minerals and the potassium has been fixed in phengite. Noteworthy, many porphyric albite crystals have phengite rims.

The composite crystals, with piemontite cores and clinozoisite rims are the result of changes in fluid composition. The early fluids leached the Mn from the crushed garnets and enabled the piemontite formation. The later fluids had less Mn to leach, their composition became Mn-poorer and they formed clinozoisite

instead of piemontite. The essential role of the fluids in the formation of the epidote minerals is proved by the fact that in the less mylonitized zones, where the garnets preserved uncrushed, the piemontite formed only as veins along cracks.

Conclusions

The piemontite porphyroids from Valea Seacă preserved a metasomatic assemblage, partly altered due to oxidizing fluids that circulated along faults. This paper reports for the first time garnet and piemontite in the East Carpathian porphyroids.

References

Brown, W. L., Parsons, I. (1981) Towards a more pratical two feldspar geothermometer. *Contributions to Mineralogy and Petrology*, 76, p. 369-377.

Catti, M., Ferraris, G., Waldi, G. (1989) On the crystal chemistry of strontian piemontite with some remarks n the nomenclature of the epidote group. *Neues Jahrbuch für Mineralogie Monatshefte*, p. 357-366.

Green, N. L., Usdansky, S. I. (1986) Toward a practical plagioclase-muscovite geothermometer *American Mineralogist*, 71, p. 1109-1117.

Massonne, H. J., Schreyer, W. (1987) Phengite geobarometry based on the limiting assemblage with K-feldspar, phlogopite and quartz. *Contributions to Mineralogy and Petrology*, 96, p. 212-224.

Roşu, E., Vodă, A., Costea, C., Niţă, P. (1998) Sphalerite geobarometry and arsenopyrite geothermometry applied to some metamorphosed sulfide ores of the Tulgheş Group, East Carpathians, Romania. *Carpathian-Balkan Geological Association, XVI Congress, Vienna Abstracts Volume*, p. 525.

Vodă, A. (1999) Contribuţii la cunoaşterea structurii geologice a zonei cristalino-mezozoice a Carpaţilor Orientali, sectorul central. *Stud. cerc. geol.*, in press.

An. Inst. Geol. Rom., 72, part. II. p. 59-66, Bucureşti, 2000

SOME ASPECTS REGARDING MORPHOLOGICAL VARIATIONS OF ZIRCON CRYSTALS FROM MUNTELE MIC MASSIF, SOUTH CARPATHIANS-ROMANIA: PETROGENETIC IMPLICATIONS

Ion Niculae ROBU, Lucia ROBU

Geological Institute of Romania, 1 Caransebeş St., RO-79678 Bucharest 32

Key words: Zircon. Morphology. Pyramid and prism faces. Granitoid, growth, typology.

Abstract: Muntele Mic is considered to belong to Caledonian granitoids of the Southern Carpathians. It is intruded in the Precambrian medium-grade crystalline formations of the Zeicani, Godenele, Măgura-Marga and Barnita Series, from the Upper Danubian Units. It is composed of granitoid rocks, as granites, granodiorites and, sometimes diorites. A specific characteristic of the massif is the small quantity of mafic minerals, as hornblende or/and biotite, the majority of the identified petrotypes being leucrocrate ones. As an exception, diorites must be mentioned, with a stronger mafic character due to a high proportion of biotite. Zircon crystals, identified using a specific methodology for heavy minerals, are usually associated with common accessory minerals of the granitoid rocks, as apatite, garnet, magnetite. Zircons are characterized by a long prismatic habit, determined by the large development of the prism faces. There is an obvious predominance of the (110) prism faces comparatively with the (100) ones. The pyramid (101) faces are much better developed, then the (211) ones. These growth differences determined two morphological types: • simple crystals, with simple terminations, determined by well-development of (110) and/or (110) prism faces associated with (211) pyramid one; • complicated crystals, with complicated terminations, that have well-developed (110) and/or (100) prism ones combined with (201) and (101) pyramid ones. The typological study (according to Pupin, 1980) has emphasized morphological types, crystallized from melts with deep source, pointing out the possibility for some crustal contamination. Sometimes zircon crystals are overgrown, zoned and contain opaque and/or transparent (zircon, apatite) minerals.

Introduction

Previous studies (Codarcea et al., 1963; Gherasi, Savu, 1969; Savu et al., 1973; Kräutner et al., 1981; Berza et al., 1983, 1993) in the Muntele Mic area have included some considerations regarding petrography, mineralogy and geochemistry of this massif, without presenting some information about accessory minerals, especially about their morphological aspects and their implications in the petrogenetic interpretations.

This paper tries to emphasize the morphology and the optical properties of zircon crystals enclosed in granitic rocks of the Muntele Mic massif, to establish the existing connections between morphological characteristics of zircons and physico-chemical conditions of their crystallization environment, and to present how could these ones be used in petrogenetical interpretations.

Geological setting

The actual geological data (Gherasi, Savu, 1969; Savu et al., 1973) include Muntele Mic granitoid body and its country rocks, Precambrian polymetamorphic crystalline formations of the Zeicani, Godenele, Măgura-Marga, Maru and Barnita Series (Fig. 1) of the Upper Danubian Units (Berza et al., 1983, 1993).

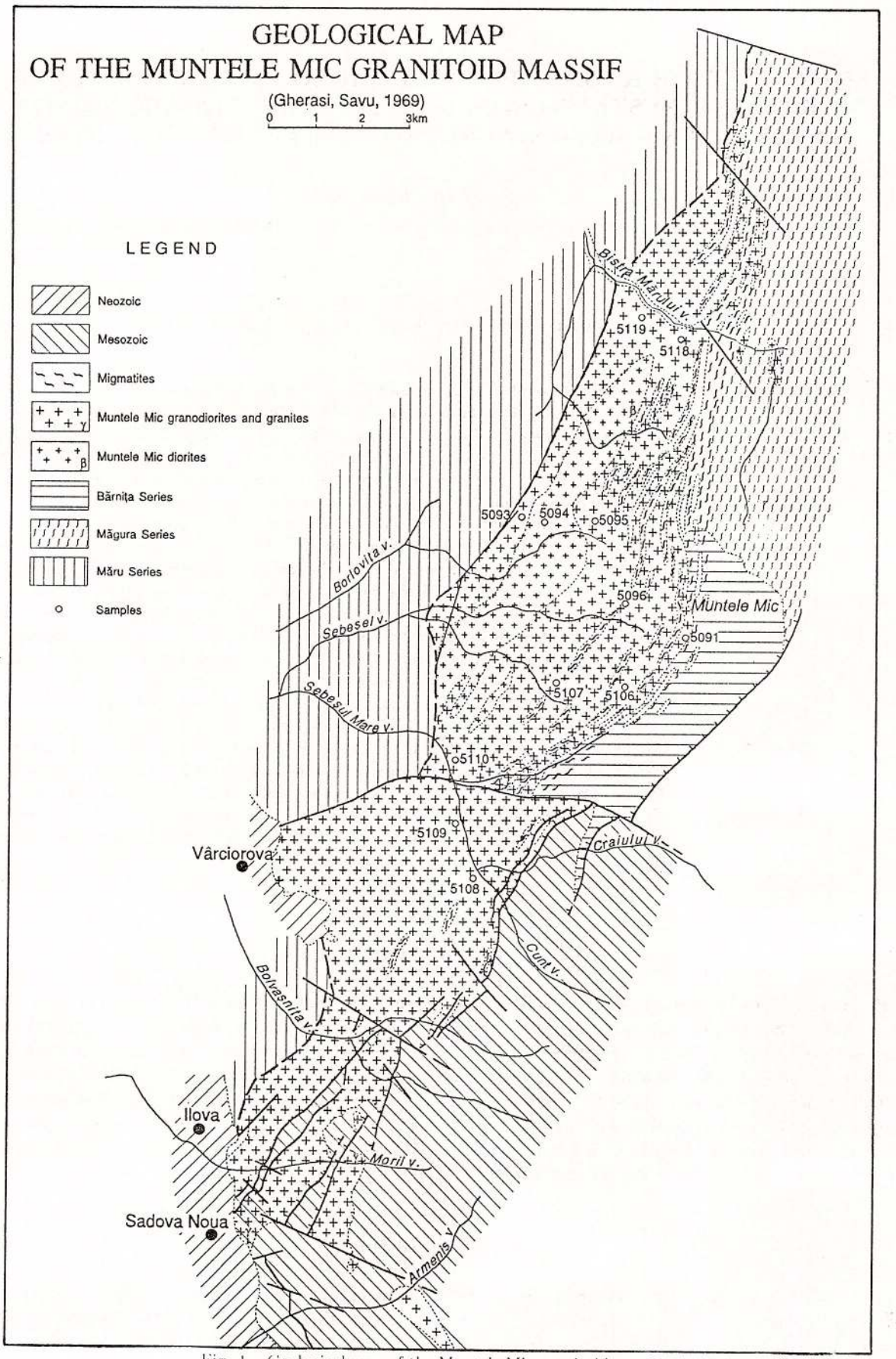

Fig. 1 – Geological map of the Muntele Mic granitoid massif.

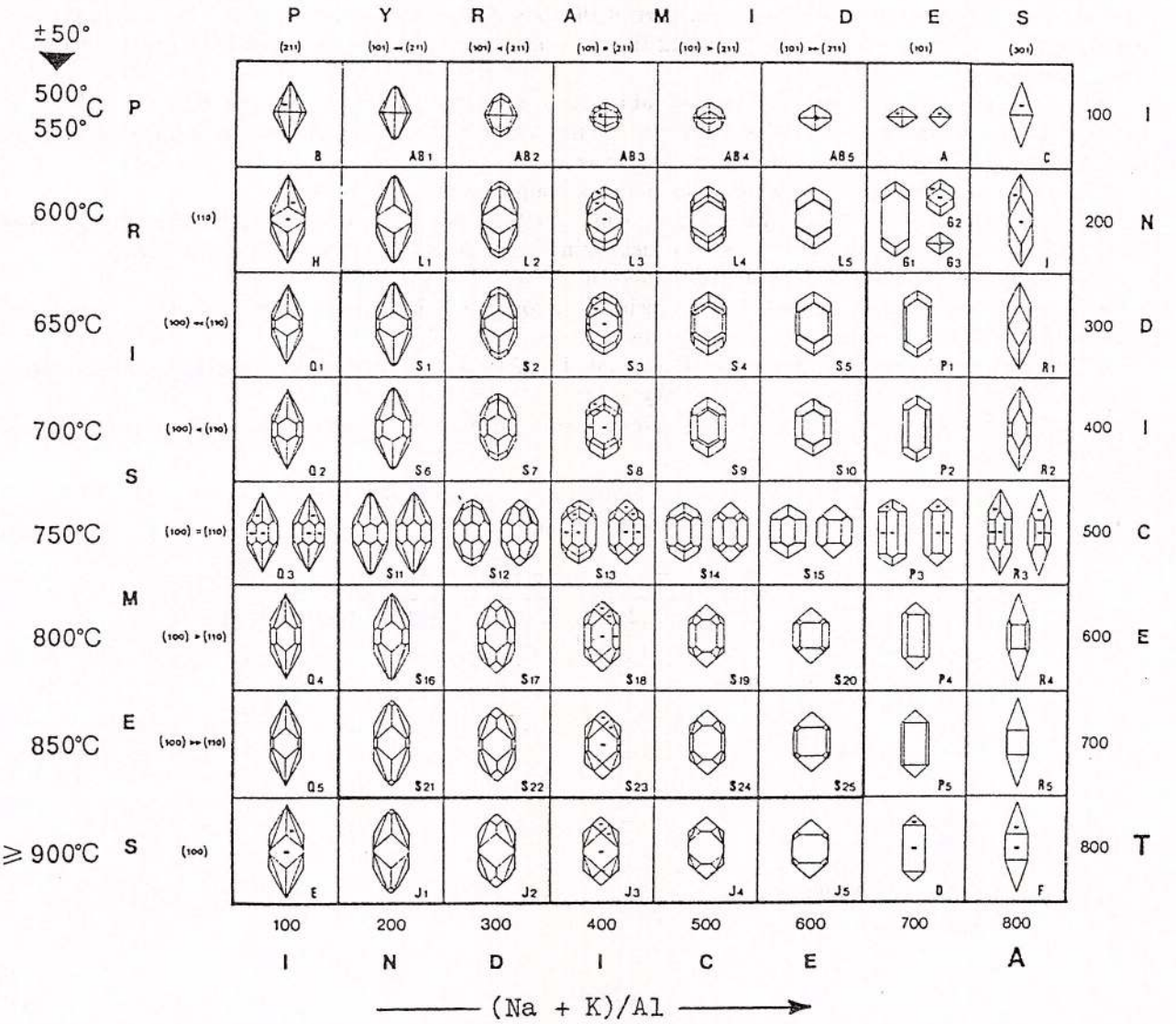

Fig. 2 – Main types and subtypes of typologic classification of zircon crystals (Pupin, 1980).

Its shape is an ellipsoid, NNE-SSW oriented, according to its long axes, parallel to an antiform structure, that included it. It is divided in two different parts, a northern uplifted part and a southern down-thrown, by the Vârciorova-Craiul fault (Gherasi, Savu, 1969).

Muntele Mic granitoid massif is surrounded by crystalline formations, grouped in some different metamorphic series, and by Mesozoic sedimentary deposits, as follows:

- *Măgura-Marga Series*, composed of quartz-biotite-chlorite schists and chlorite-albite-sericite schists and *Barnita Series*, enclosing metamorphosed basic schists, met in the Eastern part of the massif;
- *Maru Series*, constituted of amphibolites, metaquartzdiorites, metagabbros and sometimes metaultramafites, cropping out to the West of the massif;
- *Mesozoic sedimentary* formations, cropping in the Southern and South-Eastern parts of this one.

Petrography and mineralogy

Muntele Mic granitoid massif is characterized by petrographical and mineralogical homogeneity in its entire area.

Granodiorites and granites are the main petrographical types, but sometimes diorite or quartz diorites can be observed, especially in the northern part of the massif, where a narrow zone (6-7 km long and 1 km apparently thick) has been separated, having the same orientation as the long axes of the body (Gherasi, Savu, 1969).

The porphyric structure and an oriented fabric are specific for all petrotypes, but they are difficult to organize in the southern part of the massif, along the Vârciorova-Craiu fault and in the Bistra Marului Basin, where the granitoid rocks present mylonitic aspects.

Feldspar, micas and quartz have been observed as main mineralogical phases:

• *Feldspar* (plagioclase and/or alkaline-microcline-perthite) has been observed (1) in the matrix of the rocks and (2) as well-developed crystals, that determined the porphyric character of the structure.

Frequently it is partially or totally substituted by albite.

• *Micas* are represented by biotite, that includes zircons, or is intergrown with muscovite. Sometimes muscovite can be observed as main micas phases.

• *Quartz* is present as anhedral crystals, associated to feldspar and micas, constituting the last mineral phase. Frequently it is broken or presents wavy aspects.

As *accessory minerals* we have identified: *zircon, apatite, titanite, magnetite.* Mineral species and mineral associations are presented in table 1.

Table 1. Accessory minerals in investigated rocks from Muntele Mic granitoid massif

Primary minerals						Secondary minerals	
Sample	Petrotype	Zircon	Apatite	Titanite	Magnetite	Pyrite	Epidote
5091	granite	+	-	-	+	+	-
5106	granite	+	+	-	+	+	-
5107	granite	+	-	+	+	+	+
5108	granite	+	+	-	+	+	-
5110	granite	+	+	-	+	+	-
5118	granite	+	+	-	+	+	-
5119	granite	+	+	-	+	+	+
5109	microgranite	+	+	-	+	+	+
5096	granodiorite	+	+	+	+	+	-
5094	granodiorite	+	+	-	+	+	-
5095	diorite	+	-	-	+	+	+
5093	diorite	+	+	-	+	+	-

+ = yes; - = no

Chemistry

Chemical characterization of the granitic rocks from Muntele Mic massif (content, variation and interpretation) (Savu et al., 1973) is emphasized, as follows:

• *Main elements*

– SiO_2 content varies between 68.54 % and 53.24 %, determining for all investigated petrotypes an acid-intermediary character;

– alkaline elements have relatively high values, varying between 5.10 and 3.38 % for Na_2O, and 1.43 and 4.37 %, for K_2O, and their sum (Σ K_2O+Na_2O) is between 5.08 and 8.89 %.

The Na-character (K_2O<Na_2O) is obvious for the majority of the considered rocks.

– ferro-magnesian elements have lower contents in granitic rocks (0.92-2.72 % for Fe_2O_3 and 0.86-3.10 % for FeO), their sum (Σ FeO+Fe_2O_3+MgO) being 0.99-4.60 %; for diorites, the values are higher and the calculated sum is 9.41-12.1 %.

Main element variation emphasizes a typical calc-alkaline character.

• Minor elements (Pb, Cu, Ga, Sn, Ni, Cr, Co, V, Sc, Zr, Sr, Ba) present no specific variations in considered petrotypes, and their concentration is low.

• REE elements (Robu et al., 1997) have no specific concentration for each considered petrotype and their patterns are very similar, emphasizing (1) no Eu anomaly; (2) a low LREE increase; (3) a significant

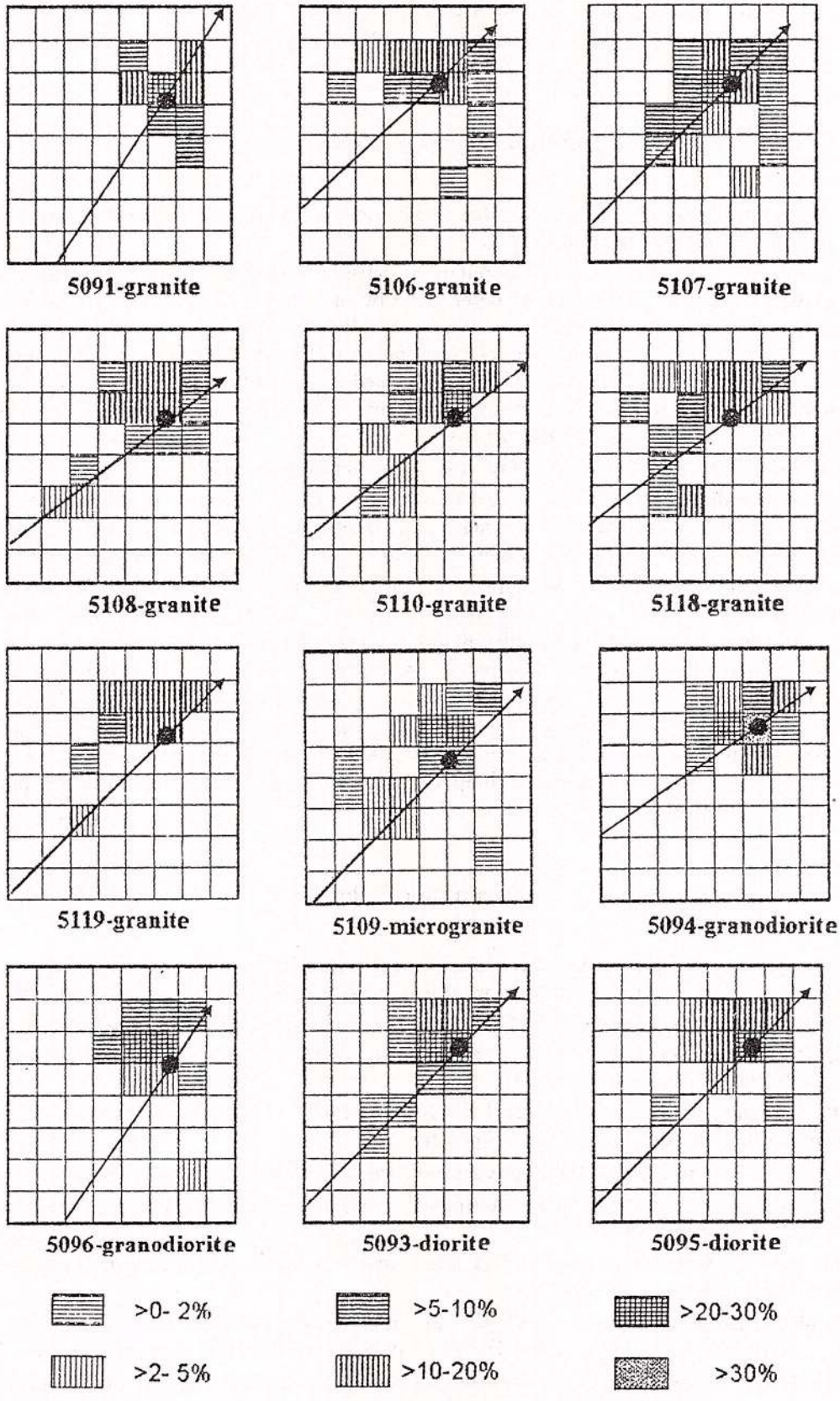

Fig. 3 – Tipologic distribution of zircon populations from Muntele Mic granitoid massif (Pupin, 1980).

HREE concentration. A petrogenetic interpretation, based on REE content and variation, envolves complex geological aspects as (1) a deep magma generation and (2) crustal assimilation processes.

Physical aspects of zircon crystals

Physical properties, important for zircon characterization and used in petrogenetical interpretations, are the colour and optical aspects (crystal inside).

Colour is variable in the zircon studied populations, without significant differences between zircons from the investigated petrotypes. These ones are determined by the number of different coloured crystals, in the same population, the majority of zircon crystals are light-dark brown and a few are light pink. In spite of these colour variations, morphological aspects are frequently the same and no connection between colour variations and morphological aspects could be established. The metamictic process, determined by the accumulation and disintegration of the radioactive elements (Th, U-Pb isotopes) enclosed in crystal network of the zircon crystals, affected most of the zircons.

Crystal's inside is not simple and in many cases is characterized by nucleus, zoning and inclusions.

Nucleus is generally disposed in the central part of the crystals, overgrowth developed arround it, being symmetric or asymmetric (plate I). This nucleus is represented by smaller idiomorphic zircon crystal, sometimes partial or total rounded ones, having the same optical orientation with the host zircon crystal.

Zoning has a small development, as number of zoned crystals or observed zones in the crystals. The way of zoning is very different, varying from crystal to crystal (plate II). Generally, zones have an unequal development, in the same crystals or in different crystals, varying from thin to thick; they are observable especially in prism grown area and disposed parallel with prism faces or sometimes pyramid ones.

Inclusions, observable in a large number of crystals, are very minute, disposed chaotically, or oriented parallel to prism faces, with different morphological aspects: needles, batons and prismatic aspects (plate III). The extremely minute dimensions have made difficult their identification by optical method, but their morphological aspects seem to be similar with apatite (long batons) or zircon (prismatic forms); the needle ones could not be identified.

Zircon morphology

Some morphological differences have been observed, determined by unequal development of two main faces of zircon crystals: prism and pyramid. Two different aspects could be identified (plate IV).

- unequal developed prism faces, when (110) prism faces are much better developed than (100) [(110) > (100)], due to some chemical change of the crystallization environment and temperature variation (Pupin, 1980): high Al-content and low temperature.
- unequal developed pyramid faces, [(211) < (101)], determined by K-content increase of the zircon crystallization medium and decrease of the temperature.

These variations have as a result the appearance of two different crystal type (plate V):

- simple crystals, with simple ending, determined by well developed (110) and/or (100) prism faces, associated with (211) pyramid ones;
- complex crystals, with complicated ending, that have well-developed (110) and/or (100) prism ones, combined with (211) and (101) pyramid ones;

Typological interpretation (Pupin, 1980) (fig. 2) emhasizes the predominance of L_{2-5}, S_{3-5}, P_{1-3} G types, a few P_5 type and S_{11-13}, S_{16-18} and D types have sporadically been observed.

No specific forms for each petrotype have been identified, but high percentage variations of these ones have been emphasized (Fig. 3).

Their tendency vectors (fig. 3) emphasize a calc-alkaline evolution and their mean calculated points plot in granodiorite, monzogranite and monzonite areas (fig. 4).

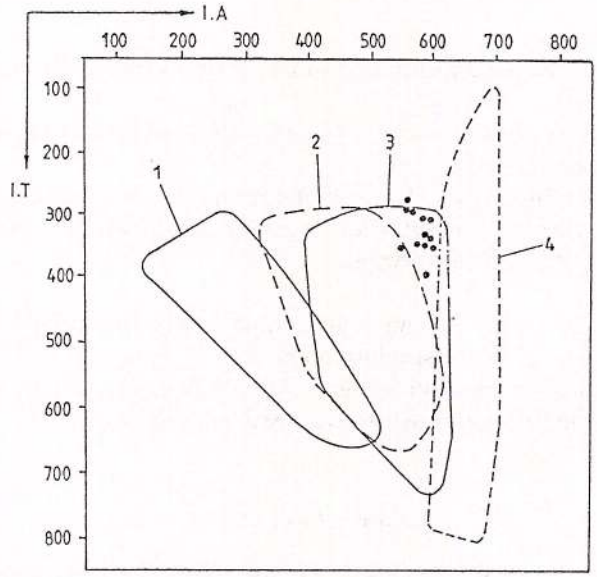

Fig. 4 – Distribution of plutonic rocks in the typologic diagram.
(1) diorites, quartz gabbros and diorites, tonalites; (2) granodiorites; (3) monzogranites and monzonites; (4) alkaline and hyperalkaline syenites and granites (Pupin 1980).

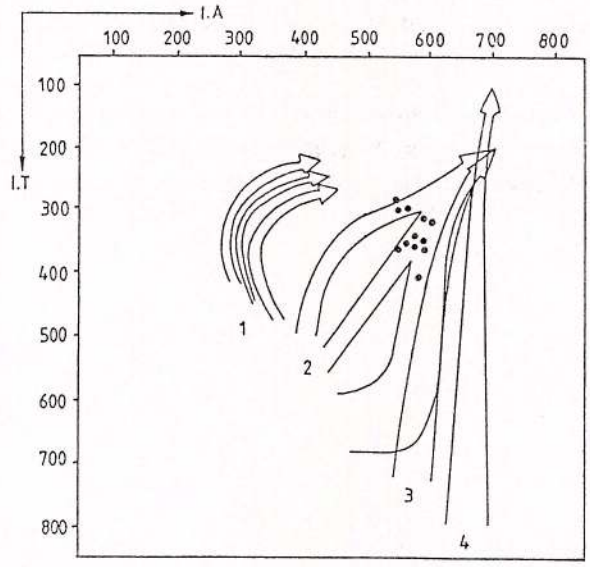

Fig. 5 – Distribution of mean points and mean T.E.T. of zircon population from granitic rocks
(1) granites of crustal origin; (2) granites of crustal+mantle origin (hybrid granites); (3+4) granites of mantle or mainly mantle origin (Pupin, 1980).

Distribution of mean points in T.E.T. diagram (fig. 5) shows a crystallization process of a granitic composition melt and mix origin (crust+mantle) for this one.

Conclusions

Some interesting data have resulted from the zircon morphological study of the Muntele Mic granitoids, as follows:

- unequal development of the prism and pyramid faces;

• for each petrographical type, the same zircon morphological types, but different zircon subtypes and different frequency;

• two different zircon crystal types:

– simple crystals, with simple ending, resulting from well developed (110) and/or (100) prism faces, associated with (211) pyramid ones;

– complicated crystals, with complicated ending, having well-developed (110) and/or (100) prism ones, associated to (211) and (101) pyramid ones;

• morphological variations, determined by chemical and temperature exchanges;

• a mix origin of the initial magma emphasized by the typological classification;

• a common origin for all investigated petrotypes;

• some interesting optical aspect:

– a variation of colour, from light pink (a few) to light-dark brown (majority)

– zoning, especially in the zones of the prism development;

– core, at the middle of crystals (frequently), or near the margins of crystals (sometimes);

– inclusions (needles, batons and minute prisms), disposed in prism zone.

References

Berza T., Kräutner, H., Dimitrescu R. (1983) Nappe structure in the Danubian of the central South Carpathians. Asoc. Geol. Carp.-Balk., Congr. XII, 1981, Bucureşti.

— , **Dimitrescu M., Seghedi, A., Oaie, Gh. (1993)** Harta geologică 1: 50.000, foaia Petreanu, Machetă.

Codarcea, Al., Pavelescu, L. (1963) Considérations sur la genèse des roches granitoides del'autochtone danubien des Carpathes Méridionales. Asoc. Geol. Carp.-Balk., Congr. V, 1961, Bucureşti.

Gherasi, N., Savu, H. (1969) Structura masivului granitoid de la Muntele Mic (Banatul de Est). *D.S.*, LIV/3, Bucureşti.

Kräutner, H., Năstăseanu, S., Berza, T., Stănoiu, I., Iancu, V. (1981) Metamorphosed Paleozoic in the South Carpathians and its Relations with the Pre-Paleozoic Basement. Asoc. Geol. Carp.-Balk., Congr. XII, 1981, Guide to Excursion A1, Bucureşti.

Pupin, J. P. (1980) Zircon and granite petrology. *Contrib. Mineral. Petrol.*, 73, p. 207-220.

Robu, I. N., Robu, L., Tiepac, I., Stoian, M., Alexe V. (1997) Raport, Arh. IGR, Bucureşti.

Savu, H., Vasiliu, C., Udrescu, C., Tiepac, I. (1973) Crystalline schists and Baikalian granitoid rocks in the Muntele Mic region. *An. Inst. Geol.*, XLII, p. 395-44, Bucureşti.

Plate I — Cores in zircon crystals

• nucleus

x1200

Plate II — Zircon crystals, different zoned

• zoning

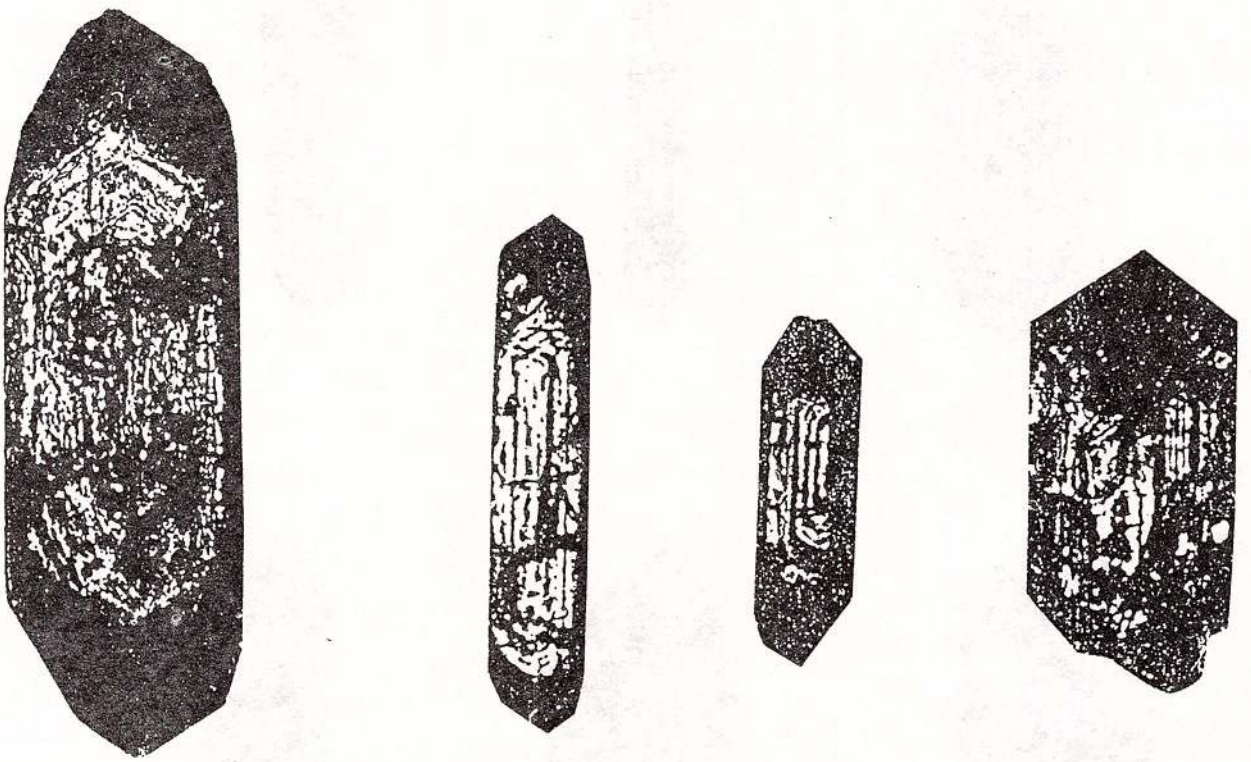

x400 x 1200

Plate III — Inclusions in zircon crystals

• inclusions

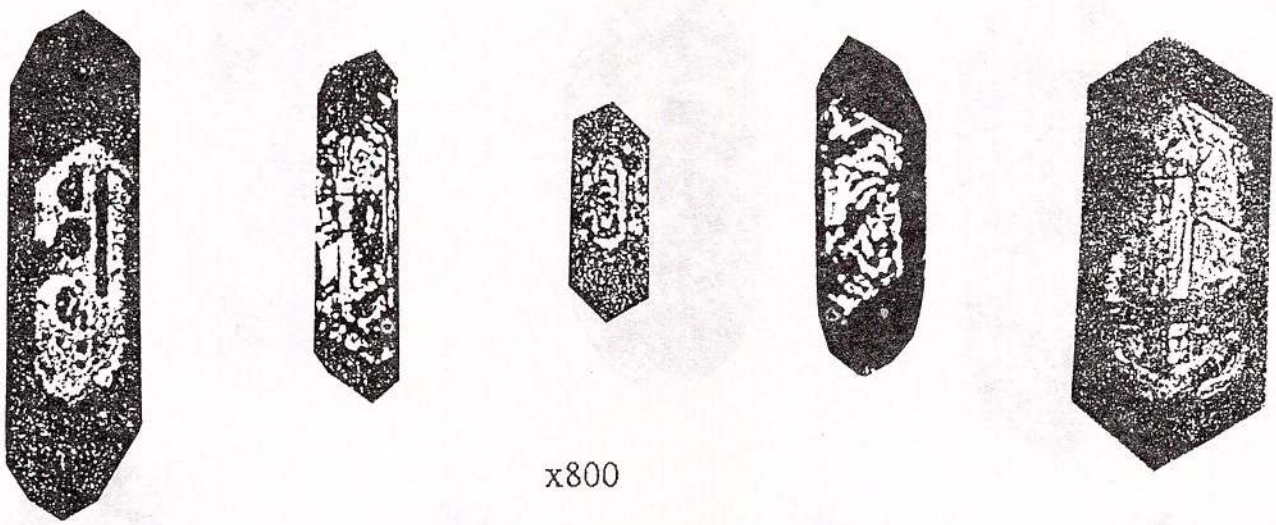

x800

Plate IV — Variation of growth way of zircon crystals:

a. • **unequal developed prism faces [(100) < (110)]**

b. • **unequal developed pyramid faces [(211) < (101)]**

x 1200

Plate V — Zircon crystal types

- **two different crystal types:**

⇒ <u>simple crystals</u>, *with simple ending, determined by well developed of (110) and/or (100) prism faces, associated with (211) pyramid ones;*

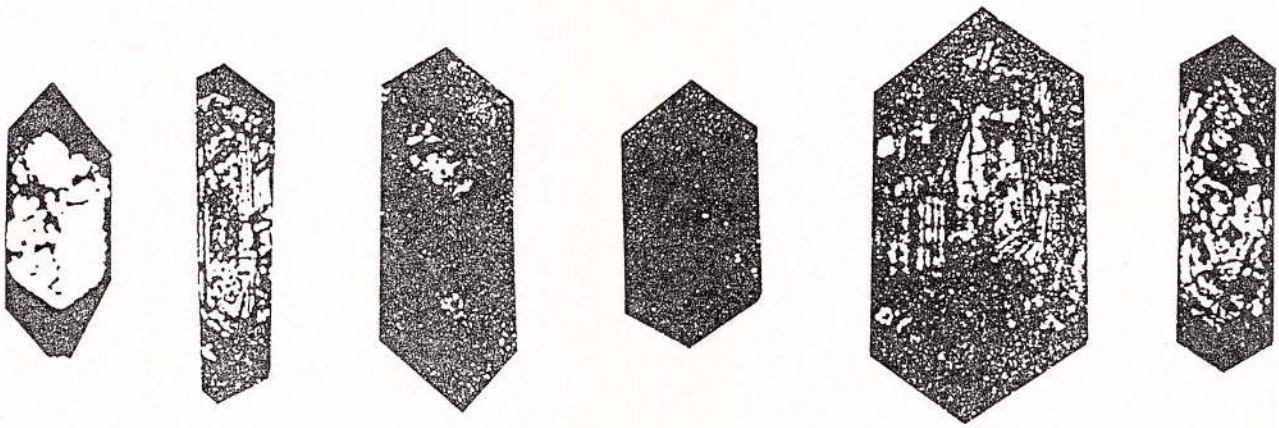

x1200

⇒ <u>complicated crystals</u>, *with complicated ending, that have well-developed (110) and/or (100) prism ones, combined with (201) and (101) pyramid ones*

x1200

An. Inst. Geol. Rom., 72, part. II, p. 67-76, Bucureşti, 2000

THE ENCLAVES IN THE EAST CARPATHIAN NEOGENE INTRUSIONS (ROMANIA); THEIR SIGNIFICANCE FOR THE GENESIS OF THE CALC-ALKALINE MAGMAS*

Eugenia NIŢOI, Marian MUNTEANU, Ştefan MARINCEA
Geological Institute of Romania, 1 Caransebeş St., RO-79678 Bucharest 32

Key words: Calc-alkaline magma. Enclaves. Andesites. Intrusive bodies.

Abstract: The subvolcanic bodies in the Rodna and Bârgău Mountains contain magmatic metamorphic and sedimentary enclaves. The study of the enclaves was used to get information about magma evolution. Several pairs host rock-cognate enclaves have been investigated. On the basis of the petrographic, mineralogical and geochemical features observed, the following conclusions can be drawn: (1) the initial magma was a calc-alkaline one, acidic or intermediary, with normative corundum. This one could be derived from a basalt-andesitic hydrated magma with normative diopside, as a result of a fractioned-crystallization process; (2) the magma has formed in intermediary crustal magma chambers at depths of about 15-20 km, where the estimated temperature has been 700-800^{0}C and the pressure 6.43-6.83 kbar. The pressure was calculated on the basis of the chemical composition of hornblende. Pressure values were obtained for both host rocks and enclaves; (3) the cognate enclaves have been considered as evidence for crystallization from a melt initially more mafic than the one the host rocks have resulted from.

Introduction

In the northern extremity of the inner part of the East Carpathians, calc-alkaline intrusive bodies were emplaced in Pannonian-Pontian time span (8.5 Ma-11.7 Ma: Pecskay et al., 1995). This area includes the Rodna and Bârgău Mountains where many shallow intrusions (rhyolites, rhyodacites, dacites, andesites, microdiorites) penetrated either a Precambrian metamorphic basement or a Paleogene sedimentary one. The intrusions occur in two alignments parallel to the Transcarpathian Flysch Fault (Fig. 1). Most of the intrusive bodies contain enclaves. The presence and the abundance of the igneous enclaves depend on the petrographic type of the host rock: they are rare in dacites, rhyodacites and rhyolites and quite abundant in andesites (especially in the quartziferous ones) and in microdiorites.

Types of enclaves

The studied enclaves can be separated (in a genetic classification) in four comprehensive groups: igneous enclaves, metamorphic enclaves, sedimentary enclaves, and xenocrysts. Each group, in its turn, can be divided, on the basis of petrographical and mineralogical criteria, in several categories, as follows:

(1) The igneous enclaves may be cognate enclaves or foreign enclaves. The cognate enclaves consist of glomeroporphyric mineral assemblages similar to the host rock with respect to their composition and origin. The foreign enclaves are rocks which differ from the host rock by their features. They may be andesites, basalts or microdiorites, modified to various degrees by a host rock-induced recrystallization; these enclaves

*Paper presented at the International Congres of Vulcanology, IAVCEI-Capetown, July 1998, South Africa

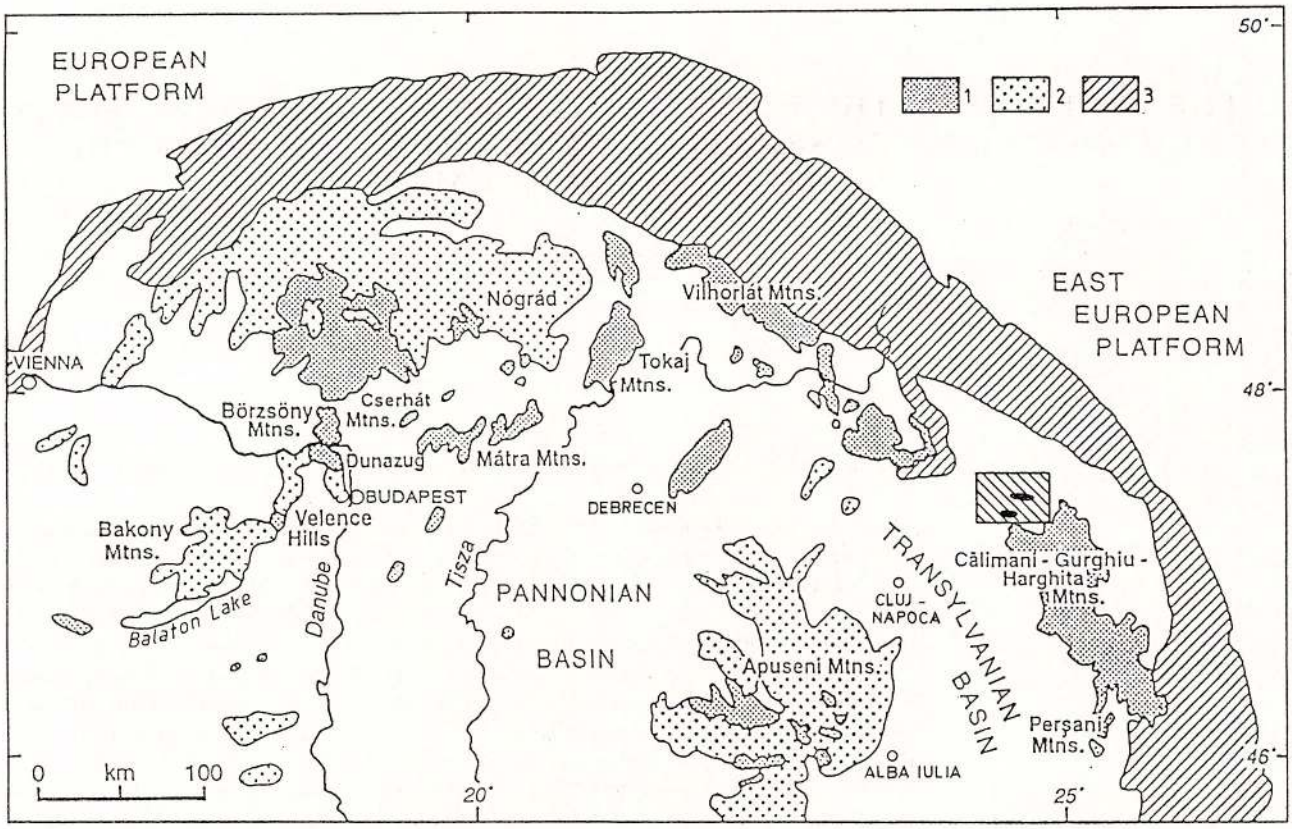

Fig. 1 – Location of the calc-alkaline intrusive magmatism in the general framework of the Carpatho-Pannonian area 1, calc-alkaline volcanic rocks: 2, Inner Carpathians; 3, Outer (flysch) Carpathians.

represent rocks of the earliest magmatic events in the area, pierced by the magmas of the younger generations which crushed and transported them to the upper levels.

(2) The metamorphic enclaves represent either regionally metamorphosed rocks or sedimentary rocks thermally metamorphosed by the host magma. The enclaved regionally metamorphosed rocks may show a superposed contact metamorphism. The new parageneses added sillimanite, andalusite, K-feldspar, corundum and spinels to the older ones containing amphiboles, quartz, feldspars, biotite, garnet, staurolite and kyanite. In the carbonaceous sedimentary enclaves the contact metamorphism produced andradite vesuvianite and wollastonite.

The general absence of quartz and muscovite as well as the common occurrence of the spinel and K-feldspar±corundum indicates a high-grade contact metamorphism of most of the feldspathic enclaves. The amphibolic enclaves seem to have been almost inert with respect to the host rock influence. The mica-rich enclaves usually show partial melting.

Two biotite generations have been observed in the metamorphic enclaves:

a) An older one, with largely developed crystals decomposed along cleavage planes. It formed during the regional metamorphism and usually grew in conformity to the schistosity of the enclave. This biotite is associated with K-feldspar and spinel produced by its breakdown.

b) A new biotite usually occurs near the contact with the host rock as tiny, rounded crystals (Pl. I, Fig. 1).

Sillimanite is most frequently fibrolitic and commonly replaces feldspars (Pl. I, Figs. 2 and 3), seldom biotite (Pl. I, Fig. 4) and only exceptionally andalusite or garnet.

Garnet occurs as newly formed crystals or as overgrowths on older garnet crystals. Spinel (Fe-rich) and corundum (Pl. I, Fig. 2) usually occur near the contact with the host rock, but may be present in the inner parts, too. Spinel occurring in the inner parts of the enclaves is more magnesian than the one near the margins. Andalusite is common only in a small sill of the Oala body, being scarce elsewhere. It forms porphyroblastic crystals, sometimes altered to a pinite mass. Noteworthy, some enclaves are surrounded by a distinct border or a reaction corona. Considering their mineralogical composition, these borders

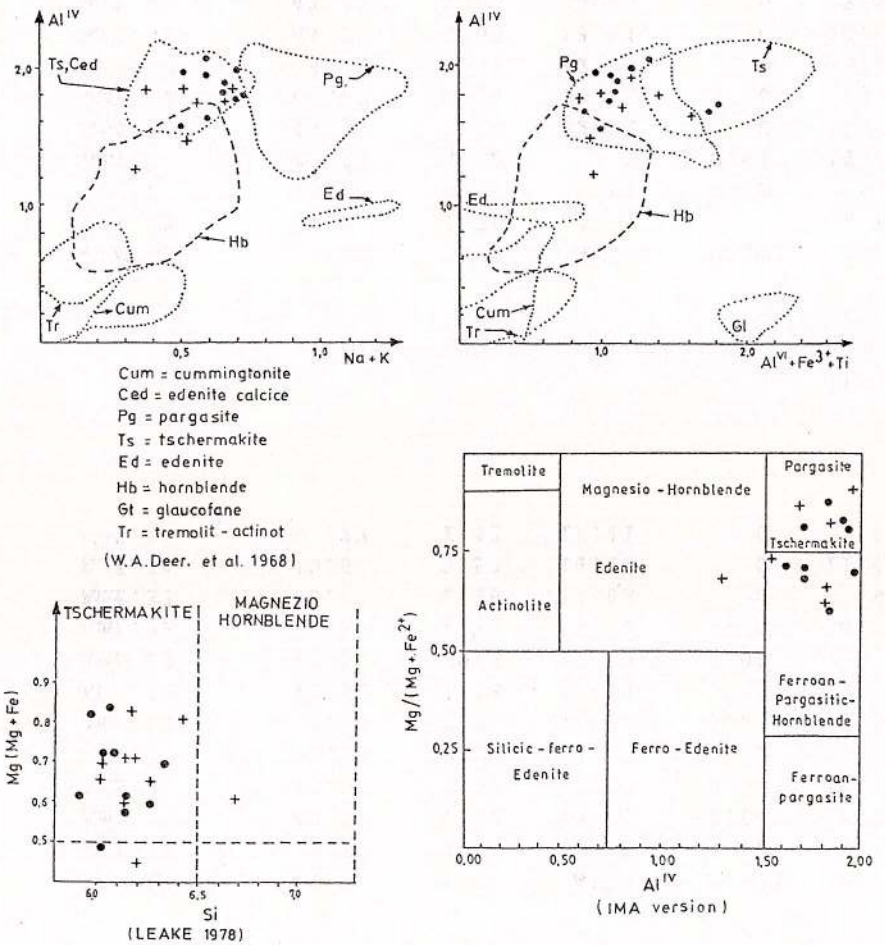

Fig. 2 – Amphibole composition plotted in several classification diagrams.

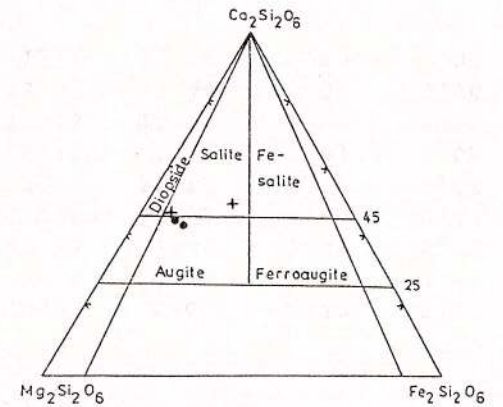

Fig. 3 – Classification of the pyroxenes in Poldervaat and Hess diagramme (1951).

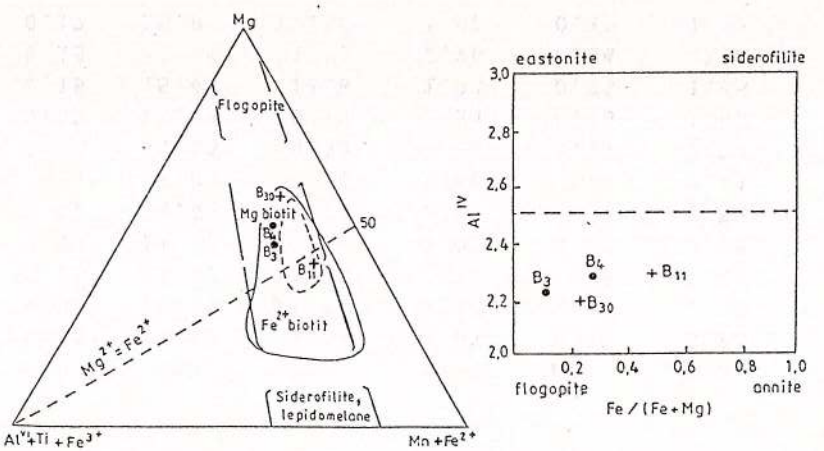

Fig. 4 – The chemical composition of the biotite in Foster diagramme (1960).

• Host rocks ; + Cognate enclaves

Table 1a
Electron microprobe analyses of selected amphiboles (A-type) from the host rocks
(Magura Arsente, Magura Cornii, Casariu, Heniu, Oala Sturzii structures)

SAMPLE	SiO2	TiO2	Al2O3	Fe2O3	FeO	MnO	MgO	CaO	Na2O	K2O	H2O
Amf 13	39.82	1.35	15.53	0	14.07	0.13	11.87	11.4	2.07	0.97	2.92
Amf 14	42.13	1.48	13.39	0.04	10.38	0.03	15.26	11.94	2.18	0.74	2.62
Amf 8	43.86	1.73	12.3	0.16	11.44	0.16	13.98	11.48	1.73	0.8	14.02
Amf 9	41.41	2.08	12.2	0	15.58	0.39	11.56	11.26	2.05	0.87	3.05
Amf 19	41.7	1.81	13.61	0.27	9.95	0.12	14.95	11.74	2.47	0.3	2.52
Amf 31	40.82	1.48	11.51	0	18.91	0.4	8.83	11.34	1.66	1.7	2.44
Amf 12	42.96	0.7	13.83	0.08	15.5	0.45	11.68	9.63	1.59	0.32	2.77
Amf.32	42.37	2.18	12.49	0	8.92	0.25	12.75	10.19	2.24	0.38	1.09
Amf.33	41.47	1.94	13.02	0	11.98	0.15	15.47	11.6	1.93	0.05	1.65
Amf.34	40.63	2.53	14.14	0	11.64	0.15	14.15	11.79	2.26	0.44	1.3
Amf.35	41.77	1.43	13.41	0	11.82	0.17	15.87	11.56	1.98	0.39	1.27

Table 1b
Electron microprobe analyses of selected amphiboles from the cognates igneous enclaves

SAMPLE	SiO2	TiO2	Al2O3	Fe2O3	FeO	MnO	MgO	CaO	Na2O	K2O	H2O
Amf.15	42.45	1.76	13.37	0	10.67	0.12	14.5	11.31	2.22	0.45	2.26
Amf.2	45.26	0.82	11.91	0.55	6.7	0.09	17.15	11.64	1.92	0.74	2.59
Amf.3	45.71	0.56	9.7	0.44	14.61	0.38	12.95	10.93	1.47	0.47	2.65
Amf.7	41.84	2.72	12.36	0	13.67	0.25	12.43	11.55	2.16	0.77	2.85
Amf.34	41.47	1.94	13.02	0	7.13	0.15	15.47	11.6	1.93	0.05	1.65
Amf.10	41.3	2.27	12.95	0	13.37	0.31	12.06	10.94	2.08	1.15	3.25
Amf. 36	41.94	1.68	13.94	0	11.66	0.14	13.88	11.44	1.83	1.06	1.2
Amf.37	41.61	1.76	13.65	0	13.36	0.27	11.5	10.14	1.99	1.07	2.23

Table 2
Electron microprobe analyses of selected pyroxenes from the host rocks (H)
and cognate igneous enclaves (E) from Oala, Heniu, Casariu structures

SAMPLE	SiO2	TiO2	Al2O3	Fe2O3	FeO	MnO	MgO	CaO	Na2O
Py 8E	55.05	0.32	1.87	0.1	13.99	0.24	27.62	1.3	0
Py1E	52.2	0.32	3.06	0.64	4.52	0.11	15.92	22.43	0.25
Py16E	49.76	0.29	3.09	0.03	13	0.53	9.44	23.51	0.35
Py17H	52.37	0.32	1.89	0	7.62	0.41	15.2	21.6	0.26
Py18H	51.66	0.42	3.63	0.27	5.39	0.14	15.54	22.15	0.3
Py 4H	51.2	0.47	4.4	0	5.6	0.41	15.7	22	0.26
Py 7H	52.4	0.28	3.4	0	7.6	0.4	15.8	21.2	0.1

Table 3
Electron microprobe analyses of selected samples of biotite from the host rocks (H)
and the cognate enclaves (E) (Valea Vinului and Cobasel structures)

SAMPLE	SiO2	TiO2	Al2O3	Cr2O3	FeO	MnO	MgO	CaO	Na2O	K2O	H2O
B3H	36.6	3.56	15.3	nd	9.63	0.3	12.38	1.28	0.49	7.55	3.19
B11E	35.84	3.9	15.48	0.05	20.98	0.25	10.36	0	0.21	9.6	1.88
B30E	36.67	3.36	15.41	0.02	14.02	0.11	14.97	0	o.5o	9.06	1.9
B4H	36.35	3.49	14.89	nd	13.44	0.32	12.3	1.53	0.4	7.43	3.7

Table 4

COGNATE ENCLAVES

Locality	Occurence	SiO_2	TiO_2	Al_2O_3	Fe_2O_3	FeO	MnO	MgO	CaO	Na_2O	K_2O	P_2O_5	H_2O	CO_2
Arsente	basalt	39.81	2.00	16.66	8.04	8.24	0.21	9.09	11.34	1.98	0.39	0.02	1.88	0
Cornii	basalt	41.72	1.89	13.8	6.12	7.33	0.23	11.25	10.68	2.05	0.92	0.10	2.52	0.98
Cornii	basalt	41.61	1.76	13.65	5.16	7.82	0.27	11.50	10.14	1.99	1.07	0.12	2.23	1.19
Heniu	basalt	42.30	1.40	13.70	3.85	7.29	0.14	14.10	11.52	2.08	0.76	0.05	2.33	0.00
Oala	basalt	43.30	1.23	22.491	3.65	4.35	0.13	7.20	12.61	2.24	0.48	0.06	2.05	0.00
Strejii	basalt	43.32	1.67	12.25	3.10	7.90	0.19	13.86	12.98	1.60	0.87	0.05	1.77	0.00
Casariu	basalt	47.16	1.87	15.17	5.70	6.22	0.18	7.73	10.22	1.89	0.33	0.04	1.91	0.00
Secu	basalt	47.62	1.23	17.70	3.99	6.00	0.17	7.34	9.51	2.77	0.81	0.06	1.94	0.00
Magurita	basalt	47.80	1.43	15.37	2.50	8.08	0.23	9.22	8.72	2.57	1.53	0.10	2.32	0.00
V.Vinului	basalt	47.91	1.73	16.65	5.70	6.99	0.29	6.55	5.19	2.45	3.30	0.12	2.56	0.00
Magurita	basalt	48.83	0.60	11.76	1.86	3.50	0.15	4.91	20.00	0.96	0.32	0.04	0.50	1.67
Arsente	basalt	50.46	0.36	2.44	2.53	2.97	0.12	20.00	19.86	0.31	0.04	0.00	0.89	0.00
Arsente	basalt	50.57	0.35	2.59	2.6	2.98	0.12	19.38	20.46	0.31	0.03	0	0.74	

HOST ROCKS

Magurita	basalt	48.54	1.07	17.20	3.12	5.82	0.16	6.54	9.48	2.41	0.73	0.14	2.66	2.01
Magurita	basalt	48.58	1.17	16.94	2.71	5.82	0.16	6.10	10.02	2.54	0.78	0.16	1.95	2.59
Oala	bas.-andesite	51.94	1.10	17.77	2.21	5.67	0.17	5.86	7.48	3.26	0.80	0.14	3.15	0.00
Heniu	ba.-andesite	52.63	1.06	18.71	9.18	2.30	0.17	3.26	8.54	3.55	1.00	0.13	0.75	0.87
Casariu	andesite	52.98	0.90	17.91	3.90	3.30	0.26	3.49	7.42	3.83	1.34	0.10	2.10	1.98
Casariu	bas.-andesite	52.88	0.77	17.91	2.59	3.63	0.16	3.53	7.51	3.14	0.91	0.19	3.24	3.13
Tomnatec	andesite	53.1	0.98	16.88	1.42	5.67	0.15	5.59	7.50	2.50	2.29	0.18	1.55	1.40
Cornii	andesite	54.90	0.81	18.60	2.93	5.89	0.18	4.62	6.18	2.42	2.70	0.20	1.64	0.00
Casariu	andesite	55.14	0.90	19.11	5.74	1.54	0.19	3.30	6.54	3.63	1.20	0.18	2.13	0.00
Secu	andesite	55.31	0.84	19.26	3.37	3.63	0.16	3.12	7.43	3.30	0.98	0.19	1.38	0.85
Colibita	andesite	57.18	0.7	18.74	2.63	3.20	0.16	2.47	6.80	3.40	1.32	0.18	1.84	1.18
P.Baii	diorite	59.72	0.73	16.98	1.85	3.52	0.14	2.54	4.91	3.31	3.30	0.36	1.03	0.63
V. Vinului	andesite	60.27	1.18	16.04	2.83	2.88	0.15	2.71	4.24	2.70	2.24	0.27	2.56	0.48
Plesii	andesite	62.23	0.51	17.15	2,79	1.47	0.10	2.14	5.33	3.91	1.34	0,05	1.69	0
Sturzii	dacite	66.03	0.44	16.42	1.64	1.87	0.30	1.36	4.92	4.37	1.37	0.09	1.25	0.48
Cormaia	riodacite	70.10	0.10	16.08	0.52	0.92	0.10	0.69	2.86	3.55	1.99	0	0	0
PV 31	andesite	61.56	0.7	16.73	3.09	2.23	0.15	2.47	4.40	3.53	3.24	0.34	0.46	0.56

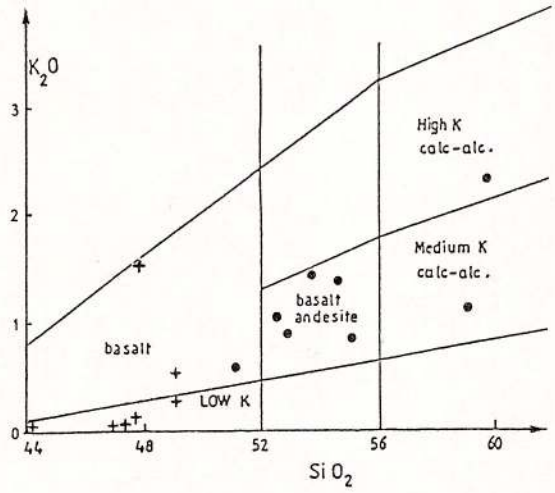

Fig. 5 – K_2/SiO_2 diagram (Peccerillo et Taylor, 1978)

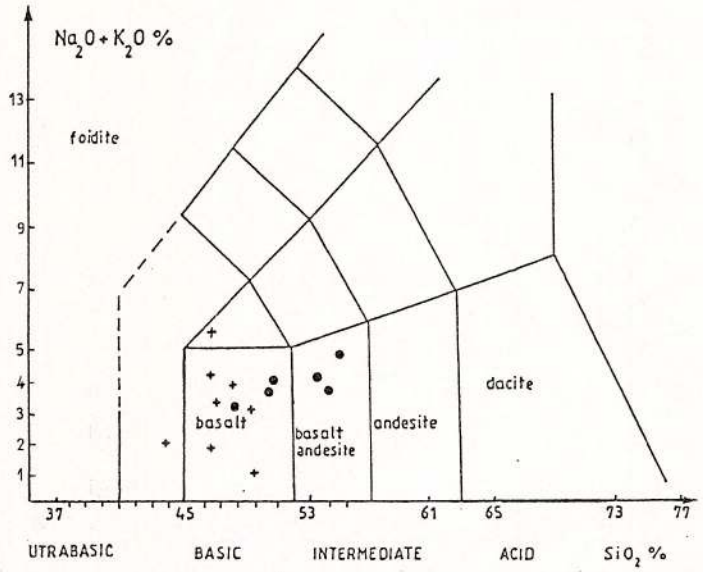

Fig. 6 – $Na_2+K_2O/Si\,O_2$ diagram (Le Maitre, 1989)

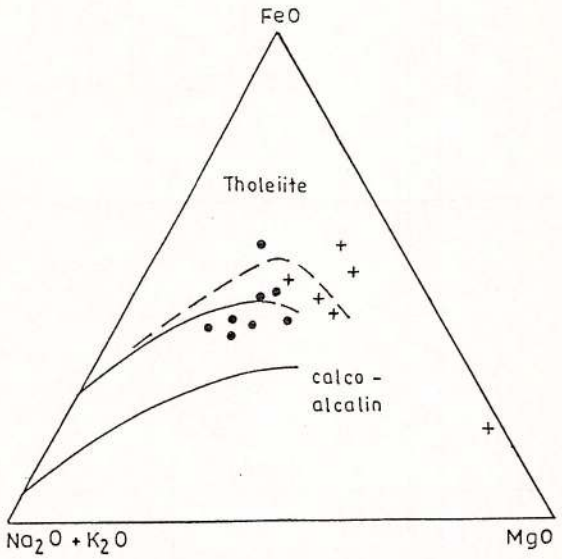

Fig. 8 – Irvine and Baragar (1971) diagram

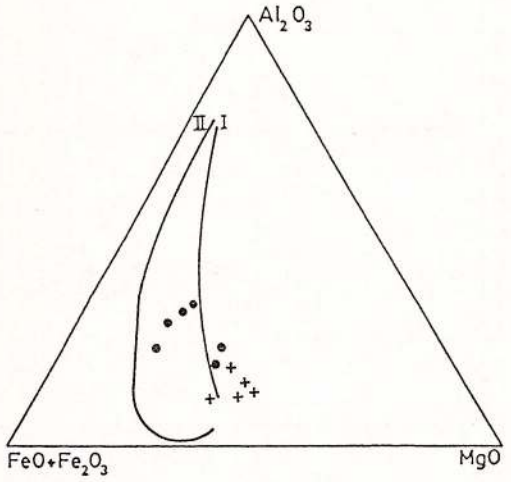

Fig. 9 – AFM diagram (Besson et Jonteilles, 1974)

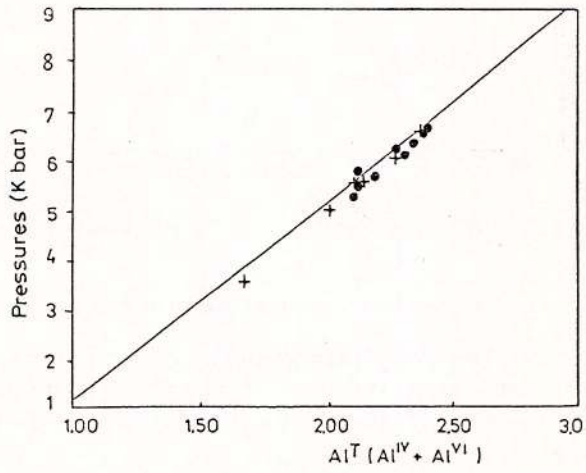

• Host rocks

+ Cognate enclaves

Fig. 10 – P=4.23 (Al^T) - 3.45 (Marie Johnson, M. Rutherford, 1989)

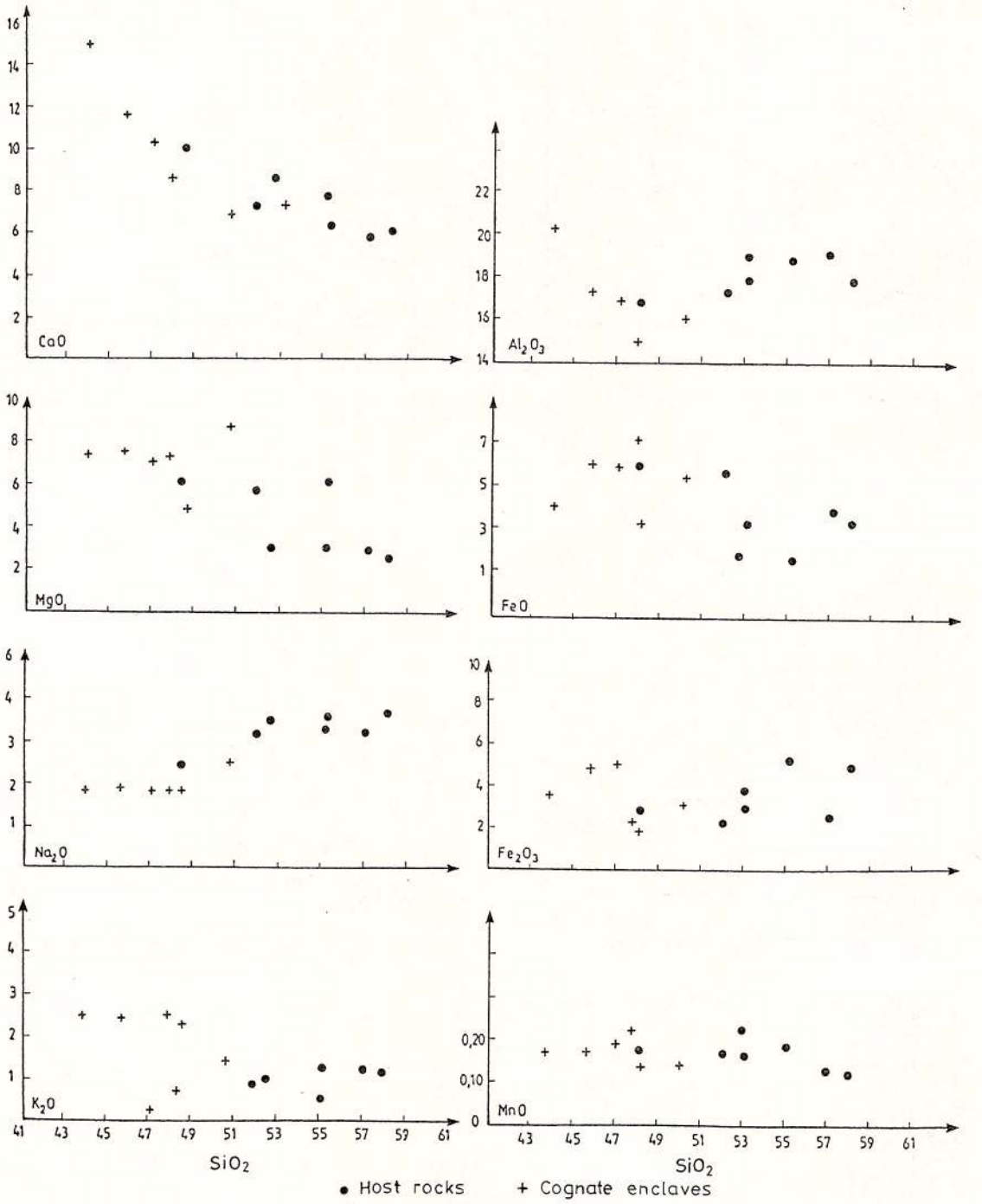

Fig. 7 – Major element Harker variation diagrams for cognate enclaves and host rocks from Bargau and Rodna Mts.

seem to be either secretions of the enclaves (quartz or amphibole rims of amphibolic enclaves) or of the host rocks (plagioclase, amphibole or pyroxene rims). The crystals in these rims are smaller than the phenocrysts in the host rocks or than the analogous crystals in the enclaves. Retrogressive rims (carbonate, epidote, chlorite) occur around several enclaves. Carbonate usually occurs near the host rock.

Most of the metamorphic enclaves show petrographic similarities with the medium-grade Bretila Group and Rebra Group that crop out in the East Carpathians.

(3) The sedimentary enclaves are rocks from the sedimentary basement that have not undergone mineralogical transformations under the influence of the host rock.

(4) The xenocrysts are represented by amphibole, quartz and garnet crystals engulfed by the volcanic matrix. The amphiboles show reaction corronas formed of opaque minerals or pyroxenes (Pl. II, Fig. 5). Quartz xenocrysts are usually corroded or have pyroxene rims (Pl. II, Fig. 6, 7). Garnets may show resorbtion shapes or reaction rims formed of opaque minerals or retrogressive assemblages (biotite-chlorite-epidote) (Pl. II, Fig. 8; Pl. III, Fig. 9).

Mineralogical features of host rocks and igneous enclaves

Most of the host rocks and their igneous enclaves consist of the following minerals:

The plagioclase is albite-type twinned, zoned (Pl. III, Fig. 10) altered or not, with an An-content of 42-70 %. It occurs either as euhedral to subhedral, 2-3 mm long crystals or as micronic, more or less idiomorphic microliths. In certain enclaves, a well developed symplektitic texture occurs at the plagioclase contact with other minerals of the rock.

The amphibole is present in all the petrographic types including the host-rocks and enclaves. Four types of amphibole were found:

- The A-type (Pl. III, Figs. 11, 12) is the most common. It forms euhedral crystals, brown-greenish in colour, sometimes marginally opacitized, up to 1 cm in size. It was formed during the first stages of magma crystallization. Its chemical composition (Table 1a) plots in the ferroan pargasite field [$(NaCaO_2Fe_2+AlSi_6Al_2O_{22}(OH)_2)$] according to AlIV vs. $Mg/(Mg+Fe^{2+})$ diagram in Figure 2. The mean composition is: SiO_2=39.82-43.86; Al_2O_3=11.81-15.53; MgO=11.68-15.26; CaO=9.63-11.94; Na_2O=1.66-2.47; Al=2.10-2.69; mg=0.75. It was found in both host rocks and cognate enclaves.

- The B-type is a poikilitic hornblende (Pl. IV, Figs. 13, 14) found only in cognate enclaves and which has been formed during the later stages. It includes earlier crystallized idiomorphic pyroxenes or plagioclases. Its mineralogical and chemical features place it in the ferroan pargasite-tschermakite field (Fig. 2). The mean chemical composition is: SiO_2=45.26; Al_2O_3=11.91; MgO=17.15; CaO=11.31; Na_2O=1.92; K_2O=0.74; mg=0.89; Al=2.00 (Table 1 b).

- The C-type is a magnesiohastingsite found only in cognate enclaves (Pl. IV, Fig. 15). Its colour is intense, with green pleochroic tints. The texture and the crystal habit indicate that it has formed by the reaction of an earlier pyroxene with the residual magma, during a later stage of crystallization. Its mean chemical composition is: SiO_2=45.71; Al_2O_3=9.70; MgO=12.95; CaO=10.93; Na_2O=1.47; K_2O=0.47; mg=0.69; Al_t=1.67. (Table 1 b)

- The D-type is a green, fibrous actinolitic hornblende, grown in bundles at the contact between the magmatic enclaves and the host rock.

The pyroxenes. Textural relations as well as the mineralogical and chemical parameters (Table 2, Fig. 3) distinguish two pyroxene generations: phenocrysts of a first generation and small crystals of a second one. The phenocrysts (Pl. IV, Fig. 16, Pl. V, Fig. 17) and formed directly from the magma and have the augite composition (En=43.14-44.96; Wo=44.07-46.06; Fs=12.75-8.98; mg=86.27). The augite has been found in both enclaves and host rocks. The pyroxenes of the second generation (Pl. V, Figs. 18, 19) have a diopside composition: En=27.82-45.96; Wo=48.79-46.53; Fs=22.38-7.5; mg=56.46. They occur only in enclaves.

The biotite was found mostly in the Magura Cornii and Valea Vinului structures. It has grown in two generations: a first one (in host rocks-quartziferous andesites), occurring as idiomorphic, inclusion-free phenocrysts, is represented by a Fe^{2+}-rich biotite (Pl. VI, Figs. 20, 21). The chemical composition (Table 3, Fig. 4) of the phenocrysts shows high Fe and low Ca content. The second generation of biotite occurs only in enclaves (Pl. VI, Figs. 22, 23).

The accessories. In most of the host rocks and enclaves, apatite and garnet euhedral crystals and opaque minerals difficult to identify usually occur.

Petrogenetic considerations

The study of the genetic relations between enclaves and host rocks has been done on 11 pairs enclave-host rock that belong to several subvolcanic structures: Măgura Arsente, Valea Vinului, Oala, Magurita, Heniu and Magura Corni. The following remarks can be drawn:

1. The SiO_2 content (Table 4) ranges between 43.92 % and 49.84 % in the enclaves and between 48.5 % and 58.06 % in the host rocks. In the K_2O vs. SiO_2 and SiO_2 vs. Na_2O+K_2O classification diagrams (Le Maitre et al., 1989) the enclaves plot in the field of low-K basalts (tholeiites) and the host rocks in the fields of andesites and medium-K basaltic andesites (Figs. 5 and 6).

2. In the Harker's binary diagrams, both for cognate enclaves and host rocks (SiO_2 vs. Al_2O_3, CaO, Na_2O, K_2O, MgO and Fe_2O_3) show a linear evolutive trend for CaO, MgO and Na_2O and a wide dispersion of the plots for FeO, Fe_2O_3 and Al_2O_3 (Fig. 7) The dispersion can be explained by the changes of the initial mineralogical and chemical features of the enclaves and host rocks under the physico-chemical and mecanical reciprocal influences.

3. In the FAM diagrams (Fig 8 - Irvine and Baragar, 1971 and Fig. 9 - Besson and Fonteilles, 1974), based on the elements less sensitive to the silica-induced dilution (Fe, Mg, Al, Mn) the features of the cognate enclaves are similar to those of the calc-alkaline melts and the features of the host rocks are similar to those of the evoluted melts, intermediary between the calc-alkaline (I) and tholeiitic (II) types.

4. The chemical and mineralogical similarities of the phenocrysts (amphiboles, pyroxenes, plagioclases) from both enclaves and host rocks, the modal and normative (CIPW) compositions support the idea of the existence of common petrological features as effect of a common origin.

5. We consider that the mafic magmatic enclaves (cognate enclaves) are formed during the earlier stages of magma evolution, when its composition was close to a basaltic one. They are syncrystallized with the host rocks or postdate them.

Conclusions

The linear evolutive trend revealed by the major components and by the FeO/MgO ratios (0.26-0.49 in enclaves, 1.07-2.09 in host rocks) support the conclusions obtained from the mineralogical study, which suggests the existence of a single calc-alkaline hydrated magma (with 3-3.5 % water) with tholeiitic tendencies. It has formed in intermediate magmatic chambers, at depths of 15-20 km, at pressures of 6.43-6.83 kb and temperatures of 700-800 ^{0}C. The pressures were determined using the Al-in-hornblende geothermometer: $P(\pm 5\ kb) = -3.46\ (\pm 0.24) + 4.23\ (\pm 0.13)\ Al^T$ given by Johnson and Rutherford, 1989 (Fig. 10). Pressure values determined for the enclaves are consistent with those for the host rocks. We consider that the fractionate crystallization of the hornblende exersized a significant influence on magma genesis and evolution.

References

Besson, M., Fonteilles, M. (1974) Relations entre le comportements contraste de l'alumine et du fer dans la differenciation des series tholeiitique et calco-alcaline. *Bull.Soc.mineral.Cristallogr.*, 97, p. 445-465.

Irvine, T. N., Baragar, W.R.A. (1971) A guide to the chemical classification of the common volcanic rocks. *Canadian Journal of Earth Sciences*, 8, p. 523-548.

Johnson, M.C., Rutherford, M. J. (1989) Experimental calibration of the aluminium in hornblende geobarometer with application to long Valley Caldera (California) volcanic rocks. *Geology*, 17, p. 837-841.

Pecskay, Z., Edelstein, O., Seghedi, I., Szakacs, Al., Kovacs, M., Crihan, M., Bernard, A. (1995) K-Ar datings of Neogene-Quaternary calc-alkaline volcanic rocks in Romania. *Acta. volc.*, 7, p. 53-61 .

PLATES

Plate I

Fig. 1 — New biotite (black) occurring as tiny, rounded crystals (s - sillimanite; f - feldspar)

Fig. 2 — Fibrolitic sillimanite (s) around pinite aggregates (pseudomorphs on feldspars?) containing corundum crystals (c)

Fig. 3 — Sillimanite (s), corundum (c), spinel (black) and new biotite (b) in a feldspathic enclave (f-feldspar).

Fig. 4 — Sillimanite (s) grown on biotite (b) in a feldspathic enclave (f-feldspar).


1

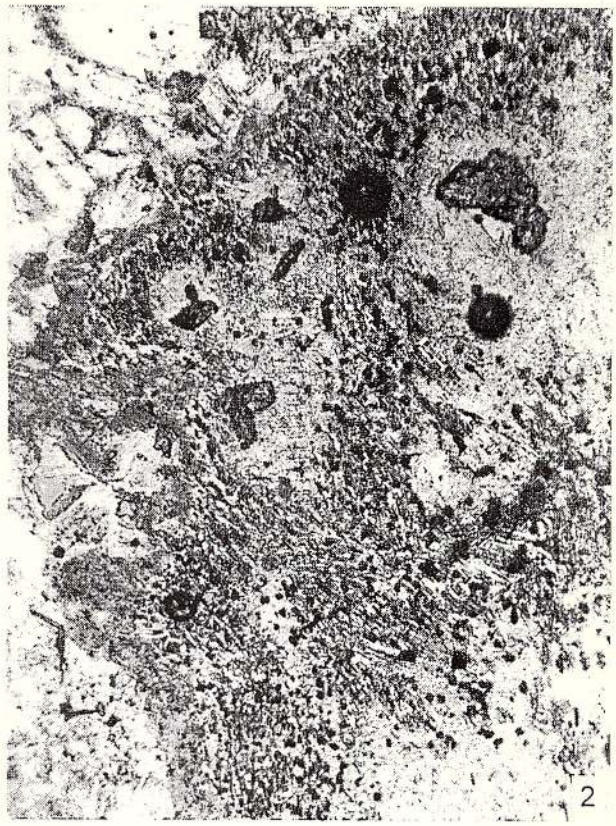
2

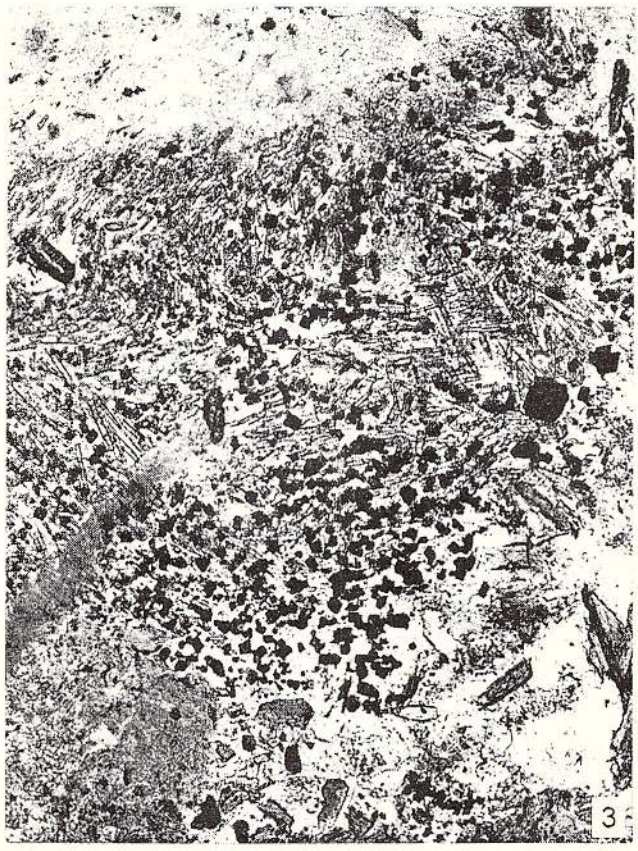
3


4

Plate II

Fig. 5 — Amphibole (hornblende) xenocryst with opaque minerals and pyroxene reaction corona. The host rock is a pyroxene and hornblende (Colibita structure).

Fig. 6 — Corroded quartz xenocrysts (Heniu structure).

Fig. 7 — Quartz xenocryst with pyroxene (diopside) reaction rim (Heniu structure).

Fig. 8 — Garnet xenocryst with resorption shape (Colibita structures).


5

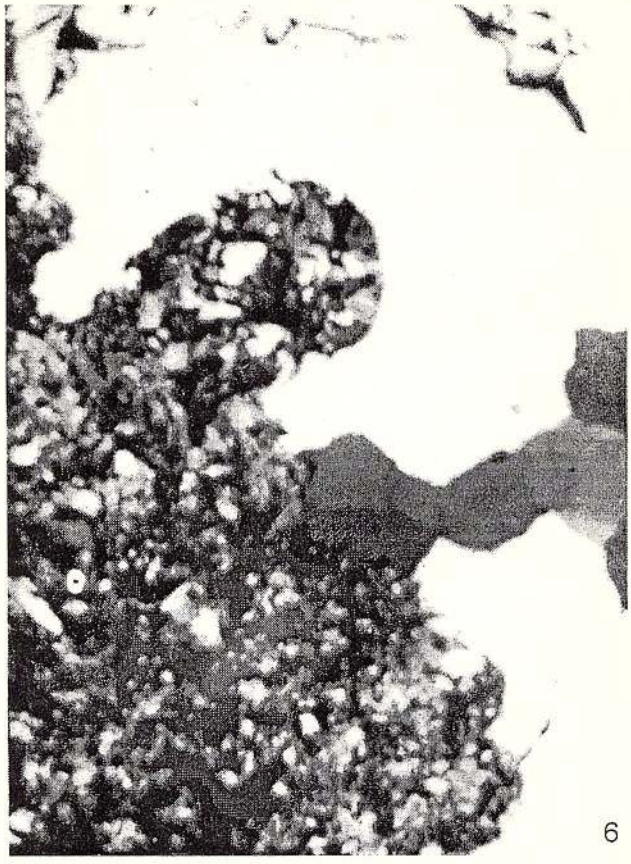
6


7

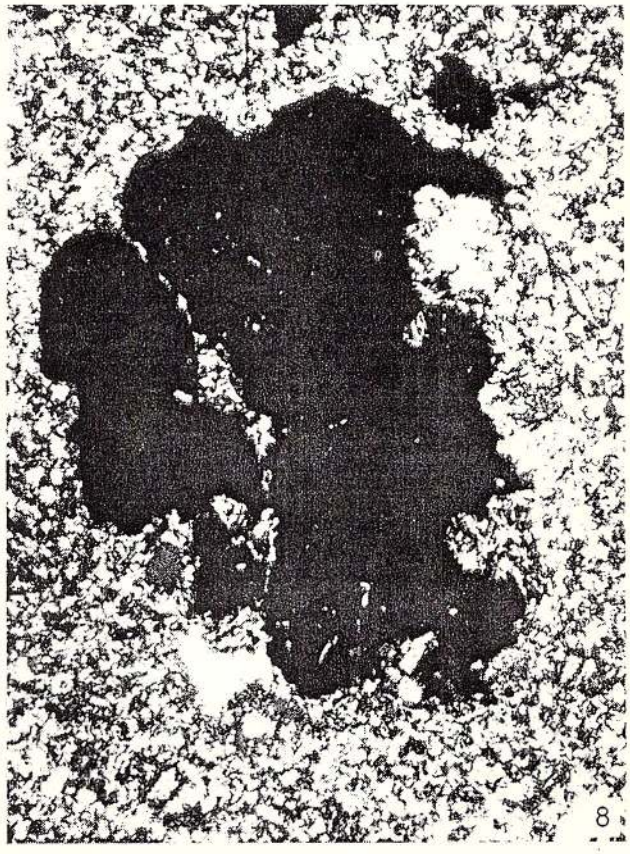
8

Plate III

Fig. 9 — Garnet xenocryst with reaction corona in the andesite host rock (Strejii structure).

Fig. 10 — Zoned plagioclase phenocryst, unaltered and showing euhedral shape (center). (Valea Vinului structure)

Fig. 11 — Zoned, euhedral A - type amphibole (ferroan, pargasite), in the andesitic host rock (Magura Arsente structure).

Fig. 12 — A-type amphibole (ferroan pargasite)).

9

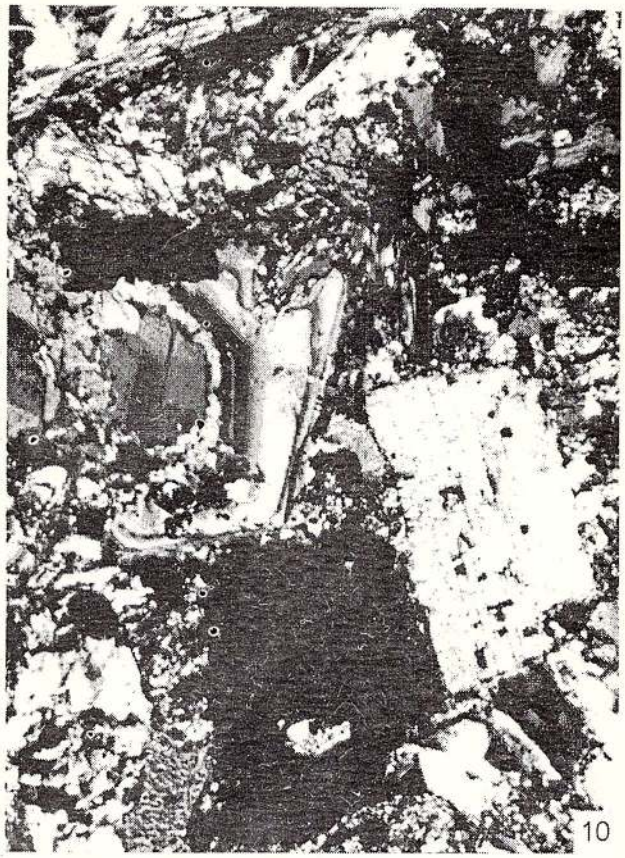

10

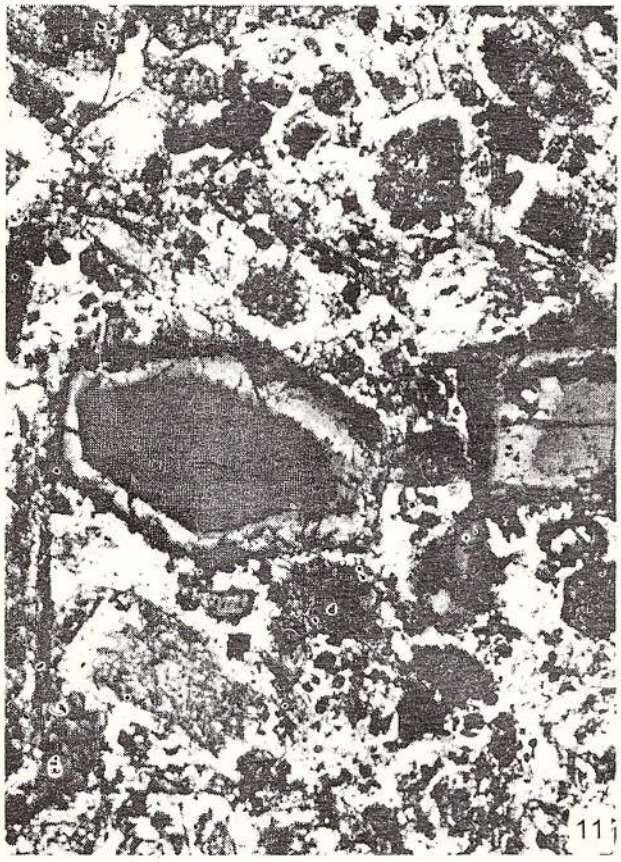

11

12

Plate IV

Figs. 13, 14, 15 — Poikilitic hornblende (B-type) in cognate enclaves. The chemical features place it in the ferroan, pargasite - tschermakite field. The host rocks is microdiorite (Arsente Structure).

Fig. 16 — Primary pyroxene (augite) phenocryst.


13


14


15


16

Plate V

Fig. 17 — Primary pyroxene phenocryst. The host rocks is an andesite. (Strejii structure).

Figs. 18, 19 — Secondary generation pyroxene crystals (diopside), from an enclave (Dornisoara structures).

Fig. 2o - First generation biotite (idiomorphic, inclusion-free) in quartz andesite host rock (Valea Vinului structure).

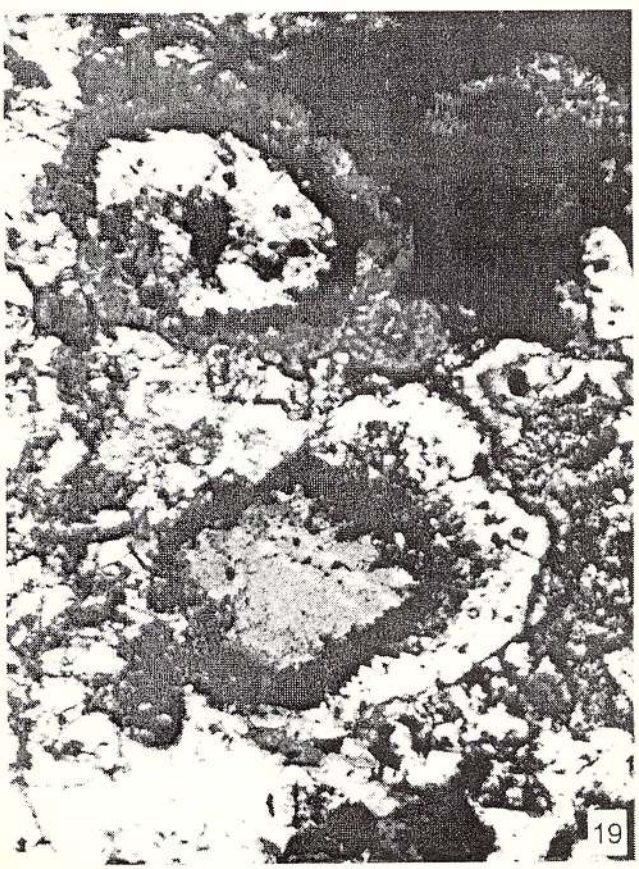

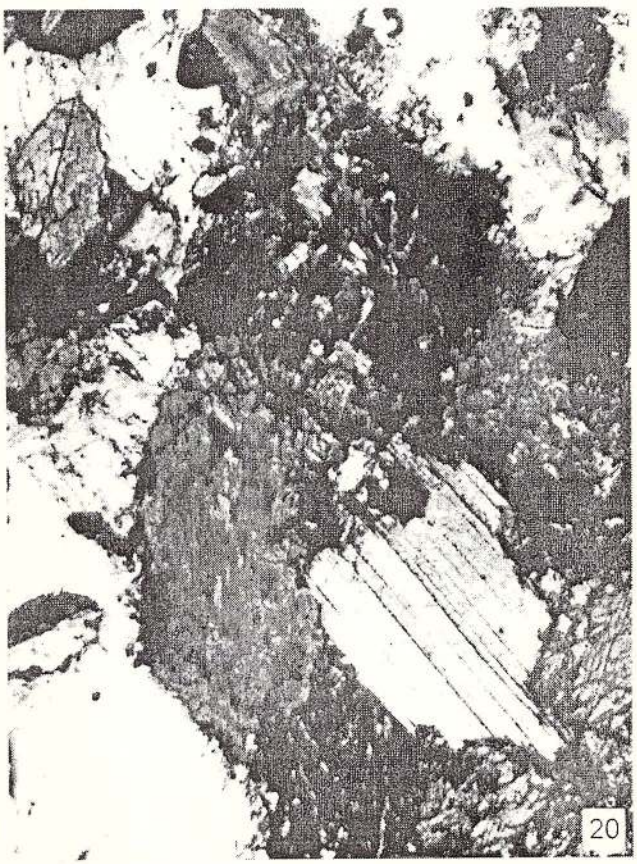

Plate VI

Fig . 21 — First generation biotite (idiomorphic, inclusion-free) in quartz andesite host rock (Valea Vinului structure).

Figs. 22, 23 — Biotite of the second generation from an enclave.

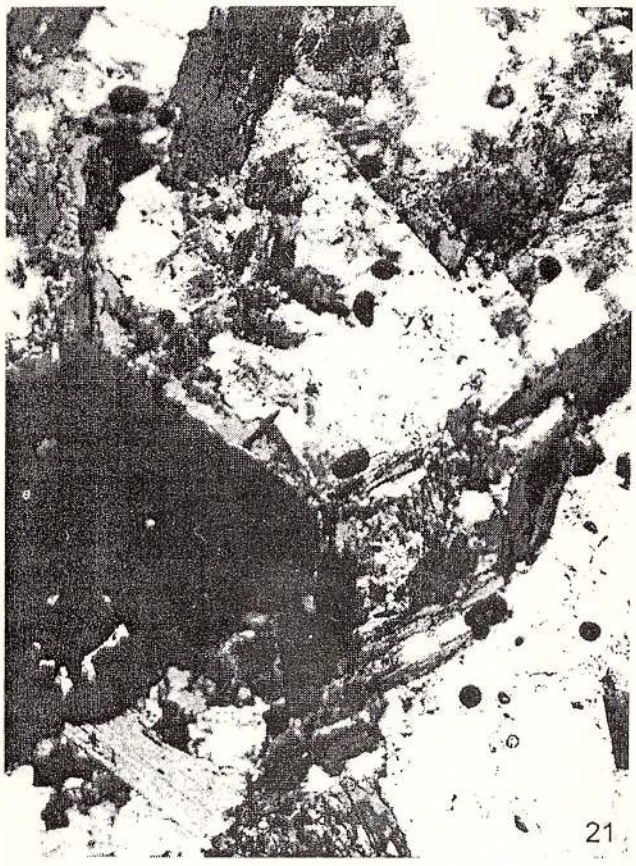

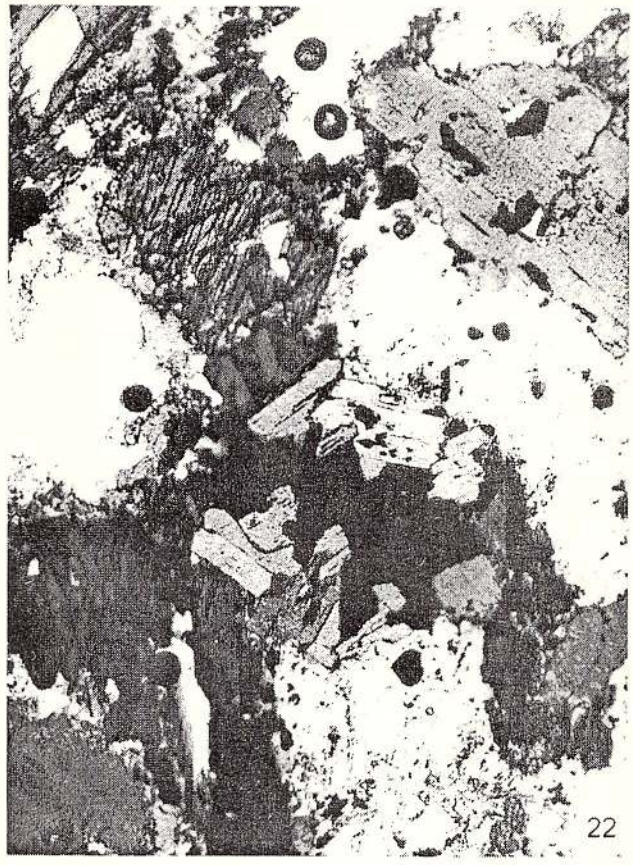

INSTRUCŢIUNI PENTRU AUTORI

ANUARUL INSTITUTULUI GEOLOGIC AL ROMÂNIEI publică contribuţii ştiinţifice originale referitoare la acest domeniu.

Vor fi acceptate numai lucrările care prezintă concis şi clar informaţii noi. Manuscrisul va fi supus lecturii critice a unuia sau mai multor specialişti; după a doua revizie nesatisfăcătoare din partea autorilor va fi respins definitiv şi nu va fi înapoiat.

Manuscrisele trebuie prezentate, de regulă, în engleză sau franceză; cele prezentate în limba română trebuie să fie însoţite de un rezumat, în engleză sau franceză, de maximum 10 % din volumul manuscrisului.

Lucrările trebuie depuse, pe disketă şi text pe hârtie în două exemplare, la secretariatul Comitetului de redacţie, inclusiv ilustraţiile în original. Manuscrisul trebuie să cuprindă: textul (cu o pagină de titlu, care este şi prima pagină a lucrării), bibliografie, cuvinte cheie, abstract, ilustraţii, explicaţii ale figurilor şi planşelor, şi un sumar cu scop tehnic.

Se va adăuga o filă separată cu un colontitlu de maximum 60 semne şi un sumar, în care se va indica ierarhia titlurilor din text în clasificarea zecimală (1; 1.1; 1.1.1), care nu trebuie să depăşească patru categorii.

Textul va fi predat pe disketă, format ASCII şi două copii pe hârtie, cu un spaţiu liber de 3 cm în partea stîngă a paginii şi nu trebuie să depăşească 10 pagini (inclusiv bibliografia şi figurile).

Prima pagină a textului va cuprinde: a) titlul lucrării (concis, dar informativ), cu un spaţiu de 8 cm deasupra; b) numele întreg al autorului (autorilor); c) instituţia (instituţiile) şi adresa (adresele) pentru fiecare autor sau grup de autori; d) text.

Notele de subsol se vor numerota consecutiv.

Citările din text trebuie să includă numele autorului şi anul publicării. Exemplu: Ionescu (1970) sau (Ionescu, 1970). Pentru doi autori: Ionescu, Popescu (1969) sau (Ionescu, Popescu, 1969). Pentru mai mult de doi autori: Ionescu et al. (1980) sau (Ionescu et al., 1980). Pentru lucrările care se află sub tipar, anul publicării va fi înlocuit cu "in press". Lucrările nepublicate şi rapoartele vor fi citate în text ca şi cele publicate.

Abstractul, maximum 20 rînduri (pe filă separată), trebuie să fie în limba engleză şi să prezinte pe scurt principalele rezultate şi concluzii (nu o simplă listă cu subiecte abordate).

Cuvintele cheie (maximum 10) trebuie să fie în limba engleză sau franceză, corespunzător limbii în care este lucrarea (sau abstractul, dacă textul este în română), prezentate în succesiune de la general la specific şi dactilografiate pe pagina cu abstractul.

Bibliografia se prezintă în ordine alfabetică şi cronologică pentru autorii cu mai mult de o lucrare. Abrevierile titlului jurnalului sau ale editurii trebuie să fie conforme cu recomandările respectivelor publicaţii sau cu standardele internaţionale.

Exemple:

a) jurnale:

Giuşcă, D. (1952) Contributions à l'étude cristallochimique des niobates. *An. Com. Geol.*, XXIII, p. 259–268, Bucureşti.

– , Pavelescu, L. (1954) Contribuţii la studiul mineralogic al zăcămîntului de la Muşca. *Comm. Acad. Rom.*, IV, 11–12, p. 658–991, Bucureşti.

b) publicaţii speciale:

Strand, T. (1972) The Norwegian Caledonides. p. 1–20. In: Kulling, O., Strand, T. (eds.) Scandinavian Caledonides, 560 p., Interscience Publishers.

c) cărţi:

Bălan, M. (1976) Zăcămintele manganifere de la Iacobeni. Ed. Acad. Rom., 132 p., Bucureşti.

d) hărţi:

Ionescu, I., Popescu, P., Georgescu, G. (1990) Geological Map of Romania, scale 1:50,000, sheet Cîmpulung. Inst. Geol. Geofiz., Bucureşti.

e) lucrări nepublicate sau rapoarte:

Dumitrescu, D., Ionescu, I., Moldoveanu, M. (1987) Report. Arch. I.G.R., Bucureşti.

Lucrările sau cărţile publicate în rusă, bulgară, sârbă etc. trebuie menţionate în bibliografie transliterînd numele şi titlurile. Exemplu:

Krasheninnikov, V. A., Basov, I. A. (1968) Stratigrafiya kainozoia. Trudy GIN, 410, 208 p., Nauka, Moskow.

Ilustraţiile (figuri şi planşe) trebuie numerotate şi prezentate în original, pe coli separate (hîrtie de calc), bune pentru reprodus. Dimensiunea liniilor, a literelor şi a simbolurilor pe figuri trebuie să fie suficient de mare pentru a putea fi citite cu uşurinţă după ce au fost reduse. Dimensiunea originalului nu trebuie să depăşească suprafaţa tipografică a paginii: lăţimea coloanei 8 cm, lăţimea paginii 16,5 cm, lungimea paginii 23 cm, pentru figuri, iar pentru planşele liniare nu trebuie să depăşească dimensiunile unei pagini simple (16,5/23 cm) sau duble (23/33 cm) şi trebuie să fie autoexplicativă (să includă titlul, autori, explicaţie etc.). Scară grafică obligatorie.

Ilustraţiile fotografice (numai alb-negru) trebuie să fie clare, cu contrast bun şi grupate pe planşe de 16/23 cm. In cadrul fiecărei planşe numărătoarea fotografiilor se repetă (de. ex. Pl. I, fig. 1, Pl. II, fig. 1).

Tabelele vor fi numerotate şi vor avea un titlu. Dimensiunea originală a tabelelor trebuie să corespundă dimensiunilor tipografice menţionate mai sus (8/16,5 sau 16,5/23).

Autorii vor primi un singur set de corectură, pe care trebuie să-l înapoieze, cu corecturile corespunzătoare, după 10 zile de la primire. Numai greşelile de tipar trebuie corectate; nu sînt acceptate modificări.

Autorii vor primi gratuit 30 de extrase pentru fiecare lucrare.

Comitetul de redacţie

INSTRUCTIONS TO AUTHORS

ANUARUL INSTITUTULUI GEOLOGIC AL ROMÂNIEI publishes original scientific contributions dealing with any subject of this field.

Only papers presenting concisely and clearly new information will be accepted. The manuscript will be submitted for critical lecture to one or several advisers. Papers will be definitely rejected after a second unsatisfactory revision by the authors. The manuscripts will not be returned to the authors even if rejected.

Manuscripts are prefered in English or French. Manuscripts submitted in Romanian will be accompanied by an abstract in English or French (maximum 10 per cent of the manuscript volume).

Papers should be submitted on diskette and typed text in duplicate to the secretary of the Editorial Board, including the reproduction ready original figures. The manuscript should comprise: text (with a title page which is the first page of it), references, key words, abstract, illustrations, captions and a summary for technical purposes.

Author(s) should add a separate sheet with a short title (colontitle) of maximum 60 strokes and a summary indicating the hierarchy of headings from the text listed in decimal classification (1; 1.1; 1.1.1) but not exceeding four categories.

Text should be on diskette, format ASCII and 2 copies, holding an empty place of 3 cm on the left side of the page. The text cannot exceed 10 typewritten pages (including references and figures).

Front page (first page of the text) should comprise: a) title of the paper (concise but informative) with an empty space of 8 cm above it; b) full name(s) of the author(s); c) institution(s) and address(es) for each author or group of authors; d) text.

Footnotes should be numbered consequtively.

Citations in the text should include the name of the author and the publication year. Example: Ionescu (1970) or (Ionescu, 1970). For two authors: Ionescu, Popescu (1969) or (Ionescu, Popescu, 1969). For more than two authors: Ionescu et al. (1980) or (Ionescu et al., 1980). For papers which are in course of print the publication year will be replaced by "in press". Unpublished papers or reports will be cited in the text like the published ones.

Abstract, of maximum 20 lines (on separate sheet), must be in English, summarizing the main results and conclusions (not a simple listing of topics).

Key words (max. 10 items), in English or French, following the language used in the text (or the Resumé if the text is in Romanian), given in succession from general to specific, should be typed on the abstract page.

References should be typed in double-line spacing, listed in alphabetical order and chronological order for authors with more than one reference. Abbreviations of journals or publishing houses should be in accordance with the recommendations of the respective publications or with the international practice.

Examples:

a) journals:

Giuşcă, D. (1952) Contributions à l'étude cristallochimique des niobates. *An. Com. Geol.*, XXIII, p. 259–268, Bucureşti.

– , Pavelescu, L. (1954) Contribuţii la studiul mineralogic al zăcămîntului de la Muşca. *Comm. Acad. Rom.*, IV, 11–12, p. 658–991, Bucureşti.

b) special issues:

Strand, T. (1972) The Norwegian Caledonides. p. 1–20. In: Kulling, O., Strand, T. (eds.) Scandinavian Caledonides, 560 p., Interscience Publishers.

c) books:

Bălan, M. (1976) Zăcămintele manganifere de la Iacobeni. Ed. Acad. Rom., 132 p., Bucureşti.

d) maps:

Ionescu, I., Popescu, P., Georgescu, G. (1990) Geological Map of Romania, scale 1:50,000, sheet Cîmpulung. Inst. Geol. Geofiz., Bucureşti.

e) unpublished papers or reports:

Dumitrescu, D., Ionescu, I., Moldoveanu, M. (1987) Report. Arch. Inst. Geol. Geofiz., Bucureşti.

Papers or books published in Russian, Bulgarian or Serbian etc. should be mentioned in the references transliterating the name and titles. Example:

Krasheninnikov, V. A., Basov, I. A. (1968) Stratigrafiya kainozoia. Trudy GIN, 410, 208 p., Nauka, Moskow.

Illustrations (figures and plates) must be numbered and submitted as originals on separate sheets (tracing papers), ready for reproduction. The thickness of the lines, lettering and symbols on figures should be large enough to be easily read after size-reduction. The original size should not extend beyond the print area of the page: column width 8 cm, page width 16.5 cm, page length 23 cm for figures; the width of line drawings should not extend over a single (16.5/23) or double (23/33 cm) page area and must be selfexplanatory (including title, authors, legend etc.). The graphic scale is obligatory.

Photographic illustrations (black-and-white only) must be of high quality and should be grouped into plates 16/23 cm in size. Each plate should have the photos numbered, i.e. Pl. I, Fig. 1; Pl. II, Fig. 1.

Tables should be numbered and entitled. Original size of the tables should correspond to the above mentioned (8/16.5 or 16.5/23) dimensions of the printing area.

Author(s) will receive only one set of preprint proofs which must be returned, with corrections, 10 days after receiving them. Only printing errors should be corrected, no changes in the text can be accepted.

Thirty offprints of each paper are supplied to the author(s) free of charge.

Editorial Board

Editat cu sprijinul Agenţiei Naţionale pentru Ştiinţă, Tehnologie şi Inovare – Colegiul Consultativ pentru Cercetare Ştiinţifică şi Dezvoltare Tehnologică

Edited with the support of the National Agency for Science, Tehnology and Innovation – Advisory Board for Scientific Research and Technologic Development

Translation and language review by:
Adriana Năstase

Editorial Staff:
Georgeta Borlea, Cristian Toth

Illustration:
Paraschiv Toader

Printing:
G. Bădulescu, N. Păleanu, F. Dumitru, P. Jurjea, C. Albu